

**POLITECNICO DI TORINO**

Collegio di Ingegneria Chimica e dei Materiali

**Corso di Laurea  
in Ingegneria dei Materiali**

**Graphene-based membranes for water  
purification processes**



**Tutori**

Prof. Giancarlo Cicero

Dr. Marco Laurenti

**Candidato**

Alberta Pellegrino

Dicembre 2019

# TABLE OF CONTENTS

RIASSUNTO .....	1
INTRODUCTION .....	14
<b>1. MEMBRANE SEPARATION PROCESSES</b>	
<b>1.1 Generalities of membrane processes</b> .....	16
1.1.1 Operation modes .....	16
1.1.2 Classification of synthetic membranes .....	17
1.1.3 Membrane modules .....	18
1.1.4 Process parameters .....	20
<b>1.2 Transport phenomena in membranes</b> .....	21
1.2.1 Mathematical models .....	21
<b>1.3 Concentration polarization</b> .....	23
<b>1.4 Classification of membrane processes</b> .....	25
<b>1.5 Pressure-driven processes</b> .....	25
1.5.1 Microfiltration (MF) .....	26
1.5.2 Ultrafiltration (UF) .....	27
1.5.3 Nanofiltration (NF) .....	28
1.5.4 Reverse Osmosis (RO) .....	29
<b>1.6 Limits of commercial membranes</b> .....	31
<b>2. NANO-STRUCTURED MEMBRANES</b> .....	34
<b>2.1 Graphene: two-dimensional carbon</b> .....	34
2.1.1. Crystal structure of graphene .....	36
2.1.2. Graphene properties .....	37
<b>2.2 Techniques for synthesis of graphene</b> .....	39
2.2.1 Top-down methods .....	39
2.2.2 Bottom-up methods .....	40
<b>2.3 Advantages of graphene-based membranes</b> .....	42
2.3.1 Single layer porous graphene membranes: state of the art .....	44
<b>3. MATERIALS AND METHODS</b> .....	53
<b>3.1 Materials</b> .....	53
3.1.1. PCTE membranes .....	53
3.1.2. Monolayer Graphene .....	54
<b>3.2 Transfer process of monolayer graphene to PCTE substrates</b> .....	56
<b>3.3 Characterization of graphene membranes</b> .....	58
3.3.1 Contact angle test .....	58
3.3.2 Field-Emission Scanning Electron Micrope (FE-SEM) .....	59
3.3.3 Raman spectroscopy .....	61
<b>3.4 Mass Transport measurements</b> .....	64

3.4.1	Side-bi-side diffusion cell .....	64
3.4.2	Calibration procedure of the probe .....	66
3.4.3	Transport study experimental procedure .....	69
<b>4.</b>	<b>RESULTS AND DISCUSSION .....</b>	<b>71</b>
4.1	Transfer process .....	71
4.2	Characterization of membranes .....	71
4.2.1	Contact angle measurements on PCTE .....	72
4.2.2	Contact angle measurements on PCTE/graphene membranes .....	72
4.2.3	FE-SEM images of PCTE membranes .....	74
4.2.4	FE-SEM images of PCTE/graphene membranes .....	75
4.2.5	Raman Spectroscopy .....	78
4.3	Transport measurements .....	82
4.3.1	NaCl transport measurements .....	82
4.3.2	Diclofenac transport measurements .....	85
<b>5.</b>	<b>CONCLUSIONS .....</b>	<b>87</b>
<b>6.</b>	<b>BIBLIOGRAPHY .....</b>	<b>89</b>
<b>7.</b>	<b>ACKNOWLEDGEMENTS .....</b>	<b>92</b>

## RIASSUNTO

Nel ventunesimo secolo il mondo si sta ritrovando a fronteggiare le più grandi sfide di sempre in termini di approvvigionamento di risorse idriche, necessità di risparmio energetico, e protezione dell'ambiente da reflui industriali pericolosi. In tale ottica, questo lavoro di ricerca nasce dal bisogno di trovare delle valide alternative ai processi di separazione e purificazione attualmente in uso per il trattamento delle acque. La separazione dei componenti di una miscela, siano essi solidi, liquidi o gassosi, è una pratica indispensabile alla realizzazione di innumerevoli attività industriali. I processi di separazione, concentrazione e depurazione sono infatti fondamentali nella nostra vita quotidiana e sono impiegati in numerosi settori: nella produzione di prodotti ultra puri nell'industria farmaceutica, nella produzione di acqua potabile, nel trattamento di acque superficiali e sotterranee per la rimozione di inquinanti ambientali, oltre che nei processi di concentrazione dell'industria lattiero casearia, nella purificazione dei prodotti di fermentazione dell'industria vinicola e birraria, nel recupero dai reflui di sostanze preziose come minerali e terre rare, ecc. Negli ultimi sessant'anni la tecnologia a membrane ha affiancato i processi di separazione tradizionali quali distillazione, cristallizzazione, sedimentazione, etc. affermandosi come la migliore tecnologia esistente per il trattamento delle acque reflue e per la desalinizzazione delle acque saline o salmastre. Le prime applicazioni industriali della tecnologia a membrana risalgono agli anni '60, anche se i primi studi teorici sui fenomeni a membrana risalgono al XVIII secolo. Questo tipo di separazione si basa sulla presenza di una membrana, che può essere definita come "un materiale attraverso il quale un tipo di sostanza può passare più facilmente di un altro, presentando così la base di un processo di separazione"[1]. In sostanza una membrana è una barriera di permeabilità selettiva che varia in materiale, struttura e funzione, caratterizzata dalla prevalenza della superficie sullo spessore, ovvero una barriera che può essere attraversata da alcuni componenti presenti nei fluidi mentre è scarsamente o per nulla permeabile agli altri. Le membrane possono essere classificate in base al materiale di cui sono costituite, alla forma geometrica (piane, a spirale avvolta, tubolari, o a fibre cave), alla struttura (dense o porose) e alla sezione trasversale (simmetriche o asimmetriche). Il principio alla base dei diversi tipi di processi a membrana è il seguente: una soluzione di alimentazione contenente soluti e/o particelle passa attraverso la membrana, dalla quale si ottiene una corrente residua (o retentato/concentrato) più ricca nei componenti trattenuti, e un flusso di permeato purificato da questi componenti, come schematicamente mostrato in Fig.1. La separazione nei processi a membrana si basa su una diversa velocità di trasporto delle varie specie chimiche. Questa velocità di trasporto dipende dalle forze motrici che agiscono sul sistema e dalla mobilità e concentrazione delle specie chimiche.

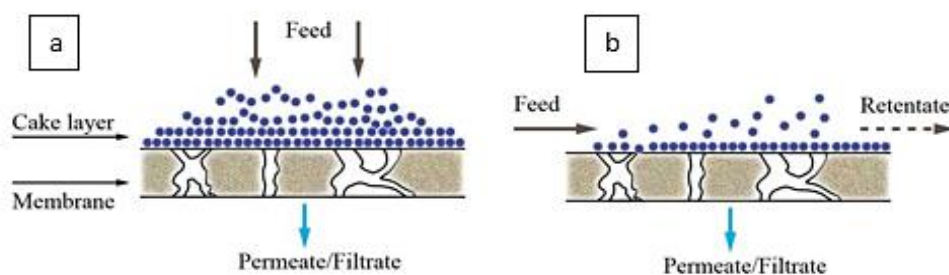


**Figura 1:** Rappresentazione schematica di un processo a membrana in modalità a) dead-end e b) cross-flow

Come si può osservare in Figura 1 la filtrazione a membrana può essere eseguita in due modalità operative: modalità dead-end, in cui il flusso di alimentazione si muove perpendicolarmente alla membrana, e modalità cross-flow, in cui il flusso di alimentazione si muove parallelamente alla superficie della membrana. Lo schema di filtrazione tangenziale si traduce in prestazioni molto più elevate rispetto a quello convenzionale (dead end), perché la velocità tangenziale del fluido rimuove dalla superficie della membrana le particelle che vi si accumulano per effetto della ritenzione.

Nei processi di filtrazione, se la differenza di pressione applicata viene mantenuta costante, il flusso diminuisce nel tempo a causa della formazione della cosiddetta "cake", costituita dal materiale in sospensione fermato dal telo filtrante. Oltre a questi fenomeni di incrostazione riconducibili alle caratteristiche intrinseche della membrana ci sono anche altri fenomeni di resistenza al flusso noti come "polarizzazione di concentrazione" dipendenti dalle condizioni fluidodinamiche che creano in prossimità della membrana stessa. Questo fenomeno, dovuto al trasporto selettivo di solvente e soluto, implica che la concentrazione di soluti in prossimità della membrana sia superiore alla concentrazione media della soluzione, con formazione di uno strato limite concentrato, come mostrato in Figura 2. Come conseguenza, si forma un flusso retrodiffusivo in competizione con quello convettivo diretto verso la membrana. L'effetto di polarizzazione della concentrazione può anche dare origine a fenomeni di "fouling" sulla superficie della membrana: la maggiore concentrazione all'interno dello strato limite favorisce la precipitazione dei soluti, con conseguente deposizione delle particelle sulla superficie della membrana. Questi fenomeni provocano una riduzione della ritenzione e una diminuzione del flusso, il quale è inversamente proporzionale alle resistenze opposte al flusso e direttamente proporzionale alla forza motrice agente sul sistema.

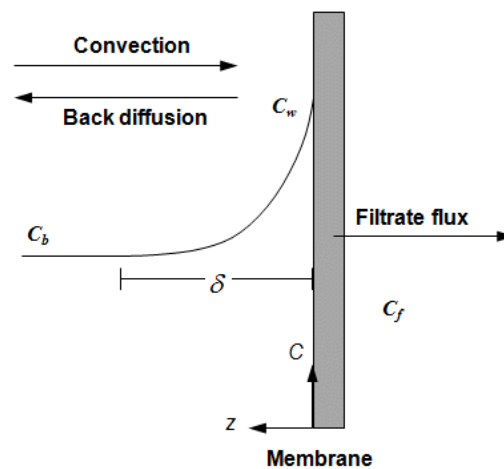


**Figura 2:** Rappresentazione schematica della polarizzazione di concentrazione

L'esistenza di una forza motrice tra i due lati di una membrana è ciò che rende possibili i flussi di solvente e soluto da un lato all'altro della barriera. La forza motrice agente sul sistema è il parametro in base a cui i processi di separazione a membrane vengono distinti e classificati, come si può vedere in Tabella 1.

**Tabella 1:** Classificazione dei processi di separazione a membrana

FORZA MOTRICE	PROCESSI DI SEPARAZIONE A MEMBRANA
Gradiente di pressione	<ul style="list-style-type: none"> <li>• Microfiltrazione (MF)</li> <li>• Ultrafiltrazione (UF)</li> <li>• Nanofiltrazione (NF)</li> <li>• Microfiltrazione (MF)</li> <li>• Separazione di gas (GS)</li> <li>• Pervaporazione (PV)</li> </ul>
Gradiente di concentrazione (o attività $a$ )	<ul style="list-style-type: none"> <li>• Dialisi</li> <li>• Osmosi diretta (FO)</li> </ul>
Temperature gradient	<ul style="list-style-type: none"> <li>• Distillazione a membrana (MD)</li> </ul>
Electrical potential gradient	<ul style="list-style-type: none"> <li>• Elettrodialisi (ED)</li> </ul>

In generale, un gradiente di pressione idrostatica implica una portata volumetrica  $J_V$ , un gradiente di concentrazione implica un flusso di molecole  $J_n$ , un gradiente di temperatura implica un flusso di calore  $J_Q$ , e un gradiente potenziale porta ad una corrente elettrica  $J_e$ . Il flusso  $J$  (espresso in  $m^3/s \cdot m^2$  oppure in  $kg/s \cdot m^2$  a seconda che si tratti di flusso di solvente o di soluti) è uno dei parametri di processo che contraddistinguono la tecnologia a membrane e rappresenta la quantità di sostanza che permea attraverso la membrana nell'unità di tempo per unità di superficie. Oltre al flusso, altri due parametri sono necessari per caratterizzare le performance di una membrana: la conversione o recupero, definita come il rapporto tra la portata di permeato e quella di alimentazione, e la ritenzione  $R$ , che è una misura della quantità di soluto trattenuta dalla membrana. Quest'ultima è definita come:

$$R = \left( \frac{C_F - C_P}{C_F} \right) \times 100 = \left( 1 - \frac{C_P}{C_F} \right) \times 100 \quad (1)$$

dove  $C_p$  e  $C_F$  sono rispettivamente la concentrazione del permeato e dell'alimentazione. La ritenzione è espressa in percentuale e quindi può variare tra 0 e 100%.

I processi di separazione a membrana più sfruttati tra quelli citati in Tabella 1 sono quelli che coinvolgono flussi di materia  $J$  significativi. Tra questi, i più comuni e diffusi sono quelli basati sulla differenza di pressione. In particolare, MF, UF, NF, NF e RO sono quelli coinvolti nella depurazione delle acque. I processi a pressione sono classificati in base alla dimensione delle particelle trattenute e alle pressioni di esercizio utilizzate. La Tabella 2 mostra le applicazioni, le dimensioni dei pori delle membrane e i  $\Delta P$  tipici di ogni processo.

**Tabella 2:** Dimensioni delle particelle trattenute e pressioni tipiche dei processi a pressione.

<b>Tipo di membrana</b>	<b>Taglia dei pori</b>	<b>Tipo di particelle rimosse</b>	<b>Pressione di esercizio</b>
Microfiltrazione	10 <sup>3</sup> -50 nm	-Particelle sospese -Colloidi -Globuli rossi -Batteri -Virus	5-500 KPa (<30 psi)
Ultrafiltrazione	50-1 nm	-Virus -Proteine -Amidi -Grassi -Molecole organiche -Coloranti	<1 MPa (20-100 psi)
Nanofiltrazione	1-0,1 nm	-Glucosio -Sali monovalenti -Pesticidi -Erbicidi	<4MPa (50-300 psi)
Osmosi inversa	< 0,1 nm	-Acqua -Sali monovalenti	>5-10 MPa (225-1000 psi)

Le membrane usate per microfiltrazione e ultrafiltrazione sfruttano un meccanismo di separazione essenzialmente di tipo "setaccio": le particelle sono separate in base alla loro dimensione. Le membrane per nanofiltrazione invece, avendo proprietà intermedie tra membrane porose e non porose, implicano meccanismi di separazione che comportano sia la setacciatura che il trasporto per diffusione. Nell'osmosi inversa invece le membrane utilizzate non sono più considerate come mezzi porosi bensì come mezzi densi. Per le membrane porose il trasporto avviene grazie alla presenza di pori, e la permeazione avviene attraverso fenomeni convettivi, mentre nelle membrane dense la permeazione è dovuta a fenomeni diffusivi. La RO è il processo a membrana a pressione più adatto per ottenere acqua potabile da acqua di mare o acqua salmastra, motivo per cui questo è sempre stato il suo campo di applicazione più ampio. In tale processo la pressione di esercizio deve superare la pressione osmotica.

Per concludere il resoconto generale su questa tecnologia relativamente nuova, si può affermare che i processi di separazione a membrana soddisfano le attuali esigenze di risparmio energetico e di riduzione dell'impatto ambientale, e sono spesso più semplici ed efficaci dei processi di separazione convenzionali, oltre al fatto che possono essere facilmente integrati nei processi di produzione esistenti. Tuttavia, i processi di separazione a membrana attualmente sfruttati si basano sull'uso di materiali polimerici convenzionali, i quali hanno dimostrato di presentare dei limiti tecnici ostativi all'utilizzo su lunga durata, di cui i più importanti sono:

- una bassa resistenza termica, chimica e meccanica;
- una spiccata tendenza al fouling che richiede frequenti lavaggi chimici, i quali aumentano il consumo energetico e riducono notevolmente il ciclo di vita della membrana;

- un'incompatibilità strutturale tra alta permeabilità e alta selettività: infatti, se il flusso è alto, il fattore di separazione risulta piuttosto basso, e viceversa.

Pertanto, nonostante sessant'anni di rapido sviluppo, è evidente la necessità di ulteriori miglioramenti in questo campo.

È in questo scenario che si colloca questo lavoro di tesi, il cui obiettivo principale è quello di dimostrare il potenziale di innovative membrane a base grafene nell'ambito del trattamento delle acque. Il grafene, scoperto nel 2004 da Gejm e Novosëlov, presenta delle proprietà fisico-chimiche rivoluzionarie tali da averlo portato al centro dell'attenzione mondiale per applicazioni nei più svariati ambiti. Il grafene è uno degli allotropi del carbonio costituito da un unico strato di atomi di C. È definito come un materiale 2D perché la dimensione dello spessore tende a 0, ovvero lo spessore di un singolo strato di grafene può essere considerato approssimativamente della dimensione di un atomo (3,5 Å di spessore). Esso è fondamentalmente un unico strato di grafite, cioè un unico strato di atomi di carbonio organizzati in un reticolo esagonale bidimensionale. In termini di simmetria cristallina, la struttura esagonale è descritta da un reticolo triangolare di Bravais con base biatomica costituita da due atomi di C.

Dal punto di vista chimico-fisico tutte le eccezionali proprietà del grafene derivano dai forti legami covalenti  $\sigma$  lungo il piano tra gli atomi di carbonio ibridizzati  $sp^2$ . L'ibridazione  $sp^2$  porta alla combinazione degli orbitali  $p_x$  e  $p_y$  con un orbitale  $2s$  e permette la formazione di tre forti legami covalenti  $\sigma$ , che portano alla struttura esagonale nel piano in cui ogni atomo di carbonio è legato ad altri tre, come avviene in grafite, grafene, nanotubi e fullerene. L'elettrone rimanente (dei 4 elettroni che occupano gli orbitali  $2s$ ,  $2p_x$ ,  $2p_y$ ,  $2p_z$ ) occupa l'orbitale  $2p_z$ , orientato perpendicolarmente al piano reticolare. Questi orbitali  $p_z$ , uno per ogni atomo di carbonio, interagiscono tra loro formando un debole legame  $\pi$ . Un foglio ideale di grafene monostrato è impermeabile a molecole piccole quanto He, grazie al fatto che la densità elettronica degli orbitali  $\pi$  forma una nuvola delocalizzata che blocca qualsiasi specie all'interno degli anelli aromatici [5]. Anche se impermeabile nel suo stato originario, modelli teorici [14] hanno previsto che con l'introduzione di pori di dimensione e densità controllate le membrane di grafene supererebbero le prestazioni delle membrane polimeriche di molti ordini di grandezza in termini di permeabilità e selettività. Ciò è possibile anche grazie alle eccellenti proprietà meccaniche di questo materiale bidimensionale: esso è infatti il materiale più resistente mai scoperto in natura, con una resistenza a rottura  $\sigma$  di 130 GPa, più di cento volte maggiore di quella dell'acciaio. Sorprendentemente, è sia rigido che elastico (come la gomma), quindi può essere allungato del 20-25% della sua lunghezza originale senza rompersi. Il modulo di elasticità  $E$  è di circa 1 TPa. L'incredibile resistenza del grafene è accompagnata da un'estrema "leggerezza" legata sia alla presenza degli atomi C che hanno un basso peso atomico sia allo spessore del piano monoatomico. Le caratteristiche del grafene che lo rendono il candidato più promettente per lo sviluppo della prossima generazione di membrane di separazione sono riportate di seguito.

- L'altissima resistenza meccanica permette alle membrane di grafene su supporto poroso di resistere a differenze di pressione molto elevate [12], requisito fondamentale nei processi a pressione e soprattutto nei processi di dissalazione dell'acqua di mare per osmosi inversa, in cui la pressione da applicare per superare quella osmotica è di circa 55 bar. L'eccellente resistenza in pressione garantita dalla resistenza meccanica permette inoltre di aumentare la portata e dunque il tasso di produzione.

- Lo spessore nanometrico rende possibile un notevole incremento di permeabilità rispetto alle membrane tradizionali, implicando dunque anche un notevole risparmio energetico. Tanugi and Grossman [13] hanno infatti osservato che un triplicarsi della permeabilità ridurrebbe la pressione del 44% per la desalinizzazione dell'acqua di mare tramite RO, il che equivale ad una riduzione del 15% del consumo energetico.
- Oltre all'elevata permeabilità, si può ottenere anche un'elevata selettività, se in presenza di una membrana in grafene nano-porosa. Questo può portare al superamento della storica dicotomia tra permeabilità e selettività tipica dei processi a membrana convenzionali.
- La tendenza al fouling è notevolmente mitigata nelle membrane a base grafene, grazie alla sua idrofobicità che riduce le forze di frizione con l'acqua di alimentazione.
- Grazie alla stabilità della struttura 2D, il grafene non è chimicamente reattivo. Questa maggiore stabilità e inerzia chimica del grafene rende possibile l'applicazione di queste membrane con una vasta gamma di solventi a svariato pH, consentendo anche una durata di vita maggiore delle membrane in cui è utilizzato.

Per quanto riguarda la produzione del grafene, a partire dal primo isolamento ottenuto per esfoliazione micromeccanica della grafite sono stati sviluppati nel corso degli anni numerosi metodi di crescita, che possono essere raggruppati in due grandi categorie: metodi top-down (esfoliazione meccanica, esfoliazione chimica, ed esfoliazione dell'ossido di grafite) e metodi bottom-up (deposizione chimica da fase vapore CVD, unzipping di nanotubi, e crescita epitassiale su cristalli di SiC). La tecnica CVD è quella adottata per produrre il grafene commerciale utilizzato in questo lavoro di tesi ed è considerata uno degli approcci più promettenti per la produzione di grafene di alta qualità. Rispetto alle tecniche di sintesi precedentemente presentate, il CVD permette di sintetizzare il grafene su superfici di diversi cm<sup>2</sup> in tempi ragionevoli, ottenendo un film di alta qualità cristallina e con la possibilità di trasferire facilmente il materiale prodotto su diversi substrati. Il processo CVD consiste nella crescita di uno strato di grafene su substrati metallici come Cu che fungono da catalizzatori della crescita, che avviene attraverso la decomposizione di molecole di idrocarburi che forniscono la fonte di carbonio necessaria per la crescita del grafene cristallino.

All'interno del forno CVD è inserito il catalizzatore, il quale viene esposto al flusso di gas precursori, come il metano CH<sub>4</sub>, miscelato con H<sub>2</sub> e Ar. Opportuni valori di temperatura e la presenza del catalizzatore consentono una reazione in cui si formano materiali solidi e gassosi, a partire dai precursori gassosi:



A tal punto il carbonio ottenuto viene riorganizzato in forma solida sul substrato metallico, il quale a fine processo risulta in tal modo ricoperto da grafene.

Un vantaggio fondamentale della tecnica di crescita del CVD su Cu è il buon controllo del numero di strati di grafene. Infatti, da uno studio comparativo [10] di CVD su Cu e Ni, emerge chiaramente che la crescita del grafene su Cu porta alla formazione di grafene monostrato. Infatti, il carbonio ha una bassissima solubilità nel Cu, quindi la quantità di carbonio disciolto al suo interno sarà molto piccola. Dunque, dopo il deposito del primo strato di grafene, non ci saranno più zone del catalizzatore esposte al flusso di idrocarburi,

per cui non si verificherà più la decomposizione dei reagenti di partenza e la crescita del grafene. Pertanto, il processo di CVD del grafene su Cu, schematizzato in Figura 3, è spesso definito come un processo di reazione superficiale auto-limitante. Grazie a questo si riesce ad ottenere un monostrato di grafene.

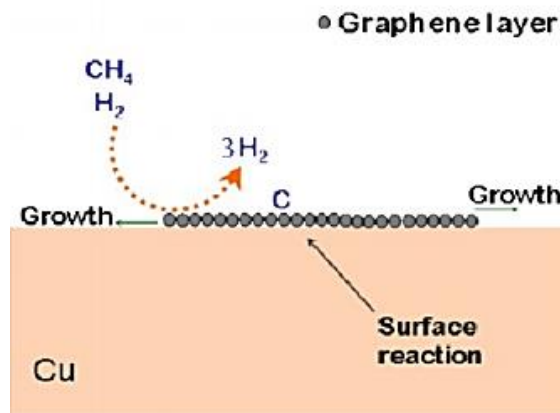


**Figura 3:** Processo CVD auto-limitante

Del grafene commerciale monostrato cresciuto tramite CVD su Cu è stato utilizzato in questo lavoro di tesi per la fabbricazione delle membrane, che costituisce la prima fase del lavoro sperimentale.

Essa consiste nel trasferimento diretto di grafene commerciale a singolo strato dal foglio di Cu a una membrana di supporto microporosa in PCTE idrofobo (con pori da 0,1 μm). Il trasferimento, illustrato in Figura 4, si effettua depositando una membrana in PCTE su un quadrato del film di grafene su Cu, lasciando poi galleggiare il tutto su una soluzione di etching FeCl<sub>3</sub> 1,5M. In seguito all'attacco chimico del rame e ad operazioni di lavaggio atte a rimuovere i residui contaminanti, il campione ottenuto è una membrana di grafene a singolo strato ben adeso a un substrato in PCTE (SLG/PCTE). Lo stesso processo di trasferimento è stato effettuato per realizzare delle membrane a doppio e triplo strato di grafene su PCTE (DLG/PCTE, TLG/PCTE).

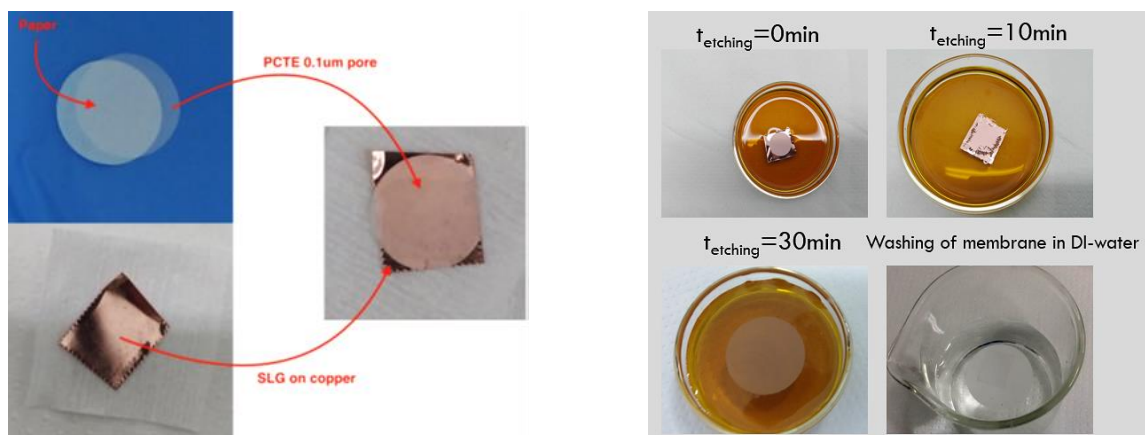


**Figura 3:** Processo di trasferimento di grafene su PCTE

Lo strato di grafene è facilmente distinguibile ad occhio nudo dopo il processo di trasferimento, come si può vedere in Figura 4. È possibile dedurre la deposizione del primo, secondo e terzo strato di grafene attraverso un cambiamento di colore della membrana in PCTE, il cui colore da inizialmente bianco diventa grigio.

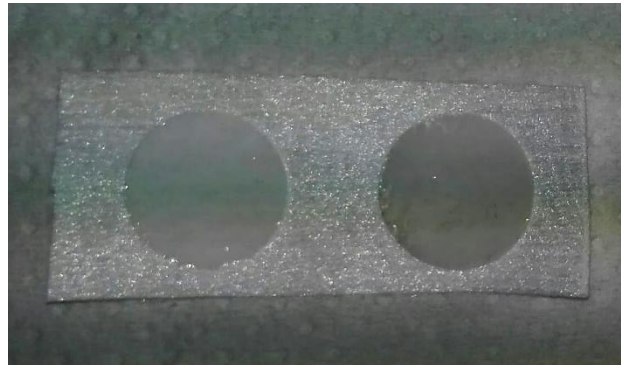


**Figura 4:** Membrana in PCTE pre trasferimento (sx) e post trasferimento (dx)

La qualità del grafene trasferito è generalmente influenzata da alcune caratteristiche del substrato. La prima è la rugosità superficiale: la superficie del supporto deve essere la più liscia possibile, in modo da garantire un buon contatto con lo strato di grafene ed evitare la presenza di fessurazioni. In secondo luogo, la dimensione dei pori deve essere la più piccola possibile, per garantire una buona sospensione del grafene sui pori ed evitare che il film collassi al loro interno. L'ultimo parametro che influenza la qualità del grafene trasferito è la bagnabilità del substrato. L'idrofobicità del supporto è necessaria per evitare che il reagente usato per l'attacco chimico si infiltri nell'interfaccia tra il grafene e il substrato, causando il distacco del grafene durante il processo di trasferimento.

Per valutare la bagnabilità delle membrane in PCTE e confrontarla con quella delle membrane grafene/PCTE, sono state effettuate misure di angolo di contatto col metodo della goccia sessile sia prima sia dopo i processi di trasferimento.

L'angolo di contatto misurato per il PCTE si avvicina a  $90^\circ$  ed è quindi rappresentativo di un comportamento idrofobico. Per quanto riguarda il grafene single layer trasferito su PCTE, è stato dimostrato sperimentalmente che tra le membrane PCTE e PCTE/SLG non c'è praticamente alcuna differenza nel valore dell'angolo di contatto, differenza che invece si accentua all'aumentare del numero di strati. È stata infatti riscontrata una bagnabilità crescente all'aumentare del numero di layer. È stato ipotizzato che ciò avvenga per effetto delle difettosità indotte, e che alcuni gruppi funzionali idrossilici (come ad esempio i gruppi -OH) potrebbero, durante i vari processi di trasferimento e lavaggio, ancorarsi ai legami insaturi presenti in prossimità di pori o difetti localizzati del film grafene.

Allo scopo di valutare la qualità del grafene trasferito, è stata condotta una caratterizzazione morfologica tramite microscopio elettronico a scansione a emissione di campo (FE-SEM) e una caratterizzazione strutturale tramite spettroscopia Raman.

Nell'immagine FE-SEM presente in Figura 5, le aree caratterizzate dalla presenza di grafene sono chiaramente distinguibili grazie alla presenza di *wrinkles* (grinze) tipiche del grafene trasferito su qualsiasi substrato. Si può anche osservare che la maggior parte dei pori sono coperti da un monostrato di grafene. Dunque, l'analisi FE-SEM conferma un buon grado di copertura e una qualità soddisfacente del film di grafene, tuttavia sono presenti alcuni difetti intrinseci su scala nanometrica e delle lacerazioni su scala micrometrica, così come alcune regioni di PCTE scoperte (indicate dalle aree più luminose).

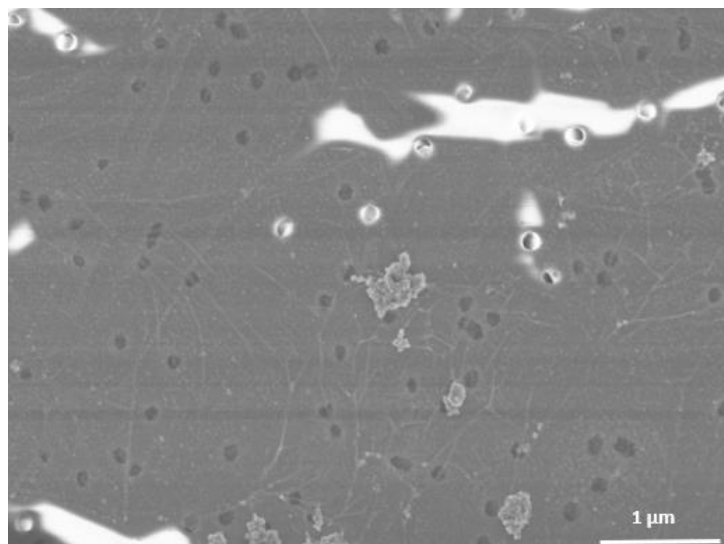


**Figura 5:** Immagine FE-SEM di una membrana SLG/PCTE. Ingrandimento 50xK

Dall'analisi al Raman emerge invece che gli spettri Raman (Figura 6 a) raccolti per le membrane SLG, DLG, TLG, TLG confermano la presenza del grafene, i cui picchi fondamentali sono denominati G ( $\approx 1580 \text{ cm}^{-1}$ ) e 2D ( $\approx 1680 \text{ cm}^{-1}$ ). In realtà, poiché la membrana in PCTE ha un picco principale alla lunghezza d'onda di  $1604 \text{ cm}^{-1}$  vicino al picco G del grafene (Figura 6 b), la presenza del grafene è più facilmente verificabile dalla presenza del picco 2D (Figura 7 a). Questo è anche il motivo per cui solo il picco 2D è stato selezionato e mappato in intensità (Figura 7 b).

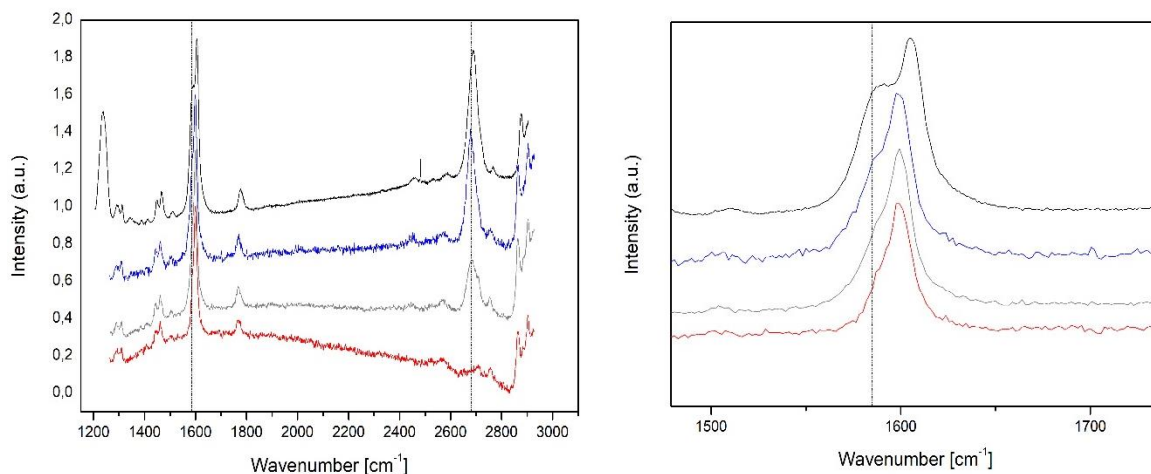


**Figura 6:** a) Spettri Raman di SLG, DLG, TLG su PCTE b) ingrandimento sul picco G del grafene sovrapposto al picco del PCTE

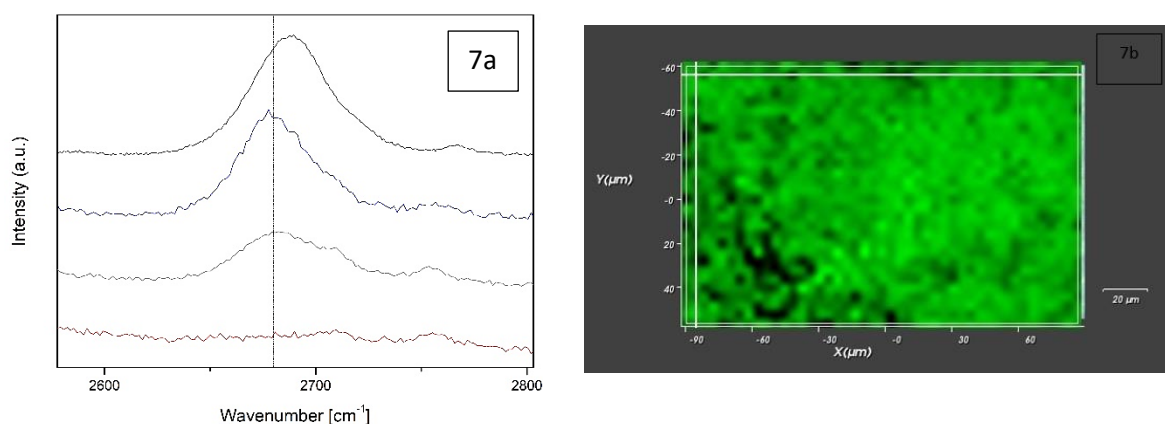


**Figura 7:** a) Ingrandimento del picco 2D b) mappatura del picco 2D con mappa Raman

Il campione su cui è stata eseguita la mappatura Raman è un campione TLG/PCTE. La regione esplorata è di circa  $120\ \mu\text{m} \times 180\ \mu\text{m}$  ed è stata divisa in  $\sim 2400$  celle. Per ogni cella è stato acquisito un singolo spettro Raman. Successivamente, la mappa spaziale Raman è stata ottenuta tracciando la modalità segnale-base a  $2680\ \text{cm}^{-1}$ , cioè normalizzando il picco di altezza massima rispetto alla linea di base dello spettro creato dal software. Il valore segnale-base è associato ad una mappa a colori, dove il verde chiaro è il massimo e il nero il minimo. È quindi possibile affermare che le zone verdi sono quelle coperte di grafene mentre quelle nere sono quelle scoperte. Questa mappa conferma una copertura ottimale del campione di grafene a tre strati, indicando che l'approccio basato sull'uso di grafene multistrato per la minimizzazione dei difetti potrebbe essere una buona alternativa alla produzione di membrane a base grafene.

Ai picchi G e 2D appena mostrati si aggiunge la banda D (Figura 9) posizionata nell'intervallo di lunghezza d'onda da  $1250$  a  $1400\ \text{cm}^{-1}$ . Il picco del grafene D fornisce informazioni sui difetti o sul grado di disordine nella struttura del grafene ed è quindi un'indicazione qualitativa della qualità cristallina del grafene. L'assenza della banda D indica che la difettosità indotta è limitata.

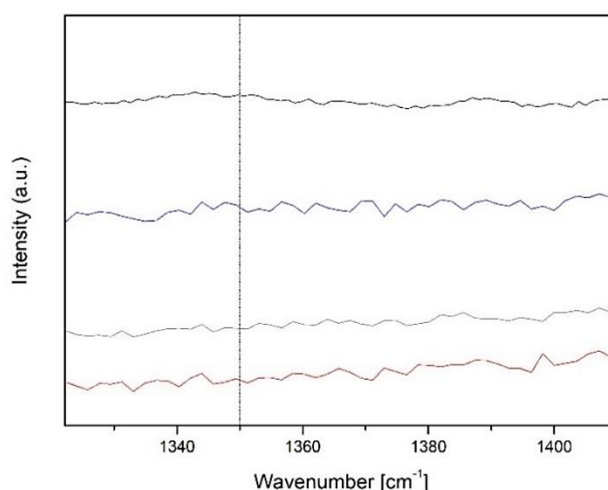


**Figura 9:** Ingrandimento della regione spettrale della banda D

Infine, è stata effettuata una caratterizzazione funzionale tramite misure di trasporto diffusivo attraverso le membrane grafene/polimero realizzate. Non conoscendo

aprioristicamente il potere selettivo e il meccanismo di esclusione dimensionale di queste membrane porose a base grafene, si sono preparate due soluzioni con diverse dimensioni dei soluti: una soluzione 0,5M di NaCl e una soluzione 10mM di Diclofenac in acqua distillata. Per valutare la diffusione di NaCl e Diclofenac attraverso le membrane grafene/polimero è stata usata una cella di diffusione Side-bi-Side in cui in una camera è stata inserita la soluzione di NaCl o di Diclofenac (alimentazione), e nell'altra camera (che sarà quella del permeato) acqua distillata. Il sistema sperimentale utilizzato è schematizzato in Figura 10. Il trasporto diffusivo è stato studiato monitorando in tempo reale la variazione di conducibilità nella soluzione di permeato grazie a una sonda a due elettrodi immersa nel liquido. L'informazione sulla variazione di conducibilità è tradotta in informazione sulla variazione di concentrazione del permeato, grazie a un'operazione di calibrazione della sonda. Per le concentrazioni impiegate nel nostro studio la relazione tra conducibilità e concentrazione è lineare.

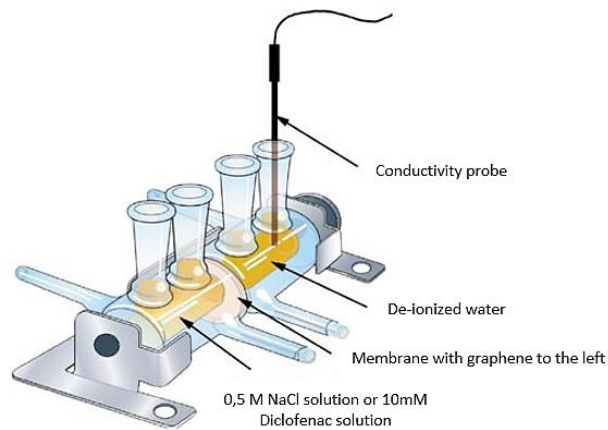


**Figura 10:** Apparato Side-bi-Side usato per effettuare le misure di trasporto

La Fig. 11 mostra l'andamento di ritenzione degli ioni di NaCl in funzione del tempo da parte delle membrane di PCTE (preso come riferimento) e di SLG/PCTE, DLG/PCTE, TLG/PCTE. La ritenzione dei soluti è stata calcolata utilizzando l'equazione (1).

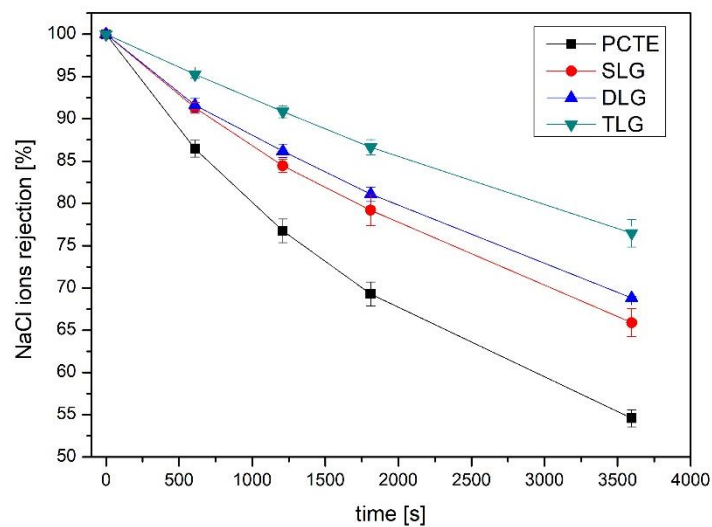


**Figura 11:** Ritenzione di NaCl in funzione del tempo

Il grafene monostrato trasferito su PCTE ha bloccato il 65,9% degli ioni di NaCl dopo 1h, mentre le membrane di grafene a doppio e triplo strato hanno bloccato rispettivamente il 68,8% e il 76,5% degli ioni. Questi risultati sono estremamente promettenti considerando che il NaCl è uno dei soluti più difficili da bloccare a causa delle sue dimensioni ridotte (0,716 nm), e che i processi utilizzati per la desalinizzazione richiedono di solito costi e pressioni di gran lunga superiori a quelli qui utilizzati.

La Figura 12 mostra invece l'andamento della ritenzione degli ioni di Diclofenac in funzione del tempo. Il Diclofenac è un farmaco la cui formula bruta è  $C_{14}H_{11}Cl_2NO_2$  e la cui molecola è significativamente più grande di quella del NaCl.

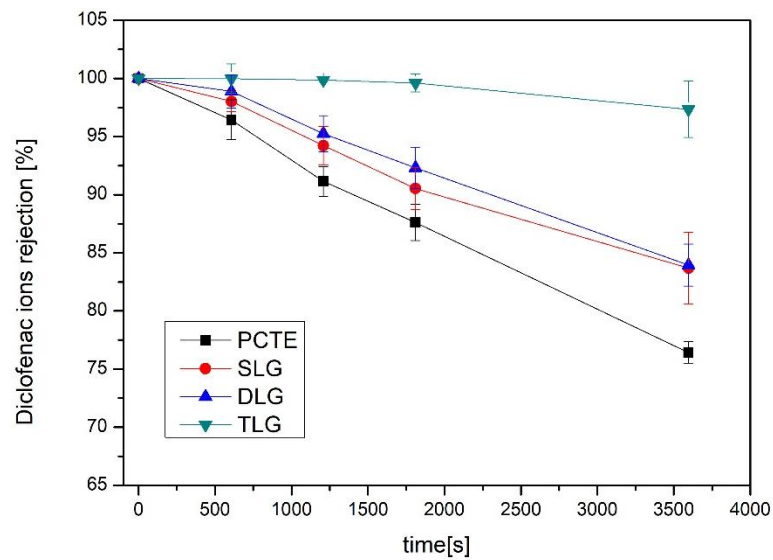


**Figura 12:** Ritenzione degli ioni di Diclofenac in funzione del tempo

Il singolo strato di grafene trasferito su PCTE ha bloccato l'83,7% del trasporto di ioni dopo 1 h, mentre le membrane grafene a doppio e triplo strato hanno bloccato rispettivamente l'84% e il 97,3% del trasporto di Diclofenac.

Dunque, il trasporto di molecole attraverso difetti intrinseci e difetti più grandi indotti dal processo di fabbricazione delle membrane è stato controllato con successo attraverso la tecnica di "sigillatura" dei difetti, sovrapponendo sul PCTE due o tre strati di grafene CVD monostrato. Ciò ha portato a una maggiore capacità di ritenzione e a un'ottimizzazione del meccanismo di esclusione dimensionale.

Grazie all'utilizzo di queste due molecole sonda (NaCl e Diclofenac) è stato quindi possibile comprendere meglio le proprietà di esclusione dimensionale di queste membrane, dimostrando la maggiore fattibilità della loro applicazione nella rimozione di molecole inquinanti dalle acque (quali ad esempio le molecole di farmaco) piuttosto che nelle applicazioni di desalinizzazione. In questa fase, infatti, queste membrane non sono ancora pronte per essere utilizzate efficacemente per dissalazione ad osmosi inversa. Infatti, anche se hanno dimostrato una buona capacità di ritenzione del NaCl con l'ulteriore vantaggio di utilizzare una tecnica molto meno costosa, le membrane a base grafene per la dissalazione ad osmosi inversa richiederebbero un ulteriore sforzo per la creazione di una generazione controllata di pori sub-nanometrici di dimensioni ben definite, per facilitare il passaggio dell'acqua respingendo al contempo quella degli ioni.

L'obiettivo qui raggiunto di realizzare membrane a base grafene con basse perdite e minimizzazione dei difetti è un passo importante verso un processo di produzione scalabile ed economico e verso la futura fabbricazione di setacci molecolari nanoporosi con un

meccanismo di esclusione dimensionale definito. Inoltre, le misure sui campioni ottenuti dal processo di trasferimento qui sviluppato godono di un'ottima ripetibilità, in quanto tutte le membrane dello stesso tipo hanno fornito risultati coerenti, sia nella caratterizzazione morfologica/strutturale che funzionale.

# INTRODUCTION

This research work was carried out in the laboratories of the “Materials and Processes for Micro & Nano Technologies Group” of the Department of Applied Science and Technology (DISAT) of the Polytechnic of Turin.

This work thesis is motivated by the need to investigate an alternative to the separation processes currently in use in wastewater treatment and desalination. In the last decades membrane separation processes have replaced conventional separation processes such as distillation, sedimentation, extraction, adsorption, crystallization etc. With sixty years of rapid development, membrane technology has found numerous applications in water and dairy purification, sea and brackish water desalination, food and beverage production, and much more. Membranes are widely accepted as the best existing technology for water treatment, but these processes are actually based on the use of membranes fabricated with traditional polymeric materials, that are found to have some drawbacks, such as low thermal, chemical and mechanical resistance, low flux, low separation factors, and above all considerable fouling phenomena that require frequent chemical washing operations that increase energy consumption and heavily reduce their life cycle. Therefore, despite the advancements, there is an evident need for further improvements in this field.

In the twenty-first century the world is facing the greatest challenges of all time in terms of potable water supplies in developing and developed countries, increasing demand for energy saving and environmental protection from hazardous waste. It is in this panorama that the present work is placed, whose main purpose is to analyse and demonstrate the potential of single layer graphene and its multi-layer declinations (BLG bilayer graphene, TLG trilayer graphene) as promising candidates for the fabrication of innovative improved separation membranes for water treatment.

Graphene, a single sheet of carbon atoms, has a key role in overcoming current shortcomings and developing high permeability and selectivity membranes, thanks to its atomic thickness, exceptional mechanical strength, and potential in size-selective mass transport thanks to nanometer-scale intrinsic pores in its lattice [16,17].

However, big advancements are required for exploiting the graphene to fabricate practical scalable membranes, including techniques for manufacturing nearly defect free graphene membranes with large areas. In this work, the mass transport is investigated through CVD graphene transferred to a microporous polycarbonate track etched membrane support (PCTE). Intrinsic defects, supposed to be of nanometric size and due to the growth of graphene [17], and extrinsic defects due to the transfer process, form leakage pathways that can be successfully used in selective molecular transport. This work is supposed to be a feasibility study towards the exploitation of these membranes, and to this end the following specific objectives were established:

1. Development of a new direct transfer procedure to transfer single layer graphene from Cu foil to PCTE substrate with the least possible damage.
2. Measurement of wettability of both the PCTE substrate and the graphene/PCTE membrane, in order to understand the relation between the contact angle and the quality of the graphene film.
3. Morphological, structural and functional characterization. Through field emission scanning electron microscopy, Raman spectroscopy and measurements of diffusive transport it was possible to show that CVD graphene on PCTE contained some

intrinsic porosity that allow for selective transport of molecules. Not knowing exactly the morphology and size of the intrinsic defects, it was not known a priori the dimensional exclusion provided by the pores. For this reason, it was decided to consider probe molecules (NaCl and Diclofenac drug molecule) to assess the capacity of dimensional exclusion provided by the membranes realized.

4. Optimization of the single layer membranes on PCTE by sealing the largest defects and the areas left uncovered by the single layer of graphene, by stacking two and three layers, in order to obtain greater selectivity and rejection ability.

The thesis work is divided in five chapters.

In chapter 1 an overview on working principles of membrane separation processes is provided, with a final insight on the limitations of the current commercial membranes.

In chapter 2 the great potential of graphene for membrane technologies will be discussed, and the state-of-the art of nano-porous single layer or few layer graphene membranes will be provided.

In chapter 3 we will report a description of the materials, equipment and experimental methodologies used for the manufacturing of these innovative membranes and for the morphological, structural, and functional characterization of the realized samples.

In chapter 4 the results obtained from the different types of characterizations will be presented and discussed.

Finally, in chapter 5 conclusions will be drawn, mentioning possible future developments of our research.

# 1. MEMBRANE SEPARATION PROCESSES

## 1.1 Generalities of membrane processes

In the last decades conventional separation processes applied on industrial scale such as distillation, extraction, adsorption, crystallization etc. have been joined by a relatively new technology based on membrane processes. Separation, concentration and purification processes are fundamental in our daily life and are involved in a lot of fields: dairy purification, food and beverage production, production of pure products in pharmaceutical industry, sea and brackish water desalination, removal of environmental pollutants, recovery of valuable substances like ores, etc. Membrane filtration technology became relevant after World War II because of the need to examine the bacteriological level in water supply systems. The first industrial applications of membrane technology date back to 1960s, although the first theoretical studies on membrane phenomena date back to the 18th century. This type of separation is based on the presence of a membrane, that can be defined as “*a material through which one type of substance can pass more easily than another, thereby presenting the basis of a separation process*” [1]. Essentially a membrane is a selective permeability barrier varying in material, structure and function, characterized by the prevalence of the surface over the thickness, i.e. a barrier that can be crossed by some substances present in the fluids while it is scarcely or not at all permeable to the others. The principle behind the different types of membrane processes is the following: a *feed solution* containing solutes and/or particles passes through the membrane, from which is obtained a residual current (or *retentate/concentrate*) richer in the retained components, and a stream of *permeate* purified of these components, as schematically shown in Fig.1.1.

The separation in membrane processes is based on a different transport velocity of the various chemical species. This transport speed depends on the driving forces acting on the system and on the mobility and concentration of the species.

Nowadays membrane separation processes are subject of countless research projects, mainly because they meet today's needs for energy savings and reduced environmental impact. In addition, they are often simpler and more effective than conventional separation processes, provide for high-performance separations and can be easily integrated into existing production processes.

### 1.1.1 Operation modes

Membrane filtration can be performed in two operation modes: **dead-end mode**, in which the feed flow moves perpendicularly to the membrane, and **cross-flow mode**, in which the feed flow moves parallel to the membrane surface, as shown in Fig.1.1.

Both in membrane processes and in conventional filtration the feed solution is forced against an obstacle (membrane or filter cloth). In the filtration, if the difference in applied pressure is kept constant, the flow decreases over time due to the formation of the so called “cake”, consisting of the material in suspension stopped by the filter cloth. A similar behaviour can be found in membrane processes as well. In this context, this effect is known as “concentration polarization” which indicates that, as a result of the rejection, the concentration of solutes in the proximity of the membrane is higher than the average concentration of the solution, with the formation of a concentrated boundary layer. The concentration polarization effect can also cause the so called “fouling” mechanism on the

membrane surface: the higher concentration within the boundary layer promotes solutes precipitation and the suspended particles begin to settle on the membrane surface.

The tangential filtration scheme results in much higher performance than the conventional (dead end) one, because the tangential velocity of the fluid removes from the surface of the membrane the particles that accumulate there due to the effect of rejection. Concentration polarization and fouling phenomena are reduced by the high turbulence that the tangential flow generate near the membrane, but on the other hand the practical implementation of a cross-flow filtration system is more complex.

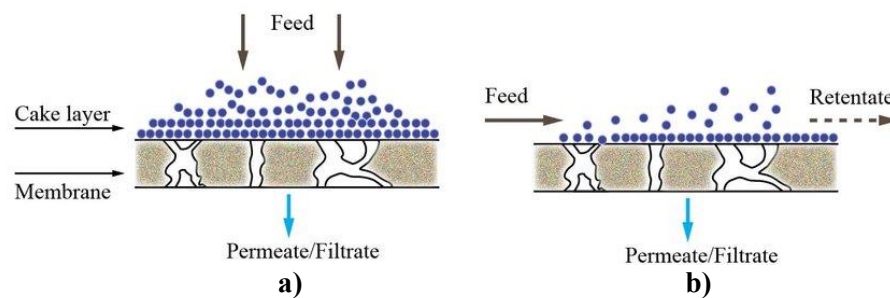


**Figure 1.1:** Operation modes of a membrane separation processes: a) dead-end and b) cross-flow

It is important to specify that the performance of a membrane equipment do not depend only on the membrane used, but also on the fluid dynamics of the solution, determined by the geometry of the channels in which the fluid moves, the physical properties of the fluid (density and viscosity) and the speed.

### 1.1.2 Classification of synthetic membranes

Leaving aside the natural membranes as being not of interest for this thesis work, there are various types of synthetic membranes that can be classified according to the parameters listed in the following and as outlined in Fig.1.2.

- Raw material: they can be divided into organic (polymer-based) and inorganic (ceramic/metallic);
- Surface charge: they can be electrically charged or neutral;
- Geometric shapes: synthetic membranes can be divided in flat, hollow fibers, and tubular;
- Structure: they can be classified as dense or porous. Dense membranes are characterized by a dense but very thin layer that is generally supported by a porous layer to increase the mechanical strength. They are mainly used in gas separation, pervaporation, reverse osmosis and in general in those processes in which the selectivity of the membrane is linked to the diffusion of molecules within the membrane itself. Porous membranes, on the other hand, are characterized by the presence of pores of a predetermined size and the selectivity of the process is related to dimensional properties;
- Cross-section structure: it is possible to distinguish between symmetrical (or isotropic) and asymmetrical (or anisotropic) membranes. Typically, the first ones have a sort of symmetry with respect to a plane orthogonal to the membrane thickness and are also characterized by the presence of pores. Asymmetrical membranes are made up of a denser layer resting on a supporting structure, such as

thin film composite (TFC) membranes, with a porous sublayer supporting a thin top layer from 0,1 to 0,5  $\mu\text{m}$  in thickness. These composite membranes consist of asymmetrical structures obtained by coupling two different materials. In this way it is possible to optimize the mechanical resistance of the support by coupling it with a specific selective dense layer.

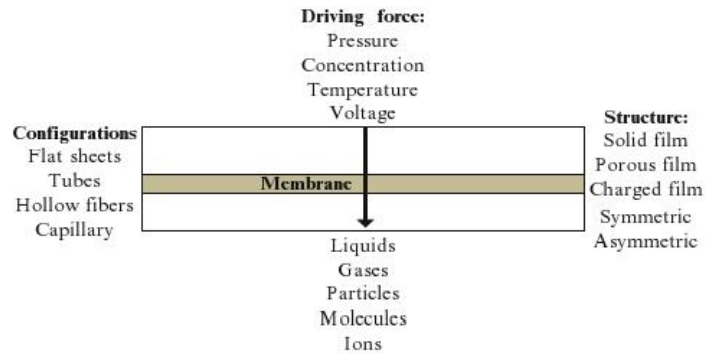


Figure 1.2: Fundamentals of membrane separation processes [2]

### 1.1.3 Membrane modules

Membrane modules are units in which there are large areas of membrane per unit volume. Inside the module the membrane can take different types of configurations, aimed at maximizing the surface/volume ratio and limiting the dirtiness. There are essentially four types of configurations: **plate&frame**, **spiral wound**, **tubular**, and **hollow fibers**.

- **Plate&frame**

In this configuration the membranes, the supports and the spacers are placed one above the other between two end plates, as shown in Fig.1.3. The spacers are in general metal meshes that also have the function of making tortuous the path of the fluid promoting the turbulence and consequently the transport of matter. These continuous changes of direction cause an increase in pressure losses.

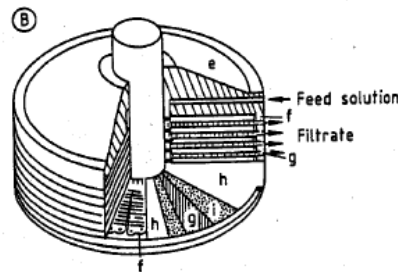


Figure 1.3: Plate and frame membrane module [1]

- **Spiral wound**

A variant of the plat and frame are the spiral wound, in which the membrane, the porous support and the spacer are wrapped around a central tube perforated and

inserted into an external tubular container, as shown in Fig.1.4. The feed flow is axial and the fluid by moving penetrates through the membrane and goes towards the central tube from which the permeate comes out. With this configuration, pressure drops are reduced and higher degrees of packing are obtained, resulting in larger specific surface areas.

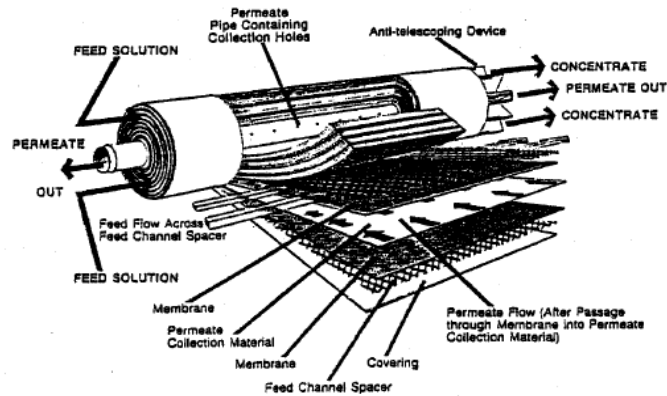


Figure 1.4: Spiral wound membrane modules [1]

- **Tubular module**

This is the simplest configuration. The membrane tubes are placed inside a porous stainless steel or glass-fibre reinforced plastic tube, as shown in Fig.1.5. The feed solution flows through the tube and the permeate is collected on the outer side of the porous steel/plastic tube that acts as a support. These modules are used in applications where the advantage of their high resistance to fouling exceeds the investment cost.

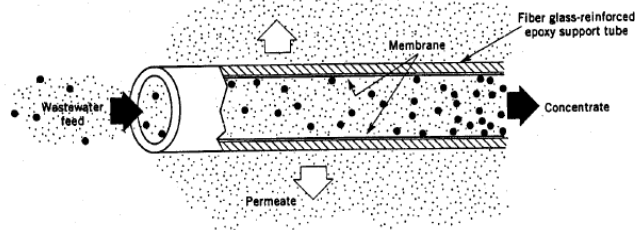


Figure 1.5: Tubular module membranes [1]

- **Hollow fibers**

In these modules, the hollow fibre membranes are arranged in a bundle of thousands of fibres closed at the ends or in such a way as to form a U, with the free ends fixed in an epoxy resin, all contained in a tube, as in Fig.1.6. The selective filter layer is placed on the outer layer of the fibres. There are two basic configurations. In the first, the feed enters from the side of the tube, the filtrate passes through the wall of the fibres and flows along the central hole of the fibres to the open part of them. In the second, the feed enters through the central hole of the fibres, which are then opened on both sides.

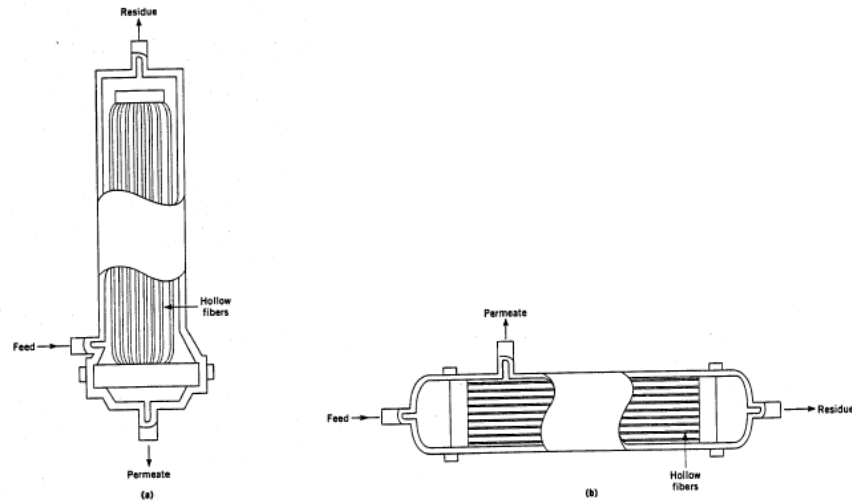


Figure 1.6: Spiral wound modules [1]

### 1.1.4 Process parameters

- The **flow** represents the amount of fluid that permeates through the membrane in the unit of time per unit area. Indicated with **J**, the flow has a unit of measure  $\left[\frac{m^3}{s \cdot m^2}\right]$ , or  $\left[\frac{m}{s}\right]$ . A flow of solvent is indicated as  $J_v$ , or  $J_w$  in case of water. The flow of a solute will be indicated as  $J_s$  and the units of measure adopted will be  $\left[\frac{kg}{s \cdot m^2}\right]$ . The flow **J** is strongly dependent on the process conditions and it influences the performance of a separation unit;
- The **conversion/recovery** is indicated with **S** and it is function of flowrates, in fact it is defined as the ratio between the permeate flowrate and the feed flowrate:

$$S = \frac{Q_P}{Q_F} \quad (1.1)$$

S can vary between 0 and 1, where the upper limit corresponds to the case of dead-end filtration. In cross-flow operation mode the typical conversion values fall in the range 0.2 - 0.5;

- The **retention** is indicated with **R** and it is function of concentrations. It is a measure of the amount of solute retained by the membrane and is defined as:

$$R = \left(\frac{C_F - C_P}{C_F}\right) \times 100 = \left(1 - \frac{C_P}{C_F}\right) \times 100 \quad (1.2)$$

where  $C_p$  and  $C_F$  are the concentration of the permeate and of the feed respectively. The retention is expressed as a percentage and therefore it can vary between 0 and 100%.

## 1.2 Transport phenomena in membranes

The existence of a driving force between the two sides of a membrane is what makes possible the flows of solvent and solute from one side to the other of the barrier. This force can be defined as the difference in potential at the sides of the membrane divided by the thickness of the membrane itself. That is, indicating with  $F$  the driving force, with  $\chi$  the potential and with  $z$  the axis normal to the plane of the membrane:

$$F = \frac{\chi}{z} \quad (1.3)$$

The majority of membrane processes originate from a difference in chemical potential which presents (in isothermal conditions) two contributions, the first one dealing with temperature and the second one with pressure gradients, as follows:

$$\Delta\mu_i = RT \ln a + v_i \Delta P \quad (1.4)$$

where the subscript  $i$  refers to the species, while  $a$  refers to the activity,  $v$  to the molar volume, and  $R$  to the universal constant of the gases.

Solvent and solute flows are related to the values of pressure and concentration on the two sides of the membrane. These concentrations differ from those existing in the bulk of the two solutions due to the increase in concentration in proximity of the membrane. The transport phenomena in membranes can be distinguished in two different flux of matter: one within the membrane and another within the portion of the fluid contiguous to the membrane.

If no external force were applied to a system subject to a potential difference, the flow would decrease in intensity until the gradient would be equal to zero, i.e. until the thermodynamic equilibrium would be reached. If an external force is applied, the flow through the membrane turns into constant flow, and the transport of material can be described by linear relationships that connect the flow to the driving force, as in the equation 1.5:

$$J_i = \sum_k L_{ik} F_k \quad (i,k=1,2,\dots,n) \quad (1.5)$$

where  $J_i$  is the flow involved,  $L_{ik}$  is a coefficient that depends on various properties of the components and the membrane, and  $F_k$  is the driving force.

In order to describe mathematically the transport phenomena, it is necessary to do a distinction between porous and dense membranes. For porous membranes the transport occurs thanks to the presence of pores, and permeation takes place through *convective* phenomena, while in dense membranes the permeation is due to *diffusive* phenomena.

### 1.2.1 Mathematical models

The mathematical models used to describe membrane processes can be distinguished into *phenomenological models* and *structural models*.

**Phenomenological models** are based on the principle that material flows are consistent with the laws of thermodynamics, but these models completely ignore the properties and structure of the membrane. The kinetic equations that come from these models contain parameters that must necessarily be measured empirically and that are not related to the

characteristics of the membranes. These models are based on the *thermodynamics of irreversible processes*. In general, the transport of chemical species through the membrane can often be described by linear relationships between driving forces and flows. However, these models based on the thermodynamics of irreversible processes include also the possibility of complex relationships between force and flows. Actually, a concentration gradient can lead not only to a flow of matter but also to the formation of a hydrostatic pressure difference and thus to a volume flow, as it happens for example in forward osmosis (FO). In the same way, a hydrostatic pressure gradient can imply a volume flow but also the formation of a concentration gradient, as it happens in reverse osmosis (RO).

**Structural models**, on the contrary, are based on a physical interpretation of the permeation mechanism occurring during the separation process. The parameters contained in the equations can be predicted according to the assumed physical mechanism and are related to the characteristics of the membrane, even if they must obviously be measured experimentally. In most cases these models assume a non-porous membrane.

The best known structural model is the **solubility-diffusion model**, that is based on the hypothesis that solvent and solute dissolve inside the membrane and move through it with diffusive flows. In the solution-diffusion mechanism the particles dissolve in the active layer of the membranes and then diffuse towards the permeate side. This mechanism is a molecular diffusion and as such is relatively slow. It is typical of membranes which have a thick active layer that increases the path that the particles must take to diffuse within the membrane.

The descriptive equations are in the form of Lonsdale-Merten linear model, where  $J_v$  is the volume flow connected to the pressure difference, and  $J_s$  is the solute diffusive flow connected to the osmotic pressure difference:

$$J_v = K_1 (\Delta P - \Delta\pi) \quad (1.6)$$

$$J_s = K_2 \Delta C \quad (1.7)$$

where  $\Delta P$  is the transmembrane pressure,  $\Delta\pi$  is the osmotic pressure and  $\Delta C$  is the solute concentration difference across the membrane.

The solubility-diffusion model is very suitable to describe the permeation in the case of dense membranes without macroscopic porosity, as the one occurring in Reverse Osmosis. If the membrane would also show macroscopic porosity, then there would also be a convective flow term in addition to the diffusive flow one and the transport mechanism would be described by the **solubility-diffusion-imperfection model**:

$$J_v = K_1 (\Delta P - \Delta\pi) + K_3 \Delta P \quad (1.8)$$

$$J_s = K_2 \Delta C + K_3 C \Delta P \quad (1.9)$$

where the second term in 1.8 and 1.9 represents the contribution of the convective flux.

Both phenomenological and structural models can be used to describe transport of solvent and solute in a membrane, although it is more convenient to use the solubility-diffusion model because the proportionality coefficient  $K_1$ ,  $K_2$  and  $K_3$  come from a physical interpretation and could be hypothesized from tests different from permeation tests.

Equations (1.8) and (1.9) are suitable to describe matter transport either in Microfiltration (MF) and Ultrafiltration (UF) or in Reverse Osmosis. In the former, the membranes are highly porous so the convective contribute is predominant, while in the latter it can be neglected in favour of the diffusive term. In MF and UF the volume flow will be simply:

$$J_v = K_3 \Delta P = \frac{\Delta P}{R_m} \quad (1.10)$$

where  $R_m$  is the resistance of the membrane to the flow.

Vice versa, in RO membranes, no defects or few defects are present, so the volume flow will be better described by 1.6 and 1.7.

There are other models that can describe the permeation mechanism in Reverse Osmosis phenomena, for example the **Sourirajan model of preferential adsorption-capillary flow**. Solvent and solute flows are once again described by equations 1.6 and 1.7 of solubility-diffusion model, although in this case the membrane is not completely dense but has pores of molecular size. Water is adsorbed onto the external face of the membrane and inside these pores, and act as a barrier against the ion passage.

To summarize, it can be stated that the flow through a membrane depends on a variety of factors, including temperature, pressure, concentration of species to be separated, thickness and material of the membrane. For example, the temperature influences the kinetic energy of the particles, the collision frequency with the membrane and so the probability that particles can cross it. For this reason, it can be concluded that temperature influences the permeability. Pressure and concentration are two of the driving forces that act on the system, while the thickness affects the path that the particles must cover and so the permeability. Finally, the material of which the membrane is made influences the affinity between the membrane and the particles constituting the fluid, reflecting on the quantity of permeated particles.

### 1.3 Polarization of concentration

The separation efficiency of a membrane depends not only on the characteristics of the membrane, but also on the fluid dynamics that determines the speed of material transport in the fluid phase adjacent to the membrane.

The solutes are transported towards the membrane, thanks to the convective motion of the solvent. As a result of the rejection capacity of the membrane, the concentration  $C_w$  near the membrane will be higher than the concentration  $C_b$  in the bulk of the solution. This leads to a diffusive flow in the opposite direction of convective flow, as shown in Fig. 1.7:

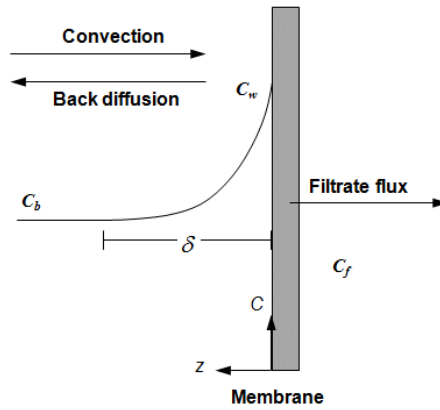


**Fig.1.7:** Schematic representation of concentration polarization

Diffusive transport of the solute, which is represented with a transport coefficient  $k$ , can be described by:

$$J_s = K \cdot (C_w - C_b) \quad (1.11)$$

According to the film model (for a detailed discussion see [3]), the resistance to transport is localized in a film of thickness  $\delta$  adjacent to the wall, in which the transport follows the Fick's law, while outside of it assumes uniform concentration.

The transport coefficient  $K$  can be written as:

$$K = \frac{D}{\delta} \quad (1.12)$$

With reference to Fig. 1.7, the material balance for the system delimited by the membrane and by the plane at distance  $z$  from it is represented by the equation:

$$D \frac{dC}{dz} = J_v (C_f - C_b) \quad (1.13)$$

where  $D$  is the diffusion coefficient of the solute and  $C_f$  is its concentration in the permeate or filtrate.

An integration of (1.13) between  $C_b$  and  $C_w$  leads to the relation between the concentrations  $C_b$ ,  $C_w$  and  $C_f$ :

$$\ln \frac{C_w - C_f}{C_b - C_f} = \frac{J_v}{K} \quad (1.14)$$

The assumption of a linear relationship between flow and difference in pressure made earlier is not coherent with reality due to the polarization of the concentration. This is evident in case of Reverse Osmosis that follows the equation 1.6: an increase in  $P$  produces an increase in flow but this increase is less than it would be without the effect of concentration polarization, because the increase in  $P$  leads also to a concentration gradient and thus to an additional pressure (the osmotic pressure) to be overcome.

The polarization of concentration has some important consequences that can severely affect the performance of the process:

- **Decrease in flow rate** due to the fact that polarization of concentration represents an additional resistance to flux;
- **Reduction in retention** due to a concentration on the membrane higher than that in the bulk. This decrease in rejection ability occurs when microsolute are involved, like inorganic salts;
- **Increase in retention** if macrosolute (e.g. proteins or starches) are involved, they accumulate on surface membrane causing the formation of a secondary membrane called “dynamic membrane” or “gel layer”. This additional barrier helps the rejection of species with lower molecular weight, as occurs in UF.

## 1.4 Classification of membrane processes

Membrane processes are kinetic and not equilibrium processes that can be classified on the basis of the driving force. This last can be a difference in pressure (as it is in most cases), a difference in concentration, in electrical potential, or in temperature. The most common classification of membrane processes is reported in Table 1.1.

**Table 1.1:** classification of membrane processes

DRIVING FORCE	MEMBRANE PROCESS
Pressure gradient	<ul style="list-style-type: none"> <li>• Reverse Osmosis (RO)</li> <li>• Nanofiltration (NF)</li> <li>• Ultrafiltration (UF)</li> <li>• Microfiltration (MF)</li> <li>• Gas separation (GS)</li> <li>• Pervaporation (PV)</li> </ul>
Concentration gradient (or activity $a$ )	<ul style="list-style-type: none"> <li>• Dialysis</li> <li>• Forward Osmosis (FO)</li> </ul>
Temperature gradient	<ul style="list-style-type: none"> <li>• Membrane distillation (MD)</li> </ul>
Electrical potential gradient	<ul style="list-style-type: none"> <li>• Electrodialysis (ED)</li> </ul>

In general, a hydrostatic pressure gradient implies a volume flow  $J_V$ , a concentration gradient implies a flow of molecules  $J_n$ , a temperature gradient implies a heat flow  $J_Q$ , and a potential gradient leads to an electric current  $J_e$ . However, driving forces and flows can also be linked together by complex relationships as said before.

The most significant processes are those involving significant material flows. Among these, the most common and widespread are those based on a difference in pressure. In particular MF, UF, NF, and RO are those involved in water purification, reason why they will be analyzed in detail in the following paragraph.

## 1.5 Pressure-driven processes

Pressure-driven processes generally have the objective of concentrating or purifying a solution. The size of the particles involved determines the choice of the type of membrane. In fact, pressure-driven processes are categorized according to the size of the retained particles and the working pressures used. Table 1.2 shows the applications, pore sizes of membranes and the  $\Delta P$  typical of each process.

**Table 1.2** – Dimensions of retained particles and typical pressures in pressure-driven processes.

Pore sizes	Types of materials removed	Filter type	Operating pressure
10 <sup>3</sup> -50 nm	-Suspended particles -Large colloids -Red blood cells -Bacteria -Large viruses	Microfilter	5-500 KPa (<30 psi)
50-1 nm	-Viruses -Proteins -Starches -Organics -Dye -Fat	Ultrafilter	<1 MPa (20-100 psi)
1-0,1 nm	-Glucose -Multivalent salts -Pesticides -Herbicides	Nanofilter	<4MPa (50-300 psi)
< 0,1 nm	-Water -Monovalent salts	Reverse Osmosis	>5-10 MPa (225-1000 psi)

### 1.5.1 Microfiltration

Microfiltration membranes are used from 1960s to separate impurities in food and pharmaceutical industry, in the former for the clarification of fruit juices or for the sterilization of wine and beer, in the latter for sterile filtration (removal of microorganisms). From 1980s the use of microfiltration in water treatment became widely diffusion as well, thanks to its low costs and mainly for the removal of phatogenic bacteria. The separation mechanism in these porous membranes is essentially "sieve" type: the particles are separated in accordance with their size, so the characterizing element of the membrane is the diameter of the pores. The typical operating pressure is of the bar order (<2 bars), lower than in the others filtration processes. Initially these membranes were made of nitro-cellulose, while over the years the use of more resistant materials became predominant, such as PP (polypropylene), PA (polyamide) and PSU (polysulfone). In microfiltration convective (and not diffusive) flows dominate the mass transport. The amount of the passage of water and therefore of the solutes depends on the characteristics of the membrane and on the pressure gradient on both sides.

Since MF membranes are porous, if the pores are cylindrical, parallel, and have a length more or less equal to the thickness of the membrane, the equation to describe the fluid transport is:

$$J_v = \frac{\varepsilon r^2}{8\eta\tau} \cdot \frac{\Delta P}{\Delta z} \quad (1.15)$$

that derives from the (1.10), in which  $K_3$  is here the term that multiplies  $\Delta P$ . In this term  $\varepsilon$  is the membrane's degree of porosity,  $r$  is the radius of the pores,  $\eta$  is the dynamic viscosity of the fluid,  $\tau$  the tortuosity of the pores (that are not always straight) and  $\Delta z$  the membrane thickness. This law is known as Hagen-Poiseuille's law for convective motion through the channels and it is valid only when the flow regime is laminar.

## 1.5.2 Ultrafiltration

Ultrafiltration membranes were introduced to the market in 1960s and have always been used in particular in two industrial sectors: in the Automotive, in order to separate electrophoretic paints from wastewater, and in dairy industry, to recover proteins and lactose from whey. However, they are also used in Pharmaceutical for sterile filtrations of solutions and in water industry as a pretreatment before Nanofiltration or Reverse Osmosis. In this process the particles are separated according to their size, so the separation principle is still a mechanical sieving. However the pores of these membranes are smaller (in the order of 1-50nm) so they allow the passage of microsolute with molecular weight  $< 300 \left[ \frac{g}{mol} \right]$ : this type of membranes are in fact used industrially to separate macromolecules from molecules with low molecular weight, for example for the concentration of dietary milk. This is the reason why in UF the characteristic parameter of the membrane is not the pore diameters but the Cut-off, i.e. the molecular weight over which complete rejection occurs. The operating pressure varies from 1 to 10 bar.

The first UF membranes commercialized were in cellulose acetate (CA), that was poorly resistant to pH changes, so over time it has been replaced by PAN (polyacrylonitrile), PA (polyamide), PSU (polysulfone), PVC (polyvinylchloride) and PVDF (polyvinylidene fluoride). These materials are resistant to a big range of pH and temperatures, and to many solvents too, so they are ideal in pharmaceutical sector where the solutions are not always water-based.

The flow through UF membranes is still convective and flux is directly proportional to applied pressure difference as in the equation 1.10, in which  $R_m$  represents the membrane's resistance in terms of pore dimension, thickness, etc.

In ultrafiltration the effect of concentration polarization is more pronounced: as the difference in applied pressure increases, the flow rapidly increases until it reaches an asymptotic value independent of pressure but dependent only on concentration and hydrodynamic conditions, as shown in Fig.1.8. This behaviour cannot be explained only by the osmotic effect, in fact for solutions of macromolecules the osmotic pressure is modest.

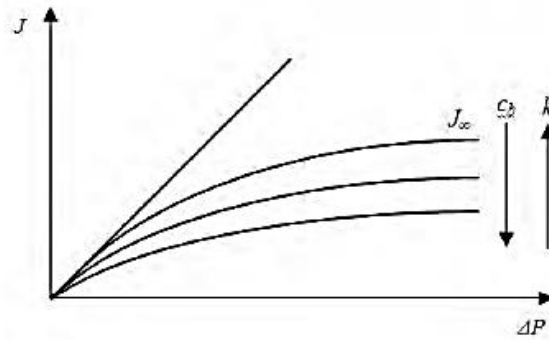


**Figure 1.8:** Flow trend as a function of concentration and material transport coefficient  $k$

The most accredited model is the gel model. As already mentioned with regard to the model of the film, the solute is transported towards the membrane by the convective motion of the solution. However, a concentration gradient  $C_w$  is generated due to membrane retention properties and therefore a diffusive transport is generated, bringing the solute back to the heart of the solution.

$C_w$  cannot increase indefinitely. For each solution there is a concentration limit value (gel concentration,  $C_g$ ) beyond which it is not possible to go.

When  $C_w$  has reached the  $C_g$  value, the driving force for diffusive back transport can no longer increase. An increase in pressure beyond  $C_g$  value tends to bring to the membrane a quantity of solute higher than that which can spread backwards, and the solutes are then deposited on the membrane forming a layer of gel. It acts as a "dynamic membrane" whose resistance is added to the hydraulic resistance of the membrane. The (1.10) becomes then:

$$J_v = \frac{\Delta P}{R_m + R_g} \quad (1.16)$$

### 1.5.3 Nanofiltration (NF)

Despite the term nanofiltration being introduced only in the late 1980s, NF membranes exist from 1960s but initially they were categorized as "poor quality" RO membranes and for this reason they were called "loose" RO or "tight" UF membranes. These NF membranes present a selectivity that lies between those of UF and RO, so they are used when the UF is found to be less selective but at the same time it is not necessary to provide the complete barrier typical of RO. Moreover, these NF membranes allow water fluxes higher than those enabled with RO and meantime lower pressure. This makes it possible lower operating costs and higher energy saving in an industrial context.

NF membranes are able to highly reject polyvalent anions and neutral solutes with molecular weight greater than 200, while monovalent salts (e.g. NaCl, KCl) are poorly retained. The dependence of rejection on valence of ions could be explained by the presence of fixed charges (generally negative) on most of these membranes, that originate phenomena of electrostatic partition.

These membranes are mainly used in dairy industry for recovery of washing water containing 4-6% of NaCl, and for concentration of whey; in textile industry for decolouration; in water industry for seawater softening, for reduction in hardness in potable water, and for decontamination of surface or subsoil water polluted by organic solids.

Rejection of NaCl results too low (30-40%) for employment in brackish water desalination.

The first NF membranes were made in CA but since they could not be applied with organic solvents due to their poor chemical stability, CA has been replaced with polymers such as aromatic PA, PSU, PAN, PES (polyethersulfone), PVA (polyvinylalcohol), and PPO (polyphenyloxide).

Having intermediate properties between porous and non-porous membranes, nanofiltration membranes imply separation mechanisms that involves both mechanical sieving and diffusion transport.

Rejection of neutral species is essentially related to the size of the compounds, such as in the case of sugars (glucose, sucrose and lactose) with values of  $R=90-98\%$ . The mechanism of salt rejection, however, is mainly due to electrostatic interactions between ions and the membrane (“Donnan effect”). These behaviors make the description of the NF particularly complex.

### 1.5.4 Reverse Osmosis (RO)

Finally, in Reverse Osmosis, the species retained are simple molecules and ions. The membranes employed in this case are no longer considered as porous media but asymmetric media with a porous sublayer and a thin, dense selective skin layer.

More than the size of the particles, separation is determined by the chemical properties of the solution’s components and of the membrane. In general, charged particles are highly retained, while neutral molecules permeate easily even if their molecular weight is relatively high. The working pressure must exceed the osmotic pressure (tens of bars) due to the low molecular weight of the retained solutes, even at relatively low solute concentration.

RO is the most suitable pressure-driven membrane process for obtaining drinking water from seawater or brackish water, which is why this has always been its largest field of application. Seawater has an osmotic pressure of 2.5-3 MPa. To obtain a good quality of the filtrate it is necessary to operate with an overpressure of at least 1 MPa.

The osmotic pressure  $\pi$  of a solution is the pressure at which the water contained in the solution is in equilibrium with the pure water at the atmospheric pressure and at the same temperature of the solution. This means that when at  $P=\pi$  the solution and the pure water are separated by an ideal semipermeable membrane, there is no flow at all. It is evident, as shown in Fig. 1.9, that for  $P<\pi$  there will be a flow of water towards the solution (forward osmosis FO) while for  $P>\pi$  there will be a flow from the solution towards the pure water (reverse osmosis RO), i.e. the osmotic pressure is the minimum value of pressure to get pure water from a solution.

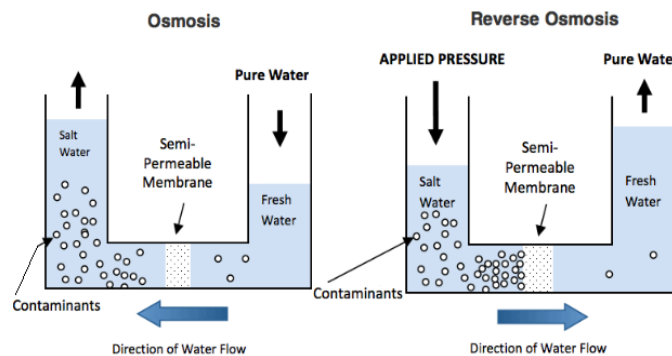


Figure 1.9: Osmosis and Reverse Osmosis

The osmotic pressure is defined as following:

$$\pi = \frac{RT}{V_w} \cdot \ln \frac{1}{a_w} \quad (1.17)$$

where  $V_w$  is the molar volume of the water,  $R$  the constant of the perfect gases ( $R= 8.314 \left[ \frac{J}{mol \cdot K} \right]$ ),  $T$  the absolute temperature in K and  $a_w$  the water activity in the solution.

$a_w$  is defined as the ratio between the vapour pressure of the water in the solution ( $P_w$ ) and that of the pure water ( $P^*$ ), at the same temperature:

$$P_w = P^* \cdot a_w \quad (1.18)$$

A form completely equivalent to (1.17) is therefore the following:

$$\pi = \frac{RT}{V_w} \cdot \ln \frac{P^*}{P_w} \quad (1.19)$$

Water activity is related to its molar fraction ( $x_w$ ) by a coefficient of activity ( $\gamma_w$ ) that measures the deviation of the solution's behaviour from ideality:

$$a_w = \gamma_w \cdot x_w \quad (1.20)$$

In fact, for fairly diluted solutions the activity coefficient tends to the value 1; an ideal solution can be defined as the solution for which Raoult's law applies:

$$P_w = P^* \cdot x_w \quad (1.21)$$

For diluted and ideal solutions (1.19) is reduced to the law of Van't Hoff:

$$\pi = C_s RT \quad (1.22)$$

where  $C_s$  is the molar concentration of the solute.

Van't Hoff equation is valid if the solution is ideal ( $\gamma_w = 1$ ), but also if the solution is diluted, i.e. the concentration of the solute is negligible compared to the concentration of the solvent ( $C_s \ll C_w$ ). Any solution tends to the ideal behaviour at low concentration values.

Fig. 1.10 shows the osmotic pressure of NaCl solution as a function of the concentration.

The straight line represents the Van't Hoff's law: it can be observed that it is valid up to concentration values higher than 1 mol/L.

In general, the linear dependence between osmotic pressure and concentration is valid across the whole range of RO application, i.e. up to 100 bar.

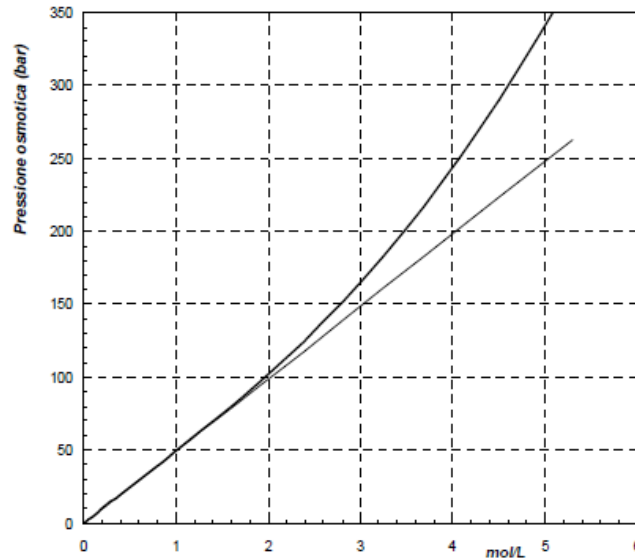


**Figure 1.10:** Osmotic pressure of NaCl solutions at 25°C.

To conclude, it should be remembered that transport through RO membranes occurs by diffusion phenomena, so permeation mechanisms are well described with equations 1.6 and 1.7 of the solubility-diffusion model.

## 1.6 Limits of commercial membranes

At present, the world is facing great challenges, one of which is the supply of water resources in developing and developed countries. Membranes are currently considered the best technology for water and wastewater treatment. However, despite the progress that has been made, it is necessary to overcome some technical limitations to make this technology competitive and reliable in the long term.

The main drawbacks of conventional polymeric membranes are:

- Membrane processes rarely produce two pure products, i.e. one stream is always contaminated with a minor amount of the second component;
- A not completely precise manufacturing process gives membranes with wide pore size distribution, leading to poor separation performance;
- Equipment costs are usually high;
- Phenomena of concentration polarization, above described;
- Tendency to fouling, that is the deposition of a layer of impurities on the membrane surface or within its pores. This leads to a decrease in permeate flux and to an increase in pressure drops across the system, with a subsequent increase in energy consumption. It affects the salt rejection of the membrane too. It has been demonstrated that subparticles of 5  $\mu\text{m}$  contribute more to fouling than bigger particles, which tend to go back in the bulk solution instead of settling on the membrane surface;
- Low resistance to biological attack: in addition to inorganic fouling (caused by the deposition of iron, calcium, sulfate, etc.), and organic fouling (caused by proteins, polysaccharides, etc.) there is the so called biofouling, caused by the adhesion of

microorganisms to the membrane surface. Biological organisms present in biofilm are bacteria, fungi, and algae. Of these, the most critical is the group of bacteria, due to the fact that they easily adapt to any type of environment, and also have the ability to multiply very quickly. In addition to an increased transmembrane pressure and a decreased permeation rate, biofouling leads also to a chemical degradation of the membrane material. It has been demonstrated that TFC membranes are generally quite resistant to biofouling;

- Feed pre-treatment, cleaning and regeneration operations are necessary, resulting in higher final costs;
- Low flux, due to slow water permeability;
- High energy consumption: there is a need for 3 KWh to produce 1 m<sup>3</sup> of drinkable water from pre-filtered seawater. One of the greatest challenges is to reduce the energy needed in separation processes. About 70% of the operating costs of RO desalination is the energy cost. Therefore, there is a need to develop energy saving techniques, because energy is important as much as the water and it is becoming scarce;
- Low separation factors: the main drawback to be overcome is that nowadays high permeability is incompatible with high selectivity and vice versa;
- Low resistance to chlorine;
- Poor durability: the fouling itself may shorten membrane life, together with the use of materials scarcely resistant at variations of pH, temperature or other parameters. Even if a big variety of membranes are available for water treatment, the membranes able to operate in aggressive conditions (such as in contact with organic compounds, oils, solvents) are very few. In fact, with these harmful chemical industry solutions, a lot of polymer-based membranes (that are the most used nowadays) can dissolve, swell, and weaken, resulting in limited lifetime and selectivity;
- Most membranes cannot operate at temperatures well above room temperature. This is due to their constituent materials: in fact, many polymers deteriorate and lose their physical integrity at  $T \geq 100$  °C. For this reason, current membrane processes are often incompatible with chemical industry separations;
- It has been proven that the high flow rates used in cross-flow operation mode damage shear sensitive materials;
- Applications are limited due to the compressibility of membranes under the high pressures that some operations (for example RO) require;
- Another phenomenon occurring in membrane processes is the so called “compaction”. It happens when a polymeric membrane is put under pressure, resulting in a change of structure due to a re-organization of the polymer. As consequence, the mechanical resistance increases but the total amount of porosity decreases. This results in a significant membrane permeability loss;
- Membrane processes are often not suitable to treat massive flows because the scale up is not yet very successful. Membrane processes typically consist of a number of membrane modules in parallel, that may be replicated many times to obtain larger feed rates;
- Usually membrane processes have only one or sometimes two or three stages. This implies that the membranes must have a really high selectivity. Thus, the compromise is often high selectivity/few stages for membrane processes against low selectivity/many stages for other processes such as distillation;
- In addition, polymeric membranes have an amorphous surface that does not allow a precise opening of the pores. Additionally, this amorphous nature of the surface has

prevented a full understanding of the mechanisms that govern the transport of matter in these membranes.

As analysed in the following chapters, this is the context in which are placed nanomaterials, that have a great potential in membrane development and improvements. In particular graphene-based membranes present innovative properties compared to conventional ones and, although still in their infancy, promise to exceed the limits above mentioned.

## 2. NANO-STRUCTURED MEMBRANES

In order to reduce the cost and energy demands associated with water treatment, innovative, selective and inexpensive antifouling materials are required to improve membrane performance. Nanomaterials with well-defined nanostructures have great potential in membrane technologies. Among these, carbon-based nanomaterials such as single layer graphene, graphene oxide (GO), and carbon nanotubes (CNTs) have attracted great interest. An ideal membrane should provide:

- High permeate flux and selectivity;
- Improved stability (chemical, thermal, mechanical);
- Resistance to fouling;
- Controlled pore sizes;
- Low thickness.

Graphene seems to be able to go beyond the filtration mechanism of current polymeric membranes. In order to understand the reason for this, a brief discussion on this material will follow.

### 2.1 Graphene: two-dimensional carbon

Carbon (C) exists in many forms due to its ability to establish different type of chemical bonds with other C atoms (carbon allotropic forms) and elements. This allows the existence of many organic compounds. The most common allotropic form of carbon is graphite, which consists of several layers of  $sp^2$  hybridized carbon atoms arranged one above the other to form a three-dimensional structure. Within each single plane, the C atoms are held together by strong covalent bonds, while the various planes are held together by weak Van der Waals forces. This is the reason why the mechanical properties of graphite in the transversal plane are significantly lower than those in the longitudinal plane.

Graphene is another allotrope of carbon consisting of a single layer of C atoms. It is defined as a 2D material because the thickness of a single graphene layer can be approximately considered and the size of an atom (3.5 Å in thickness) while it is characterized by an extended structure (ideally infinitely periodic) along the in plane directions. Graphene is basically a single layer of graphite, i.e. a single layer of carbon atoms organized into a two-dimensional hexagonal lattice. "Graphene" is a word introduced by the chemist Hanns-Peter Boehm in 1986 and it is a combination of "graphite", in relation to carbon in its ordered crystalline form, and the suffix -ene, in relation to the polycyclic aromatic hydrocarbons forming its typical honeycomb structure, as shown in Fig. 2.1.

For decades the existence of 2D crystals was considered impossible by theoretical physicists because they thought that these structures would be thermodynamically unstable, in relation to the formation of curved structures such as fullerenes and nanotubes, so graphene was studied only as an "academic" material. In 2004, Kostya Novosëlov and Andre Gejm at University of Manchester succeeded in isolating a layer of graphene using the scotch-tape technique. This is a micromechanical exfoliation which consists of pulling graphene layers from graphite and transferring them on silicon wafers through a piece of adhesive tape. They won the Nobel Prize for Physics in 2010 "for groundbreaking experiments regarding the two-dimensional material graphene [4]." Since then, this innovative material has received worldwide attention thanks to its exceptional properties, not only from an experimental point of view, but also from a theoretical one.

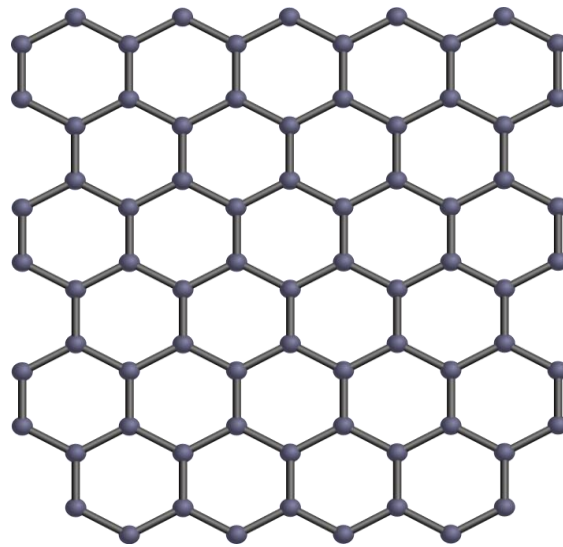


**Figure 2.1:** Graphene honeycomb structure

Moreover, graphene can be considered as the basic structure for the construction of other C allotropes known as fullerene (0D), carbon nanotubes (1D), graphite (3D), as shown in Fig. 2.2.

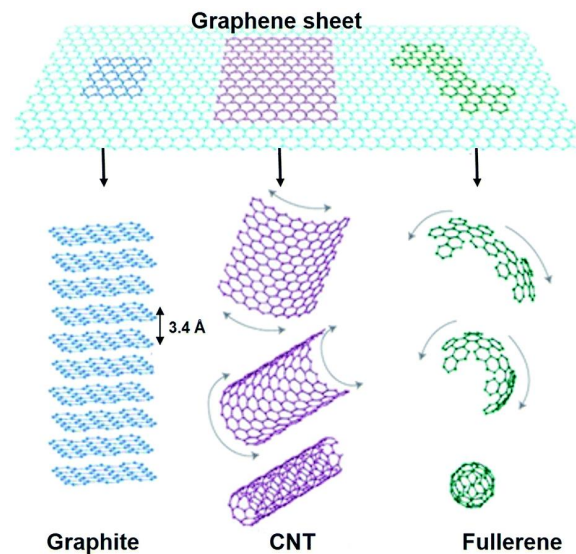


**Figure 2.2:** Allotropes of carbon

In order to describe the chemical bonds that form the crystalline structure of graphene, it is necessary to introduce the concept of hybridization of atomic orbitals. Each carbon atom has 6 electrons in the electronic configuration  $1s^2 2s^2 2p^2$ . The two electrons of level 1s are tightly bound to the nucleus and shield part of the nuclear charge, so these “core” electrons do not contribute to the bonds. Four other electrons occupy the orbitals 2s,  $2p_x$ ,  $2p_y$ ,  $2p_z$  and are available for the formation of covalent bonds. The  $sp^2$  hybridization, shown in Fig. 2.3, leads to the combination of the  $p_x$  and  $p_y$  orbitals with a 2s orbital and allows the formation of three strong covalent  $\sigma$  bonds, which lead to an hexagonal structure in the plane in which each carbon atom is bound to three others, as occurs in graphite, graphene, nanotubes, and

fullerene. The remaining electron occupies the orbital  $2p_z$ , oriented perpendicularly to the reticular plane. These orbitals  $p_z$ , one for each carbon atom, interact with each other forming a weak  $\pi$  bond, i.e. a band of mobile electrons responsible for the conductive properties of graphene. An ideal single layer graphene sheet is impermeable to molecules as small as He, thanks to the fact that the electron density of  $\pi$ -orbitals forms a delocalized cloud that blocks any species within the aromatic rings [5].

In graphite, as well as in graphene in its multi-layered declinations (BLG bilayer graphene, TLG trilayer graphene, FLG few layer graphene) the main interaction is the one between the atoms of the same crystalline plane while the interaction among the planes is relatively weak.

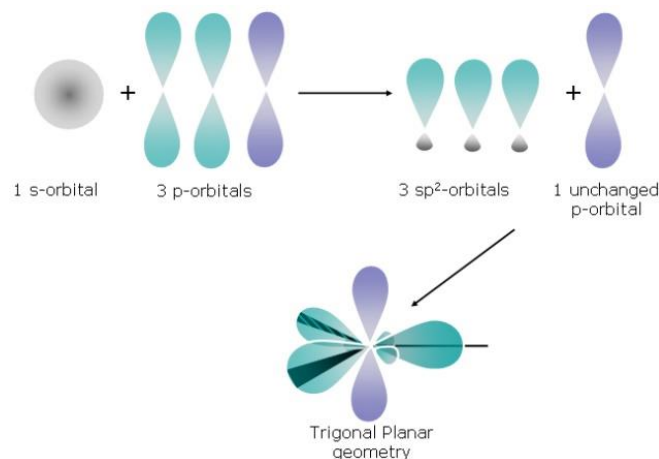


**Figure 2.3:**  $sp^2$  hybridization of carbon atomic orbitals

### 2.1.1 Crystal structure of graphene

In the hexagonal honeycomb structure each atom is bound to three adjacent atoms, placed at  $120^\circ$  from each other, with an interatomic distance  $d = 1.42 \text{ \AA}$  and a centre-centre distance of  $2.46 \text{ \AA}$ . In terms of crystalline symmetry the hexagonal structure is described by a triangular Bravais lattice with a diatomic base (Fig. 2.4). The two carbon atoms of the base are represented in dark grey and light grey. Note how the graphene lattice can also be described by two triangular sublattices A and B, corresponding to the two sets of carbon atoms shown in dark grey and light grey, respectively. Each carbon atom has as nearby atoms at distance  $R$  (vector in the drawing) 3 carbon atoms of the other sublattice.

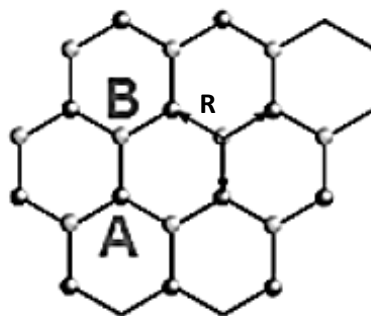


**Figure 2.4:** Graphene crystal lattice [6]

### 2.1.2 Graphene properties

An overview of the most important graphene properties will follow, although up to now a complete physical and chemical characterisation of the material has not yet been achieved. From a chemical-physical point of view all the exceptional properties of graphene derive from the bond between the  $sp^2$  hybridized carbon atoms arranged in space according to the typical hexagonal structure.

- **Electronic properties:** One of the most important characteristics of graphene is that it is a zero-gap semiconductor with a very high electrical conductivity. In graphene each atom is bound to three others in the same plane x-y, leaving a free electron in the third dimension -z. These mobile electrons, called " $\pi$  electrons", are delocalized above and below each sheet of graphene, and are responsible for its high conductivity.
- **Mechanical properties:** graphene is characterized by high mechanical performances which originate from the strength and stability of the  $\sigma$  bonds between  $sp^2$  orbitals that characterize the bond between the carbon atoms in the plane. Graphene is supposed to be the strongest material ever discovered in nature, about 200 times stronger than steel. Surprisingly, it is both rigid and elastic (like rubber), therefore it can be stretched by 20-25% of its original length without breaking. The breaking strength  $\sigma$  is of 130 GPa and the modulus of elasticity E is of about 1 TPa. However, when it reaches to fracture, it behaves like a brittle material, with a fracture toughness  $K_{IC}$  of  $4\text{MPa}\cdot\sqrt{m}$ , so quite similar to any ceramic material. The incredible resistance of graphene is accompanied by an extreme "lightness" linked both to the presence of the C atoms that have a low atomic weight and to the monoatomic plan thickness. However, the elastic properties of graphene can be changed by varying temperature, sample size or density of the defects. In fact, these values vary in a big range because there is always a difficulty in determining the precise geometry of graphene samples and because the intrinsic defects are never completely absent in the material. It is to be specified too that the breaking strength and the elastic modulus decrease (by one order of magnitude) in presence of intrinsic defects resulting from the synthesis method or other defects. Despite this, graphene is sufficiently strong for most applications.
- **Thermal properties:** Graphene is a perfect heat conductor. Its thermal conductivity, of about  $5000\text{ Wm}^{-1}\text{K}^{-1}$ , has recently been measured at room temperature and is much higher than all the values observed for copper, silver, and carbon structures such as nanotubes, graphite and diamond. However, there is a strong reduction in the value of thermal conductivity when the graphene layer is deposited on a substrate, due to scattering of the phonons with the impurities at the interface with the substrate.

In Fig. 2.5 there is a comparison between graphene mechanical properties and those of common materials.

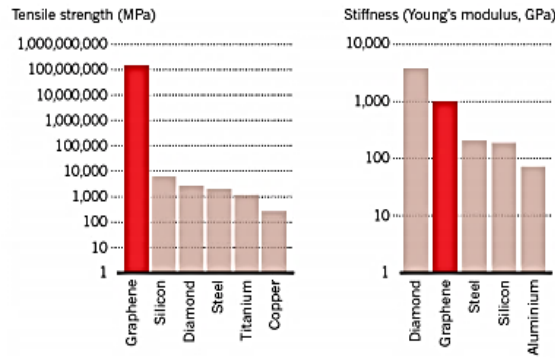


**Figure 2.5:** Mechanical properties comparison between graphene and other materials [6]

- Optical properties:** graphene has good optical transparency (97.7%). This means that graphene, even if it has the thickness of only one atom, is surprisingly able to absorb a fraction of incident white light, equal to 2.3%. From the analysis of membranes coated with single or multi layers of graphene emerges that as the number of layers increases, transmittance decreases and absorption increases, as shown in the Fig. 2.6:

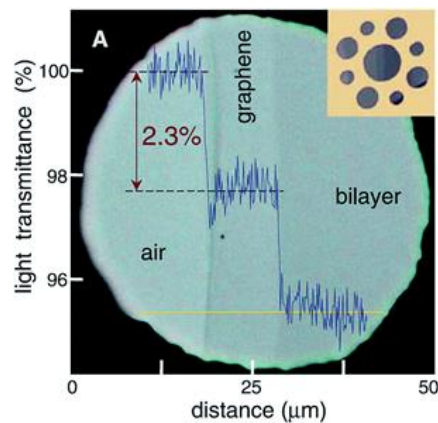


**Figure 2.6:** Intensity of the light transmitted through: 1) the air, 2) single layer, 3) bilayer [7]

- Magnetic properties:** Graphene also has magnetic properties and presents the co-existence of ferromagnetic and anti-ferromagnetic domains. The origin of this magnetic behaviour is supposed to be the presence of defects in the structure and irregularities in the edges of the graphene sheet.
- Chemical properties:** The covalent bond established among C atoms leaves the graphene chemically inert and gives its extreme strength. In any case, it must be specified that real graphene sheet shows several kinds of defects, and the extent to which defects increase reactivity is strongly dependent on the type of attached functional groups and on their number [8]. Moreover, a single layer of graphene is supposed to be more reactive than a bi- or tri- layer sheet [9]. However, graphene remains quite inert and does not react in a short time, even if exposed to severe conditions of reaction. This makes graphene suitable for the application in a wide range of conditions and with a large variety of solvents.

## 2.2 Techniques for synthesis of graphene

Since the first graphene isolation in 2004, numerous graphene growth techniques have been developed over the years, which can be grouped into two broad categories: top-down methods and bottom-up methods. The following is a general summary of the most commonly used techniques, although a lot of research is currently being carried out to try to improve graphene production. It should be specified that progress in the production of graphene would also optimise significantly the fabrication of graphene-based membranes.

### 2.2.1 Top-down methods

The top-down techniques start from a “bulky” carbon source material and allow to obtain single layers of planar graphene, through appropriate chemical or physical methods.

The main techniques that fall under this category are:

- **Mechanical exfoliation:** this is the method through which in 2004 Geim and Novosëlov isolated graphene for the first time. By using simple adhesive tape on the surface of a graphite sample, it is possible to break the weak Van Der Waals bonds that hold the carbon planes together in graphite. By repeating this exfoliation process several times, it is possible to isolate an individual graphene plane. In order to observe the samples obtained, it is necessary to place the graphite layers on a silicon/silicon oxide substrate. Despite the simplicity, this technique has many defects: it does not allow to control the thickness and size of the graphene layers and is not suitable for large-scale production.
- **Chemical exfoliation:** in this technique, graphite is immersed in a solution and the separation of the graphene planes takes place thanks to surfactant molecules present in the solution. Typically, organic solvents are used in combination with ultrasonic techniques. In this way, the solvent molecules separate the crystalline planes intercalating between the graphite layers, the solution is sonicated for a few hours and then centrifuged, to induce the deposition and the removal of the thickest graphite flakes. The dispersion and centrifugation can be repeated several times to increase the exfoliation efficiency.  
The graphene obtained in this way is typically multilayer (from a few layers up to ten layers). These techniques are inexpensive and allow the production of graphene on an industrial scale. However, the quality of the graphene grown is not of the best quality since it often contains contaminants such as the chemicals used in the solution.
- **Graphite oxide exfoliation:** in this type of technique, graphene is obtained from graphite oxide (GrO). Graphite oxide can be considered as a series of stacked oxidized graphene layers in which carbon atoms are bound to a number of oxygen atoms. The starting graphite is oxidized by means of strong acids that increase the interplanar distance. In addition, as a consequence of the oxidation process the layers becomes hydrophilic, so they tend to disperse in organic solution or in water. Through sonication, water molecules intercalate between the graphite oxide planes and cause their almost total exfoliation in monolayer oxidized graphene. The bonds with oxygen make graphene oxide a strong insulator, unlike normal graphene, which is very conductive. Electrochemical reactions can be then used to reduce back graphene oxide and thus achieve pure graphene. The disadvantage of this type of

process is that the graphene obtained in this way presents many defects and often contains high percentages of residual graphene oxide.

## 2.2.2 Bottom-up methods

Bottom-up methods allow to synthesize graphene from carbon in atomic or nanostructured form, depositing it on specific substrates. This category includes the following techniques:

- Chemical vapour deposition (CVD):** this technique is the one adopted to produce the commercial graphene used in this thesis work and it is considered to be one of the most promising approaches for the production of high-quality graphene. Compared to the synthesis techniques previously presented, CVD allows to synthesize graphene on surfaces of several  $\text{cm}^2$  within a reasonable time frame, obtaining a film of high crystalline quality, and with the possibility to easily transfer the material produced on a wide range of substrates. A graphene layer is deposited on metal substrates through the decomposition of hydrocarbon molecules, which provide the carbon source necessary for the growth of crystalline graphene. Fig. 2.7 shows the diagram of a tubular furnace generally used for growing graphene by CVD processes. The substrates on which the graphene will be grown are inserted in a hot wall furnace. Usually metal substrates are used, such as thin sheets of Cu or Ni, which act as catalysts. After a heating ramp that brings the system to about  $1000^\circ\text{C}$ , these substrates are subjected to an annealing process in a reducing atmosphere with  $\text{H}_2$  to remove any oxidized metal layer from the catalyst surface and also to avoid the presence of  $\text{O}_2$  in the reaction environment.

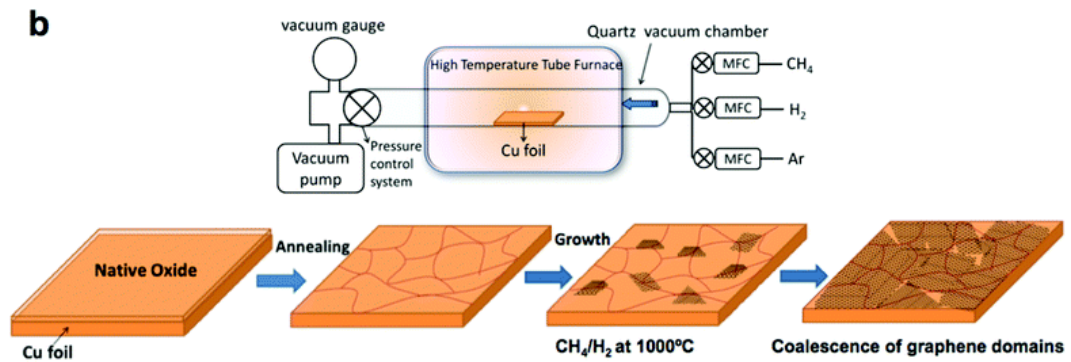


**Figure 2.7:** Scheme of the CVD process used to grow graphene on a Cu foil

Inside the CVD furnace the catalyst metal is exposed to the flow of precursor gases, such as methane  $\text{CH}_4$ , mixed with  $\text{H}_2$  and a gas carrier, usually argon (Ar). In the deposition phase, suitable temperature values together with the presence of the catalyst allow a reaction in which solid and gaseous materials are formed, starting from a gaseous precursor, as following:



Once the methane molecule has been split, the carbon obtained is reorganised into solid form onto the metal substrate, while gaseous  $H_2$  is carried out of the furnace thanks to carrier gas flow.

At the end of the deposition the metallic substrate is covered by graphene on top. The final step of the synthesis process consists in the cooling of the furnace and in the extraction of the samples. In this phase, the temperature decreases until it reaches room temperature, with a slow or rapid cooling ramp, also depending on the kind of catalyst. It is important to note that this phase plays a fundamental role, in fact possible residual thermal stresses can cause defects and breakages in the graphene film.

A fundamental advantage of CVD growth technique on Cu is the good control of the number of graphene layers. In fact, from a comparative study [10] of CVD on Cu and Ni, it clearly emerges that graphene growth on Cu leads to the formation of single-layer graphene. From optical images of graphene transferred from the catalyst support to  $SiO_2/Si$  substrate, it is evident that graphene on polycrystalline Cu is a uniform single-layer film, as shown in Fig.2.8 (a), while graphene on Ni presents many multilayer flakes, which are the darkest flakes present in Fig.2.8 (b). This difference suggests that the growth mechanism of graphene on Cu is different from that on Ni. In fact, in the case of Ni the growth mechanism is supposed to be a segregation mechanism which makes it difficult to avoid the formation of multilayer flakes. It is represented in Fig. 2.8 (c). On the contrary Cu has a very low carbon solubility, therefore the carbon amount dissolved inside it will be very small. This is valid even if the temperatures and the hydrocarbon concentrations are high, and if the growth time is long. In fact, after the first layer of graphene is deposited, there are no more areas of the catalyst Cu exposed to the flow of hydrocarbons, so it will no longer occur decomposition of starting reagents and growth of graphene. Therefore, the process of CVD of graphene on Cu is often defined as a self-limiting surface reaction process. It is represented in Fig. 2.8 (d).

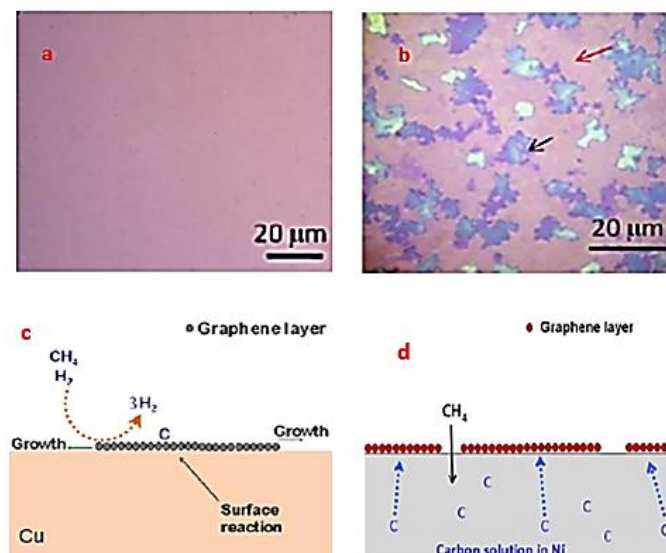


**Figure 2.8:** Optical images of graphene of graphene transferred to Si-based support from Cu(a) and Ni(b) substrate. Schematic representation of graphene growth mechanisms on Cu(c) and Ni(d). [10]

- **Unzipping of nanotubes:** graphene synthesized by this technique generally contains few defects. It consists in opening the cylindrical structure of carbon nanotubes by depositing them on a silicon substrate and coating it with PMMA. Subsequently, through an argon plasma, the structure of the nanotube is opened and, once the PMMA is removed, graphene is obtained.
- **Epitaxial growth on SiC crystals:** it consists in producing layers of graphene by recombining the carbon present on the surface of a SiC crystal. SiC is subjected to a series of processes under vacuum and high temperature conditions (up to 1450 °C). In this way, the silicon on the surface sublimates and the remaining carbon atoms recombine to form graphene. However, the graphene grown in this way is difficult to be transferred because it is strongly linked to the SiC substrate.

## 2.3 Advantages of graphene-based membranes

Graphene plays a key role for the manufacture of innovative membranes for water purification and desalination. There are a lot of graphene-based materials that could be used for the next generation membrane technology. In order to name a few: single-layer nanoporous graphene membranes, multilayer graphene membranes, graphene surface-modified membranes, graphene oxide (GO) membranes, polymeric membranes incorporated with GO, graphene membranes incorporated with CNTs [11] etc. Fig. 2.9 is a schematic summary of the different graphene-based separation membranes (GBSMs).



**Figure 2.9:** Classification of GBSMs [11]

In general, graphene-based membranes are supposed to be able to overcome the limitations mentioned in Chapter 1, for several reasons, some of which have still to be demonstrated experimentally. In particular, the following ground breaking results can be mentioned:

1. Wang et al. [12] experimentally demonstrated that a graphene membrane on a porous support, thanks to its excellent mechanical properties, can withstand high pressure differences. This is a very important aspect for pressure-driven membrane processes, especially RO, in which the pressure to be applied in seawater desalination to overcome the osmotic pressure varies in the range 50-55 bar. This high-pressure resistance leads to another benefit too: an increasing production rate. These graphene membranes show a great resistance to high pressure especially in areas with absence of wrinkles, which can withstand pressures higher than 100 bar, that is a pressure higher than the working pressure of most membrane processes. The use of substrates with smaller pores can improve the homogeneity of suspended graphene film.
2. The atomic thickness of porous graphene increases the permeance, compared with the state-of-the-art membranes. This leads to a faster water transport and so to an increase in production rates. The improved permeability implies low pressure requirements, and so a remarkable energy saving. Cohen-Tanugi et al. [13] observed that a tripling in permeability would decrease pressure by 44% for RO seawater desalination, and this is equivalent to a reduction of 15% in energy consumption. This energy saving would be significant because of the high cost of energy, which accounts for 50% of the total water desalination cost.
3. In addition to high permeability, high selectivity can also be achieved, if in presence of an ideal nano-porous graphene membrane with tailor-made pores. In fact, although graphene is impermeable in its pristine state, theoretical models [14] predicted that with the introduction of pores of controlled size and density, graphene membranes would outperform polymeric membranes by many orders of magnitude in terms of permeability and selectivity. This could overcome the eternal dichotomy between permeability and selectivity in the actual membranes. The tuning of the selectivity of graphene through narrowly distributed pore sizes represents a challenge for the development and the scaling-up of nano-porous graphene membranes.
4. Thanks to the stability of 2D structure, graphene is quite unreactive with other substances. This improved stability and chemical inertness of graphene makes possible the application of these membranes with a wide range of chemical species, in addition with a longer life-time.
5. The tendency to fouling is mitigated with graphene-based material. The work of Leenaerts et al. [15] has demonstrated through density functional theory that graphene is hydrophobic. They stated that the binding energy between water molecules is stronger than the energy between water droplets and graphene sheet, so graphene tends to absorb less water molecules than water droplets do. These hydrophobic properties imply a reduction in the frictional force between the membrane and the water. In this way the contamination rate decreases because the particles are not easily attached to the membrane surface. This decrease in fouling implies higher lifetime too, because of the fact that fewer cleaning operations are required.
6. Graphene has high wear resistance and unlike metals, it is not affected by corrosion.

### 2.3.1 Single layer porous graphene membranes: state of the art

In this section a discussion on the state-of-art of single layer graphene porous membranes will follow, presenting the results available till date.

The first studies on the feasibility of graphene membranes for water purification processes were based on molecular dynamic (MD) simulation approach [13,16]. Tanugi and Grossman established that nano-porous graphene, either alone or on a porous substrate, could withstand high pressures and allow ultra-fast water permeability due to its atomic thickness. In addition to these qualities, high salt rejection was predicted, thanks to a strict control of pores size and density. In this study Tanugi and Grossman innovatively hypothesized that pore chemistry had a fundamental influence on water permeation and salt rejection ability of nano-porous membranes [13]. In order to examine the effect of pore chemistry they studied hydrogen-terminated (hydrophobic) and hydroxyl-terminated (hydrophilic) pores. The pores considered had a size between 1,5 and 6,2 Å. As result, water permeability increased linearly with the increasing area of these pores and it is significantly enhanced by hydroxylation, due to hydrophilic functional groups that increased the water flux (Fig. 2.10).

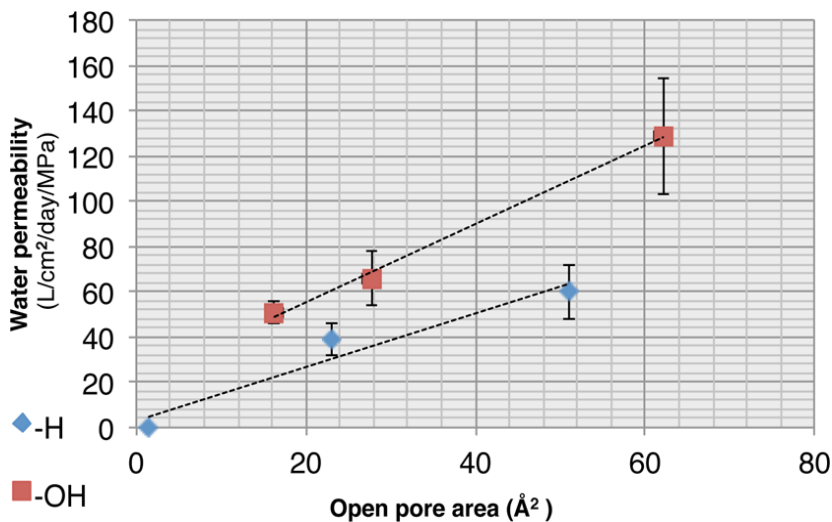


**Figure 2.10:** Computed water permeability for graphene with hydrogen and hydroxyl groups on nanopores [13]

As consequence, hydrogenated pores showed a stronger salt rejection than hydroxylated ones. The salt rejection decreased also with increasing pore size and applied pressure, reaching a minimum of 33% for the biggest OH-pores at pressures higher than 200 MPa. For the pores that exhibited a salt rejection close to 100%, the water permeability varied between 39 and 66 L/cm²·day·MPa, that is 2/3 orders of magnitude lower than real experimental calculations.

These theoretical studies were followed by several experimental attempts of manufacturing nanoporous graphene membranes. The first approach used for creating controlled nanopores was based on the possibility of suspended graphene sheets to be controllably nanosculpted with a focused electron beam of a transmission electron microscope (TEM) at a room temperature [17]. The electron beam irradiation during few seconds created stable nanopores that do not evolve over time (Fig. 2.11). The minimum pore diameter drilled by a focused electron beam was supposed to be between 2 and 5 nm, that make these membranes suitable for water decontamination of bigger molecules but not for desalination.

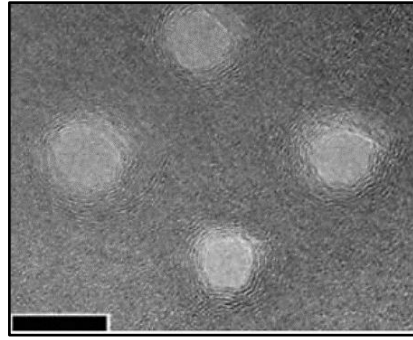


**Figure 2.11:** Multiple nanopores in proximity to each other. Scale bar 10 nm. [17]

A similar approach, but based on focused ion beam perforation (FIB) of suspended graphene, was used by Celebi et al. [18]. The membranes were manufactured with a transfer process that placed two layers of graphene onto a SiN<sub>x</sub> frame punctured with 4 μm diameter pores.

After transferring, nanopores between 14 nm and 1 μm were created using Ga-based FIB, while pores with diameter less than 10 nm were created using He-based FIB (Fig. 2.12 a,b,c,d).

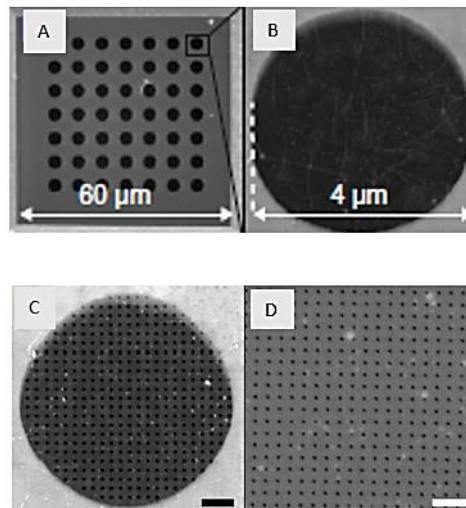


**Figure 2.12:** a) Porous freestanding SiN<sub>x</sub> before graphene transfer. b) Graphene transferred on one of the 4 μm SiN<sub>x</sub> open pores. c) Ga-FIB pores, scale bar 500 nm. d) He-FIB pores, scale bar 100 nm [18]

Few million pores ( $\sim 10^3$ - $10^6$  per membrane) with narrowly distributed diameters between less than 10 nm and 1 μm were obtained. These porous graphene membranes were found to permeate water several times faster than do ultrafiltration membranes such as acrylic, cellulose, and polysulfone, meanwhile reducing the pressure requirements (Fig. 2.13).

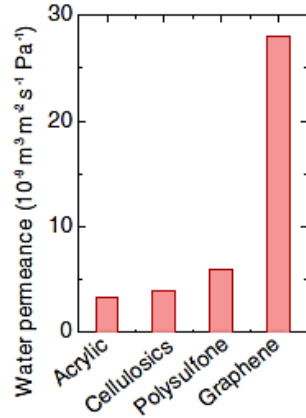


**Figure 2.13:** Water permeance for nano porous graphene and other ultrafiltration membranes [18]

One of the most striking experimental works is that of O’Hern et al [19], which for the first time evaluated the ionic transport through a SLG membrane transferred on a polycarbonate track-etched (PCTE) support with a direct transfer process. In order to achieve a molecular selective transport this study exploited the natural presence of intrinsic 1-15 nm diameter pores in CVD graphene. It was observed a KCl transport rate in the range 46-71% of that through the PCTE bare membrane, confirming that CVD graphene was quite permeable to KCl. It was then measured the diffusive transport of molecular species of greater size: tetramethylammonium chloride (TMAC), Allura red dye (AR), and tetramethylrhodamine dextran (TMRD). It emerged that the graphene membranes permitted transport of KCl and TMAC but blocked TMRD (Fig. 2.14 a). This means that intrinsic defects were able to reject TMRD (12 nm of diameter), resulting in a TMRD diffusive transport attenuated by 1 order of magnitude compared to the smaller species. The results are shown in Fig. 2.14 b.

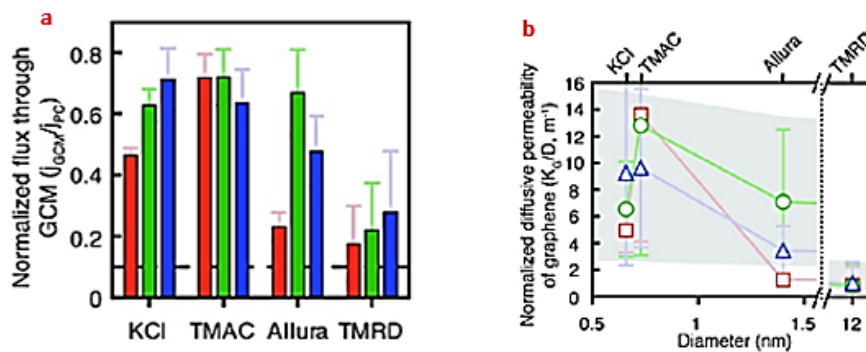


**Figure 2.14:** a) Diffusive flux of molecules through SLG/PCTE membranes normalized by that through PCTE membranes. b) Permeability of graphene normalized by the diffusivities of the molecules indicates that the transport of TMRD was significantly lower than that of smaller molecules [19]

Once again O’Hern et al [20] also investigated in another research work the possibility to obtain sub-nanometric pores over SLG/PCTE in a more controlled way. In this case the pores were formed intentionally by a two-step process (Fig. 2.15). The first step consists in nucleating reactive isolated defects through  $\text{Ga}^+$  ions bombardment, at a density of  $6 \cdot 10^{12}$

ions/cm<sup>2</sup> with 8 kV acceleration voltage. The second step consists in enlarging the starting defects by oxidative etching with acidic potassium permanganate, an oxidant that attacks unsaturated carbon bonds. Stable pores with an average diameter of  $0,40 \pm 0,24$  nm were formed after etching.

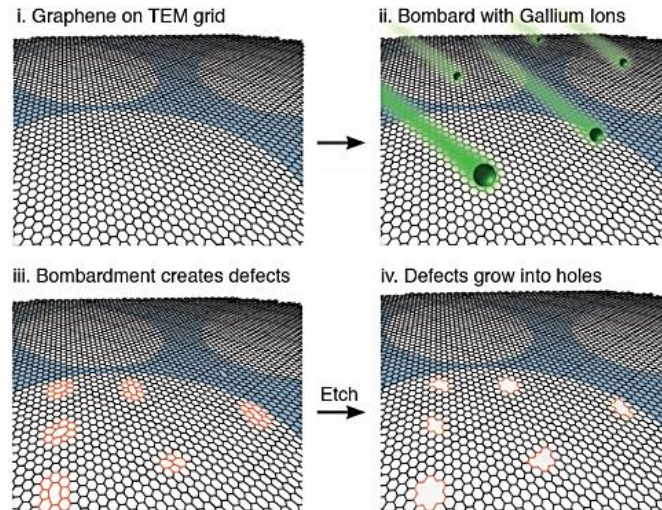


**Figure 2.15:** Schematic representation of the process employed to create controlled nanopores in SLG/PCTE membranes [20]

In this case it was evaluated the transport of KCl and Allura red dye across these formed pores. Etching time was found to be a key parameter to control pore density and pore sizes. Selectivity of K<sup>+</sup> and Cl<sup>-</sup> crossing the nanoporous SLG membrane depends on etching time too. This was due to the change in membrane potential after the etching process (Fig. 2.16). In particular, a greater membrane potential allowed for a selectivity of K<sup>+</sup> over Cl<sup>-</sup> ions. This selectivity is due to electrostatic interactions with the negative charge at the edge of the pores. As the etching time increased, the membrane potential decreased up to 0, indicating the loss of selectivity between K<sup>+</sup> and Cl<sup>-</sup> ions. As shown in Fig. 2.16, before etching the transport of KCl and AR was obtained and was similar to that through intrinsic defects in CVD graphene. As the etching progressed during the first 25 min, the transport of KCl gradually increased, while that of AR remained unchanged. This occurred because as the pores increased in size during etching the influence of electrostatic effects on K<sup>+</sup>/Cl<sup>-</sup> selectivity decreased, and the transport became dominated by steric hindrance, that excluded AR from crossing the graphene. At even longer etching time transport of AR started to increase too.

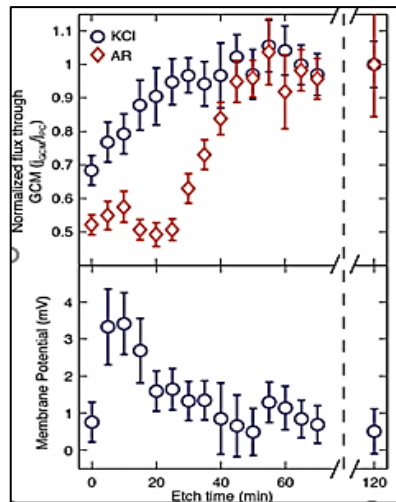


**Figure 2.16:** Diffusive flux through the SLG/PCTE membrane normalized by flux at 120 min etch time and membrane potential measurements [18]

Agrawal et al. [21] used a similar technique to create molecularly size pores in SLG membranes. They manufactured SLG membranes suspended on a W substrate with a 5  $\mu\text{m}$  hole, demonstrating their remarkable chemical and mechanical stability over weeks of testing at pressure 0,5 bar, temperature cycling from 25° to 200°C, and exposure to 15 mol % ozone up to 3 min to create pores in the size range 1 nm-100 nm. This stability opened the possibility of using  $\text{O}_3$  exposure as a method for in situ pore formation without damaging the membrane.

An alternative approach to manufacture single layer graphene membranes is that used in [22]. This study pointed out the ability to create graphene/polymeric membranes with minimized leakage pathways, important for the subsequent development of nanoporous graphene membranes. After transferring the SLG over polypropylene (PP) or polyvinylidene difluoride (PVDF) substrates, 57% and 40% blockage of KCl was obtained, compared to bare PCTE. Transport measurements were repeated after sealing the defects with interfacial polymerization (IP), resulting in an improved rejection ability, from 57% to 67% and from 40% to 67% for PP and PVDF based membranes, respectively, as shown in Fig. 2.17. IP occurs selectively at defect sites and optimization of its process parameters leads to a maximum ion blockage of 84% in the case of PP based membranes.

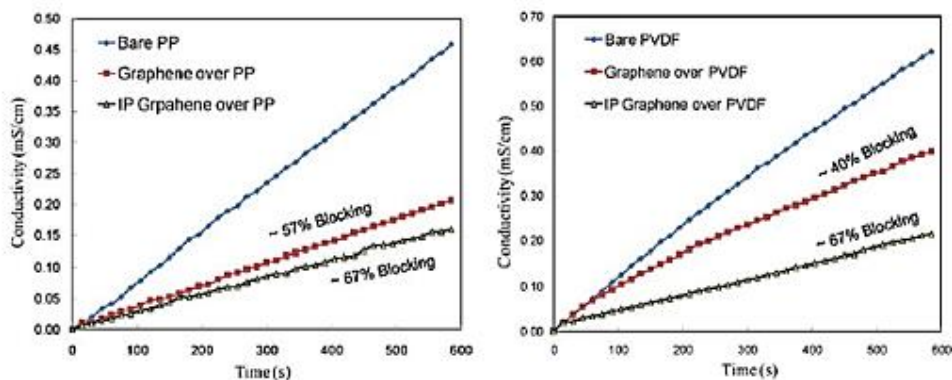


**Figure 2.17:** KCl conductivity measurements of substrate, graphene, and IP graphene on PP and PVDF [22]

A similar approach based on sealing defects [23] consists of a two-step sealing procedure. In the first step nanometer-sized intrinsic defects in SLG (1-15 nm) were selectively filled with Hafnia by atomic layer deposition (ALD). In the second step larger defects in SLG (100-200 nm) were sealed by Nylon-6,6 using IP. The flux of KCl across the SLG/PCTE membrane before defect sealing was 65% of that through the bare PCTE, thanks to intrinsic defects in SLG. After the sealing procedure, KCl flux decreased to 8% of that through PCTE. Moreover, after sealing defects the formation of controlled pores was achieved through  $\text{Ga}^+$  ions bombardment and oxidative etching. In this way it was obtained a mean diameter pore of 0,162 nm and a pore density of  $3,89 \cdot 10^{13} \text{ cm}^{-2}$ . In order to study the transport properties of thus obtained SLG nano-porous membranes four solutes were tested via forward osmosis. As shown in Fig. 2.18, the membranes showed  $\sim 90\%$  rejection of AR ( $\sim 1\text{nm}$  size),  $\sim 83\%$  rejection of Dextran ( $\sim 3,7\text{nm}$  size) and  $\sim 70\%$  rejection of  $\text{MgSO}_4$  (0,86 nm size). The higher rejection of AR was supposed to derive from electrostatic repulsions between the anionic AR molecule and the negatively charged pore terminations. NaCl ( $\sim 0,716$  nm size) rejection was negative, indicating that the NaCl transport rate due to diffusion exceeded the transport rate due to nonselective convective flow. This rate transport of NaCl could also be attributed to the increased permeability of Nylon-6,6 to monovalent ions.

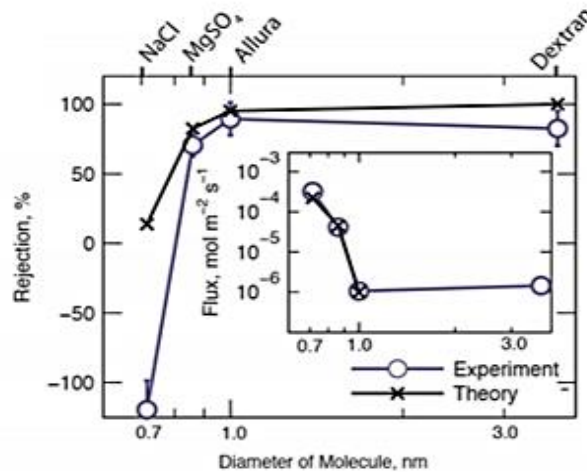


**Figure 2.18:** Rejection and molar flux of solutes [23]

Another way to fabricate SLG membranes was reported by Surwade et al [24], whose study provided striking results. Samples used are obtained transferring CVD single layer graphene from Cu foil to a SiN microchip characterized by 5  $\mu\text{m}$  diameter hole. It was established that the plasma etching process was the most convenient method to create tailored nanopores in suspended single layer graphene (Fig 2.19 a). As shown in Fig 2.19 b,  $\frac{I_D}{I_G}$  ratio increased as the exposure time increased, indicating the formation of detectable defects.

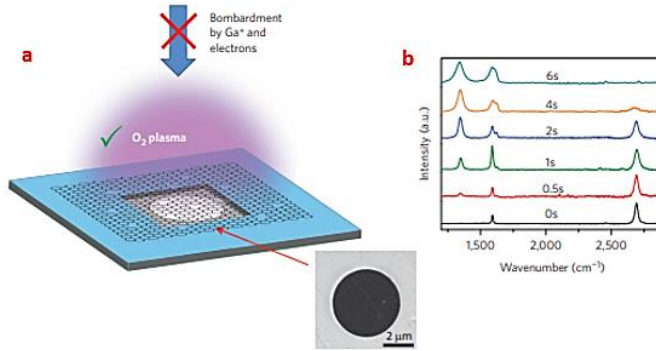


**Figure 2.19:** a) O<sub>2</sub> plasma treatment on a SLG suspended on a 5 μm diameter hole. b) Raman spectra of SLG at different exposure time to O<sub>2</sub> plasma [24]

With 0,5-1,5 s exposure to oxygen plasma, pores of 0,5-1 nm size were obtained. These membranes exhibited ~100% of salt rejection and a water flux of 250 l/m<sup>2</sup>·h·bar with osmotic pressure as driving force. Water transport was evaluated by monitoring the loss of DI water mass vs time. The pristine graphene before plasma etching showed no water loss after 24h, indicating an intact membrane. Even at short exposure times, that induce a low defect density ( $\frac{I_D}{I_G} \approx 0,5$ ), the porous SLG exhibited high water passage, that increased as the defect density increased (Fig 2.20 a). Water/salt selectivity is excellent for short etching times (Fig 2.20 b).

It can be deduced that nanoporous graphene with low defect density ( $\frac{I_D}{I_G} \leq 0,5$ ), exhibited good H<sub>2</sub>O/KCl selectivity ( $S \approx 1 \cdot 10^5$ ) and measurable water transport, i.e. it worked well as a desalination membrane.

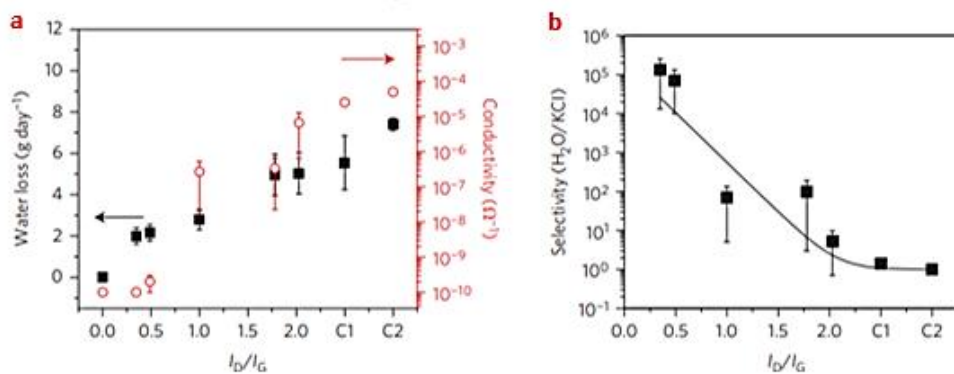


**Figure 2.20:** a) water loss after 24 h and ionic conductivity as function of  $\frac{I_D}{I_G}$  ratio. b) H<sub>2</sub>O/KCl selectivity as a function of  $\frac{I_D}{I_G}$  ratio [24]

The most recent studies [25,26] focused on manufacturing of novel supports able to maintain a mechanical stability over large SLG areas. Kazemi et al [25] successfully fabricated nano porous graphene with large total area using TEM grids as mechanical porous support and O<sub>2</sub> plasma treatment to create nanopores. The samples were placed in a plasma cleaner at 20 W power in a vacuum chamber with a flow of pure O<sub>2</sub> at 550 mTorr. These fine mesh grids were found to increase the mechanical strength over large areas of suspended graphene. SLG was transferred onto grids with various hole sizes. As the grid

mesh increased, the graphene sheet conformed better to the grid surface, resulting in a reduced number of wrinkles. By using 1m column of salty water as driving force for water transport, they measured high water permeation ( $1,6 \cdot 10^7 \text{ L/m}^2 \cdot \text{h} \cdot \text{bar}$ ) and a NaCl rejection rate of 76% for a suspended graphene area of  $\sim 2,8 \cdot 10^4 \mu\text{m}^2$ . In Fig 2.21 there is a comparison between salt rejection obtained in this work and that obtained in other aforementioned works.

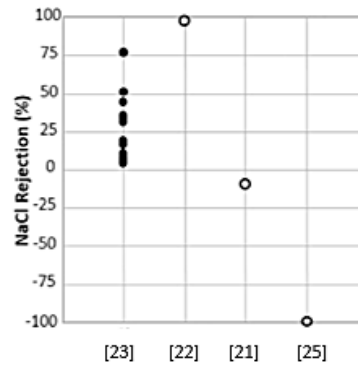


**Figure 2.21:** NaCl rejection in Kazemi et al work [25] compared to that of nanoporous single layer graphene on 5  $\mu\text{m}$  size aperture in Si [24], on PCTE with 200 nm pore size [23], and on PES with 50-500 nm pore size [27]

The same research group manufactured a novel support based SLG membrane [26] with tunable salt rejection and water permeation. Using a fine mesh grid as initial support and SiN/Si with an array of holes as secondary support, they designed a mobile nanoporous graphene membrane, shown in Fig. 2.22. This single layer CVD graphene membrane with support of 2000 mesh Ni grid was put over various SiN/Si hole arrays with different size and spacing. Thanks to the movement of graphene/grid over fixed silicon hole arrays, a big range of high permeation ( $4,3 \cdot 10^7$ - $5,9 \cdot 10^7 \text{ L/m}^2 \cdot \text{h} \cdot \text{bar}$ ) and NaCl rejection (58%-100%) was achieved.

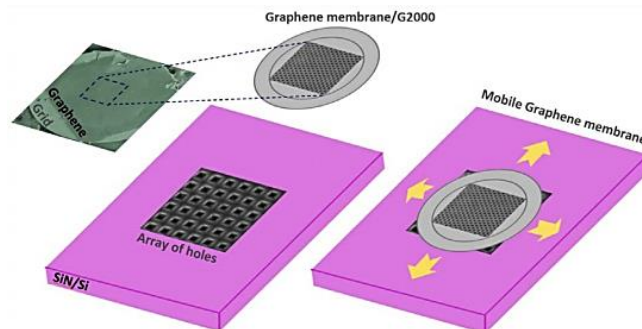


**Figure 2.22:** Scheme of transferred graphene onto grid (G/G2000) and its overlaying and movement on SiN/Si hole arrays [26]

Summarizing, top-down and bottom-up methods can be distinguished for the production of nano-porous graphene. One of the first top-down methods is based on the removal of carbon atoms from the lattice by above mentioned electron beams. Other methods are exposure to helium beams or methods based on chemical attacks. In bottom-up methods, the

nanostructures are created on a nano-porous substrate on which the graphene will then be grown, so that it can already be formed with the nanopores.

Up to now the fabrication of nano-porous graphene has been accomplished at a very small scale and under quite ideal operating conditions; new methods to create uniform nanopores in a simple and controlled way need to be developed. However, the challenges with mass application of nano-porous graphene membranes are not only relative to the fabrication of nanopores on graphene film, but also to the integration of graphene layer with supports.

The methods presented above have demonstrated the potential of graphene, but they are supposed to be not scalable, while in this work an attempt has been made to develop a scalable manufacturing method.

### 3. MATERIALS AND METHODS

This section describes the experimental procedure carried out in the laboratories of Nano Sciences and Electrochemical Characterizations of the Department of Applied Science and Technology (DISAT) of the Polytechnic of Turin. Firstly, the list of materials is presented and then the instrumental equipment used for the characterization of the membranes here fabricated are also discussed.

#### 3.1 Materials

The materials used for this thesis work are hydrophobic polycarbonate track-etched membranes and monolayer graphene grown by CVD on copper (Cu) foil. Since it was necessary to transfer the graphene film from the Cu substrate to the PCTE one, a copper etching solution was used. Wet etching is a process that utilizes a chemical solution, or an etchant, to remove or “etch” metals. The etchant solution used to dissolve the Cu substrate was iron chloride III ( $\text{FeCl}_3$ ) 1,5 M. It was prepared by mixing 51 g of  $\text{FeCl}_3$  powder with de-ionized water, heating to 30 ° on a plate to speed up the dissolution.

##### 3.1.1 PCTE membranes

Hydrophobic Polycarbonate Track-Etched (PCTE) membranes with 0,1  $\mu\text{m}$  pore size have been employed as porous supports to which single layer graphene (SLG) has been then transferred. These membranes were purchased from Sterlitech Corporation (USA) and are made from a thin, microporous polycarbonate film material. The PCTE disks considered in this work are PVP-free, i.e. free of Polyvinylpyrrolidone, a water-soluble polymer. For this reason, they exhibit a hydrophobic behaviour. These membranes are characterized by precisely controlled cylindrical pores with narrow pore size distribution. The pores act as small capillaries; when the hydrophobic membranes come into contact with water, surface tension acts to repel the water from the pores.

Table 3.1 shows some specifications of the PCTE membranes with pore size of 0,1  $\mu\text{m}$  while Fig. 3.1 shows an image representative of the membranes used in this work.

**Table 3.1:** PCTE (0.1  $\mu\text{m}$  pores) membranes specifications

Pore density [pores/ $\text{cm}^2$ ]	$4 \cdot 10^8$
Open area [%]	3,1
Nominal weight [ $\text{mg}/\text{cm}^2$ ]	0,7
Nominal thickness [ $\mu\text{m}$ ]	6
Water flow rate [ $\text{ml}/\text{min}/\text{cm}^2$ ]	2.5
Maximum Operating Temperature [ $^{\circ}\text{C}$ ]	140 $^{\circ}\text{C}$
Diameter of membrane [mm]	25
Surface wetting	Hydrophobic
pH range	4-8
Max operating temperature	140 $^{\circ}\text{C}$



**Figure 3.1:** Sterlitech PCTE membranes. The pore size is 0.1  $\mu\text{m}$ .

### 3.1.2 Monolayer Graphene

Monolayer graphene used for this thesis work is produced by Graphenea company. It is grown on a copper foil substrate with aforementioned CVD synthesis (see section 2.2.2). In Fig. 3.2 it is possible to see the aspect that Graphenea films on Cu have before their use.



**Figure 3.2:** Monolayer Graphene on Cu - Processed in Clean Room Class 1000

With regard to the single layer graphene film and the Cu substrate, the tables 3.2 and 3.3 illustrates their main characteristics, provided by the manufacturer.

**Table 3.2:** Graphene film specifications

Grown method	CVD synthesis
Appearance (color)	Transparent
Optical transparency	> 97%
Appearance (form)	Film
Coverage	> 95%
Number of graphene layers	1
Thickness (theoretical)	0,345 nm
Grain size	Up to 20 $\mu\text{m}$
Quality control	Electron Microscopy and Raman Spectroscopy

**Table 3.3:** Cu foil specifications

Thickness	18 $\mu\text{m}$
Roughness	$\sim 80$ nm
Pretreatment for easier bottom layer removal	Partial

As mentioned in Table 3.1, Graphenea provides the results obtained from the quality control on monolayer graphene. Fig.3.3 shows an example of electron microscopy image and Raman spectrum characteristics of the commercial monolayer graphene used in this thesis work.

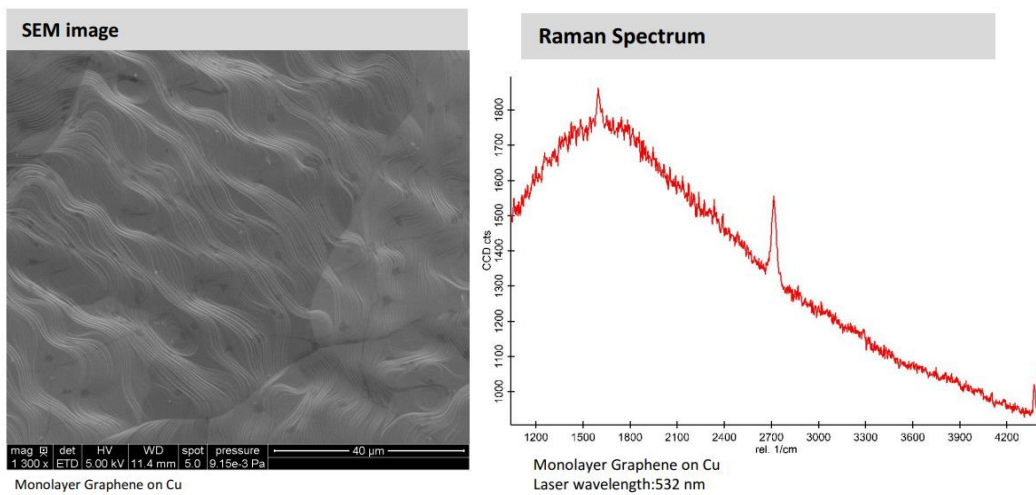


**Figure 3.3:** Results of quality control made on monolayer graphene provided by Graphenea

As it will be explained in detail in section 3.2.3.3, graphene usually shows three main Raman peaks, corresponding to the D ( $\approx 1350$   $\text{cm}^{-1}$ ), G ( $\approx 1580$   $\text{cm}^{-1}$ ), and 2D ( $\approx 2700$   $\text{cm}^{-1}$ ) bands.

The quality control made on graphene film provides the ratios between the peaks:  $\frac{I_{2D}}{I_G} < 0,5$ ;  $\frac{I_D}{I_G} < 0,05$ . The absence of D peak is representative of a negligible number of defects. Since

the intensity of 2D peak is almost three times G peak as shown in Fig. 3.3., Graphene CVD graphene is a monolayer [28].

It is advisable to keep graphene films in a vacuum or in an inert atmosphere to avoid oxidation phenomena. In this work, the graphene samples have been stored under vacuum in a dryer. As far as the pre-treatment on the copper substrate is concerned, monolayer graphene on the back side of copper is only partially removed, so an additional treatment like oxygen plasma would be necessary to eliminate the bottom layer totally before transferring the graphene film onto the desired substrate.

### 3.2 Transfer process of monolayer graphene to PCTE substrates

Monolayer graphene was transferred on the PCTE commercial microfiltration membranes with a direct transfer method. The fabrication of SLG-PCTE membranes was carried out following the procedure schematically shown in Fig. 3.4 a) and b), which consists of the following steps:

1. The PCTE membrane is deposited on a SLG/Cu sample: in this way the target substrate and the monolayer graphene on Cu are put in direct contact (Fig. 3.4 a);
2. The overall PCTE/SLG/Cu system is let floating over the etchant solution ( $\text{FeCl}_3$  1,5 M) for 30 minutes, to chemically etch away the Cu foil and directly transfer the SLG to the PCTE support (Fig. 3.4 b);
3. After chemical etching of the Cu foil, the graphene monolayer results to be well-attached on the hydrophobic PCTE membrane (Fig. 3.4 b);
4. SLG/PCTE membrane is washed three times in de-ionized water for 10 minutes each time, to provide a complete removal of the etching solution contaminants;
5. The SLG/PCTE membrane sample is finally air-dried (Fig. 3.4 b).

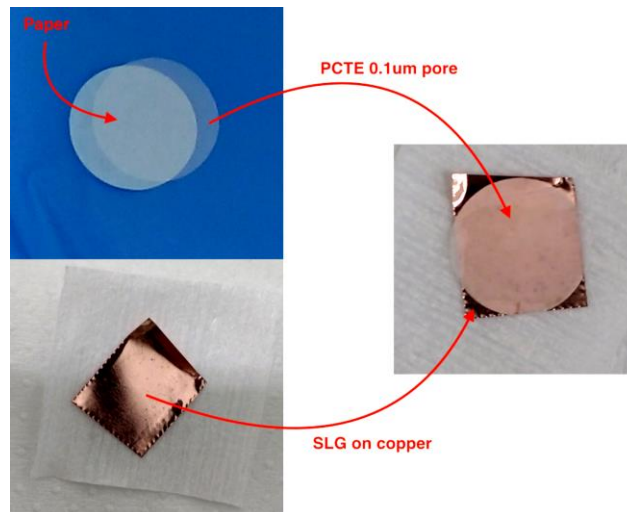


**Figure 3.4:** a) First transfer process step

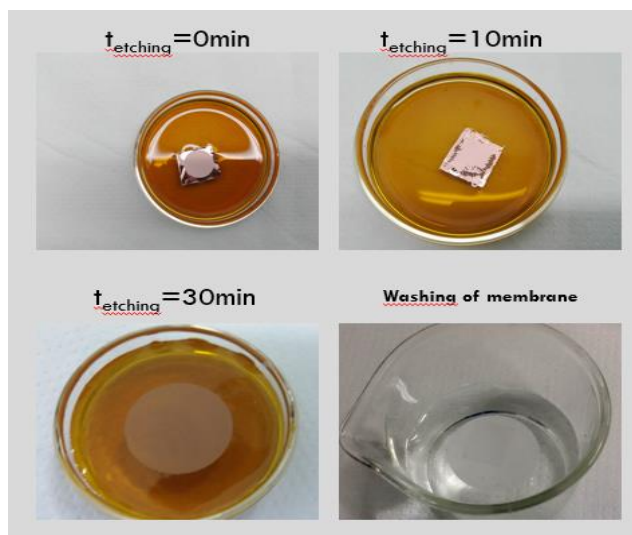


**Figure 3.4:** Transfer process steps (steps 2-3-4)

A similar transfer process has been carried out also to manufacture a bilayer or trilayer graphene membranes, simply by repeating the transfer of the monolayer graphene from the Cu sheet to the previously prepared SLG-PCTE membrane, after letting it dry. The experimental procedure is the following:

1. The previously obtained SLG/PCTE membrane is deposited on a new Graphenea SLG/Cu sample;
2. The single layer graphene membrane over the new piece of monolayer graphene on Cu is let floating for 30 minutes in  $\text{FeCl}_3$  solution with a little piece of Silicon on top, as shown in Fig. 3.5. A little weight is needed in order to help the second deposition. This step is necessary because the previously prepared SLG/PCTE membrane and the new piece of SLG/Cu tend to repel each other when let floating over the etchant solution;
3. After chemical etching of the Cu foil, it is obtained a bi-layer graphene membrane on the hydrophobic PCTE support;
4. BLG/PCTE membrane is washed three times in de-ionized water for 10 minutes each time, to provide a complete removal of the etching solution contaminants;
5. The BLG/PCTE membrane sample is finally air-dried.

The method is repeated every time a new layer of graphene must be deposited on the previously obtained membrane.

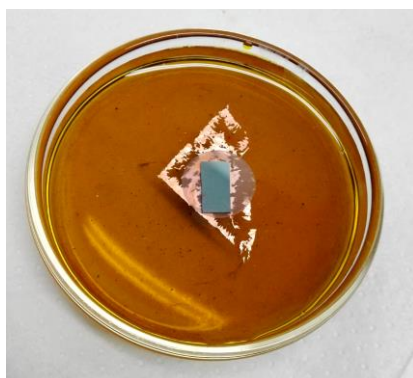


**Figure 3.5:** Deposition of the second layer of graphene

### 3.3 Characterization of graphene membranes

The obtained monolayer graphene membranes on micro-porous PCTE support can at this point be studied and characterized, as well as bilayer and trilayer ones.

Each characterization was carried out first on the PCTE membranes alone and then on those of graphene coated PCTE, for comparison purposes. Both direct and indirect characterizations were carried out. The former includes contact angle measurements to test the surface wettability, FE-SEM measurements for morphological characterization and Raman Spectroscopy for structural characterization. The latter, on the other hand, include mass transport measurements, which can be considered as a kind of indirect characterization since deductions on the homogeneity of the graphene coating can be made on the basis of the membrane rejection capacity.

#### 3.3.1 Contact angle test

The wettability of a solid in relation to a liquid is quantified by a quantity known as contact angle. This quantity is defined as the angle that forms the surface of a drop of liquid resting on an ideal solid, therefore a smooth, flat, homogeneous, inert, non-porous solid.

Among the various methods for determining  $\theta_c$ ; the wettability by spreading has been considered in this work and the sessile drop method has been used. After a certain period, the drop on the surface stops expanding, since the balance between the cohesive forces inside the liquid and the adhesive forces that favour the spreading has been reached. The angle between the drop and the surface is the well-known contact angle.

On the basis of the contact angle a classification is realized, shown in Fig. 3.6.

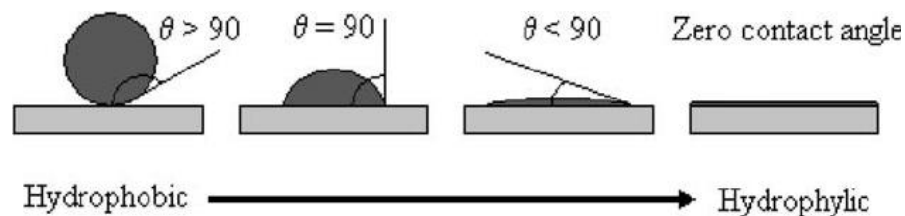


**Figure 3.6:** Contact angle classification

The measurements were carried out with DATAPHYSICS OCAH 200 high-speed optical contact angle measuring device for the spreading determination, with up to 360 images per second.

The experimental procedure is the following:

- A water drop with a volume of 1.5  $\mu\text{L}$  is dispensed. The drop is viewed in profile during the measurement;
- The integrated camera allows the acquisition of the image of the drop on the sample;
- Once the images have been obtained, it is possible to extract drop profile,
- and measure the value of the contact angle using dedicated software. This software recognises the drop contour and the base line at the solid-liquid interface, assigning a mathematical function to the drop shape (Laplace-Young fitting tool).

For each analyzed sample, three water drops were dispensed at different positions on the surface of the sample and then the average value of the contact angle was calculated.

### 3.3.2 Field-Emission Scanning Electron Microscope (FE-SEM)

Field-Emission Scanning Electron Microscope (FE-SEM) is an electronic microscope through which it is possible to carry out a detailed morphological and compositional surface characterization. It is useful for high resolution imaging in the fields of nano materials science, in fact it allows to observe structures as small as 1 nm.

It is a non-destructive analysis technique that does not use light as a source of radiation. In fact, this microscope works with electrons instead of light. The electron beam is generated by an electron source, concentrated by a series of electromagnetic lenses and deflected by a system of coils that induces the controlled deflection of the beam to allow scanning line by line of a rectangular area on the sample surface. These electrons are captured by a special detector and converted into electrical pulses, which are sent in real time to a monitor.

Conventional scanning electron microscope generates electrons by heating a tungsten, LaB<sub>6</sub> or CeB<sub>6</sub> filament through a current (thermoionic emission). Instead, in FE-SEM the so-called "cold" source is employed. It is made by an extremely thin and sharp tungsten tip with a cusp geometry (tip diameter  $10^{-7}$  –  $10^{-8}$  m). The electron beam produced by the FE source is about 1000 times smaller than that of a conventional SEM, so the image quality and resolution is considerably better (the diameter of the beam is strictly related to the resolution: very small beams lead to high resolutions).

The experimental apparatus (Fig. 3.7) is essentially composed of an electronic column at the top of which is placed the emitter of electrons and a device that gives acceleration to the electron beam emitted. Then, the electron beam crosses the electromagnetic lenses system that allow the focusing of the beam. These ones can be distinguished in condenser and objective lens. The current in the condenser determines the diameter of the beam: lower current results in a small diameter and vice versa. The objective lens is the lowest lens of the column and it focuses the electron beam on the object. Openings are placed between the lenses, and they have the role to filter the electrons and reduce the size of the beam to provide a better resolution.

The lenses are focused by changing the excitation voltage of the coils (EHT) and the working distance (WD) that is the distance between the end of the column and the sample. Moreover, scan coils deflect the electron beam over the object according to a zig-zag pattern. The formation of the image on the monitor occurs in synchrony with this scan movement.

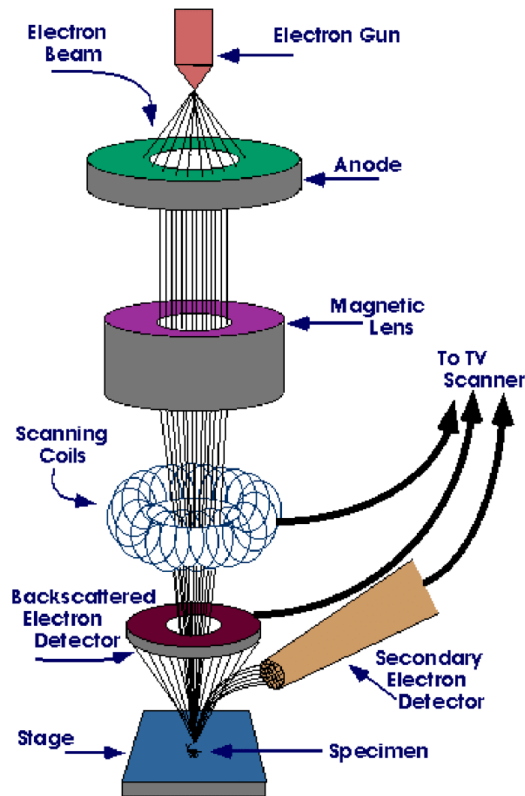


**Figure 3.7:** FE-SEM experimental apparatus

An electron is much smaller than the atoms of which the sample is made, so the electron beam will not only affect the surface but also the layers below. Therefore, an interaction volume is defined. The geometry of the interaction volume is strongly influenced by the energy of the incident beam (the higher the energy, the greater the interaction volume) and by the nature of the atoms of the sample. As  $Z$  increases, the electrons will penetrate the sample less and less, resulting in a smaller interaction volume.

The electrons detected by the detectors can therefore come from different depths of the interaction volume and thus carry different information with them. There are four zones from which four types of electrons come, as shown in Fig. 3.8.

- Auger electrons that come from the most superficial zones (1-5nm) and have energies between 50 and 1000 eV;
- Secondary electrons that come from superficial layers (5-50 nm) and that have energies between 0 and 50eV;
- Back-scattered electrons that have energies close to those of the primary beam (~50 eV) and therefore can re-emerge from deeper zones (hundreds of nm);
- X-rays coming from the deepest areas.

Since there are different types of signals, there will be various detectors:

- Back-scattered electrons detector;
- Detector for secondary electrons (Everhart-Thorley detector);
- X-ray detector.

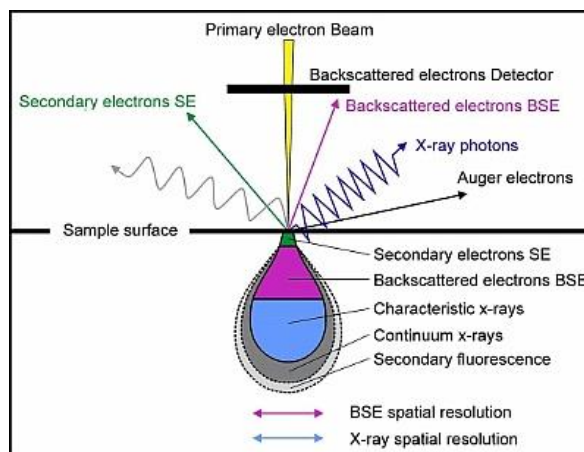


**Figure 3.8:** Interaction between electron beam and sample

FE-SEM needs an ultra-high vacuum (in a range between  $10^{-8}$  and  $10^{-10}$  Torr) in the column of the microscope. The vacuum is needed to minimize the interaction between air and electrons, optimize the efficiency of signal detection, and avoid the dispersion of the beam before it reaches the sample, allowing the reduction of the spot size (it is the diameter that the cone of the incident beam forms with the surface of the sample area).

A SUPRA™ 40 (ZEISS) FE-SEM was used for this thesis work, equipped with a point source thermal FE (Schottky), which exploits both the thermionic effect and the Field Emission one. The measurements have been performed with an acceleration voltage of  $\sim 1,2$  kV and with a working distance of 5 mm.

### 3.3.3 Raman Spectroscopy

In general, vibrational spectroscopy is used to determine the vibration frequencies of a molecule. When a monochromatic electromagnetic radiation interacts with a sample, it can (depending on the wavelength of the light and on the nature of the sample) either be transmitted, i.e. pass through it without undergoing modifications, or be absorbed. In the latter case, an infrared (IR) absorption spectrum is obtained. A small part of the incident radiation is also diffused by the sample elastically, that is with the same frequency as the incident radiation. This effect is known as Rayleigh diffusion. Another even smaller amount of radiation is then diffused by the sample inelastically, i.e. with a frequency greater or lower than that of the incident beam; this is the case of Raman effect, which consists essentially in the inelastic diffusion of photons. Therefore, Raman spectroscopy is a vibrational optical spectroscopy, i.e. a technique of material analysis based on the phenomenon of diffusion of a monochromatic electromagnetic radiation by the sample.

A typical Raman scattered light spectrum is given by scattered light intensity as a function of the shift in frequency from the incident radiation. This shift is defined as the difference between the wavelength of the scattered radiation emitted by the sample and the wavelength of the incident radiation emitted by the source.

The choice of the excitation source in Raman spectroscopy is fundamental. In most samples the faint Raman signals are obscured by background fluorescence. Fluorescence is the property of some substances to re-emit the received electromagnetic radiation, in most cases

with longer wavelength and therefore with lower energy. Generally, the fluorescence decreases if the energy of the excitation source decreases, that is if its wavelength passes from the visible to the near IR region (NIR). This means that, as excitation sources, laser are commonly chosen, because they emit in the far infrared and in the NIR, reducing background fluorescence. Not only the fluorescence, but also the intensity of the Raman signal decreases with increasing wavelength, which is why the longer wavelength that can be used for source radiation is in practice 1064 nm. The ideal situation is to choose the lowest laser wavelength that is able to prevent the phenomena of fluorescence, but without introducing problems due to the corresponding higher energy, such as overheating of the sample or photodegradation (in this last there would be a break in the structural bonds of the sample material at the moment of relaxing the excited state).

Moreover, Raman spectroscopy is an immediate non-destructive technique that can be carried out directly on the sample without any preparation and that doesn't need particular conditions for the execution of the test. Raman spectroscopy is considered the most suitable material analysis for the family of carbon-based materials [29].

A Raman microscope is made of the following components, as shown in Fig. 3.9:

- A monochromatic excitation light, that is a laser source;
- A sampling system to send the laser beam onto the sample, consisting in the objective lens;
- The sample: from it the scattered light is distributed in all directions. Two observation geometries are generally used: one, in which the light diffused at  $90^\circ$  with respect to the direction of the incident beam is observed, and the other in which the light diffused at  $180^\circ$  with respect to the direction of the incident beam is observed (back-scattered light, more intense than the first);
- A filter to separate the Raman signal from the light scattered in an elastic way. In fact the light diffused by the sample contains both the Rayleigh and Raman components. The first must be eliminated because it is too intense compared to the second. The filter has to cut only the light with the same frequency of the incident light. For this purpose Notch filters are used, and every type of laser must have a Notch filter designed for its specific wavelength;
- A spectrometer, i.e. a part dedicated to the dispersion of the light, that occurs thanks to one or more diffraction gratings. These diffract each wavelength of the incident beam at different angles. Each of these rays will follow a different path, before they are recombined together in a detector;
- A detection system. For this purpose, devices CCD are nowadays generally used (Charge Coupled Devices). CCDs are integrated circuits formed by a grid of semiconductor Coupled elements that accumulate an electric Charge proportional to the intensity of the electromagnetic radiation that hits them. By sending sequence of pulses to the Device, an electrical signal is obtained in output, thanks to which it is possible to reconstruct the matrix of the pixels that make up the image projected on the surface of the CCD itself. This information can be used directly in its analogical form, to reproduce the image on a monitor, or it can be converted into digital format for storage in files.

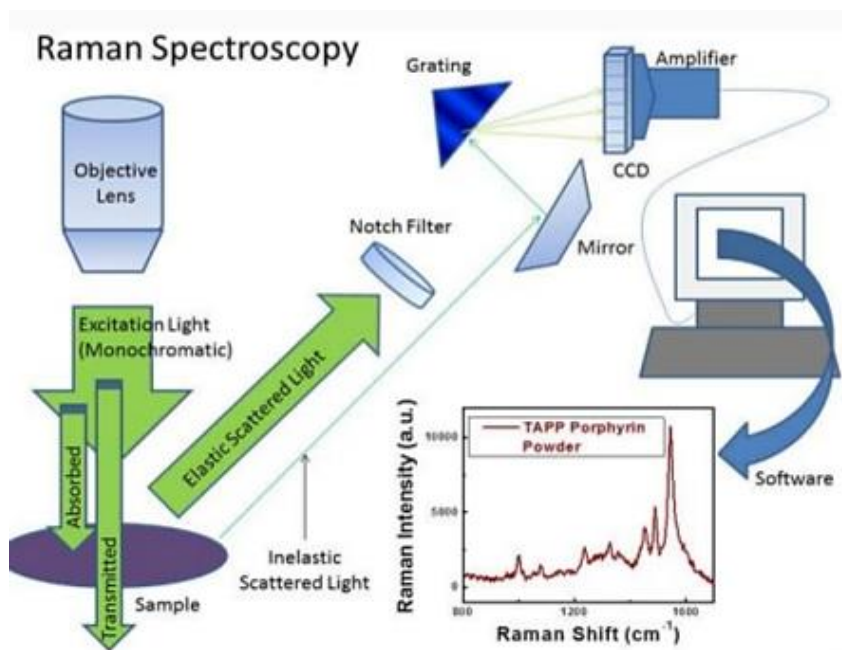


**Figure 3.9:** Raman spectroscopy equipment

The Raman equipment used in this work is that in the Fig. 3.10 and it is a Renishaw InVia Qontor Raman microscope. The inVia Qontor micro-Raman, thanks to an innovative LiveTrack focusing technology developed by Renishaw, allows to analyse samples with irregular, curved or rough surfaces. The system is able to maintain an optimal focus during data acquisition, allowing to show 3D Raman chemical images and chemical/topographical pictures. It is equipped to work up to 100X magnification, with measurements in backscattered light configuration with a cooled CCD camera as detector.

Four laser excitation wavelengths are available for this system:

- 325 nm, He-Cd laser (Kimmon IK Series), with a maximum power of 200 mW;
- 442 nm, He-Cd laser (Kimmon IK Series), with a maximum power of 300 mW;
- 532 nm, solid state diode (Renishaw), with a maximum power of 500 mW;
- 785 nm, solid state diode (Renishaw), with a maximum power of 500 mW.

The system is equipped with edge filters and four diffraction gratings (1200 l/mm, 2400 l/mm for excitation in the visible range, 2400 l/mm for excitation in the UV range, and 600 l/mm) for Raman mapping of surfaces in different conditions. Raman mapping can be performed in point configuration or in streamline configuration. Data analysis and elaboration can be performed with Wire 5.1 software by Renishaw.

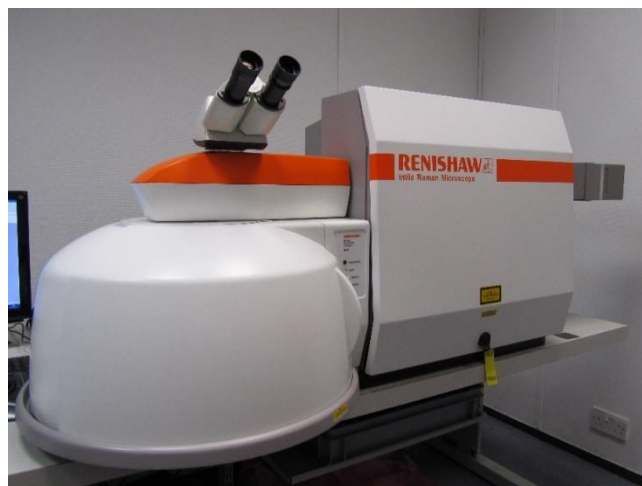


**Figure 3.10:** Renishaw InVia Qontor Raman microscope

The experimental conditions used to obtain Raman spectra and maps are:

- Wavelength: 532 nm;
- Beam power: 1%;
- Magnification: 50X.

### **3.4 Mass Transport measurements**

Diffusion transport study can be used as an indirect characterization to evaluate the quality of the transferred graphene. Diffusion measurements through graphene/PCTE membrane were carried out using NaCl solution and Diclofenac solution.

NaCl solution (500 mM) was prepared by mixing 1,461 g in 50 ml of de-ionized water while Diclofenac solution (10 mM) was prepared by dissolving 0,159 g diclofenac sodium salt in bidistilled water under vigorous magnetic stirring for 30 min at room temperature. NaCl and Diclofenac diffusion through the graphene membranes obtained in this work thesis were tested by employing the side-bi-side diffusion cell described below and by measuring the change in conductivity of the permeate solution as a function of time. In fact, as NaCl or Diclofenac ions diffuse through the membrane from the feed to the permeate side (initially containing only distilled water) the conductivity increases.

#### **3.4.1 Side-bi-side diffusion cell**

A 5 ml Side-Bi-Side glass diffusion cell from PermeGear Inc., USA, was used for this study, and it is shown in Fig. 3.11.



**Figure 3.11:** Side-Bi-Side cell on a stirrer

The system has one port on each side for filling and sampling the chambers. It is composed of two facing glass chambers having the same volume on each side of the joint. The Side-Bi-Side cell is supplied with Teflon stoppers and stir bars for both sides.

After the membrane sample is placed between the cell chambers, a stainless steel cell clamp is placed around them. The knob is at this point tightened to keep the glass chambers and the membrane together. The overall system is then positioned above the H-Series Stirrer shown in Fig. 3.12 by placing the clamp holes over pins on the stirrer surface. The stirrer used is an H1C stirrer produced by PermeGear Inc., USA.



**Figure 3.12:** H1C stirrer: 1-station Side-Bi-Side cell stirrer with cell clamp

A scheme of the complete assembly above described is shown in Fig. 3.13:

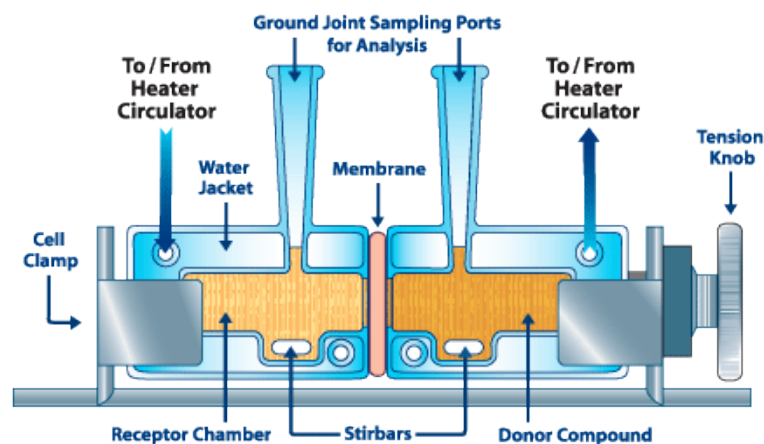
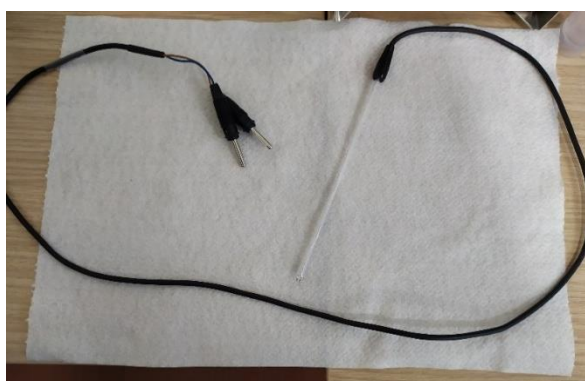


**Figure 3.13:** Side-Bi-Side cell viewed straight on

### 3.4.2 Calibration procedure of the probe

To quantify the amount of NaCl and of Diclofenac diffused through the membrane into the permeate side of the cell, a calibration of the electrode probe was carried out. Calibration is necessary to obtain connect the linear correspondence between the conductivity value read by the electrode probe and the concentration of NaCl or Diclofenac in the solution. The mass transport measurements were then carried out introducing in the Side-bi-Side left chamber NaCl or Diclofenac solutions, and in the right chamber de-ionized water. Thanks to the calibration procedure, it is possible to directly monitor the change in concentration on the right side of the cell over time. The calibration was carried out following this procedure:

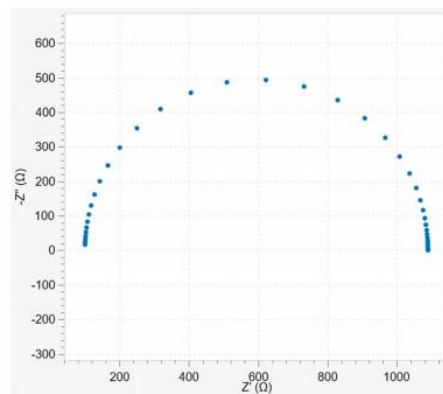
- 6 different NaCl or Diclofenac solutions were prepared from a mother solution with the method of serial dilutions. In the first case the mother solution was a 500 mM NaCl solution and in the second case it was a 10 mM Diclofenac solution;
- The two chambers of the cell are clamped together using the cell clamp and regulating the tension knob, after positioning a polymeric o-ring between the empty chambers;
- Both chambers of the Side-Bi-Side were filled with known concentration solutions;
- A two-tips electrode probe (shown in Fig. 3.14) is immersed into the Side-Bi-Side cell, dipping it into the solution.



**Figure 3.14:** Two-tips platinum electrode

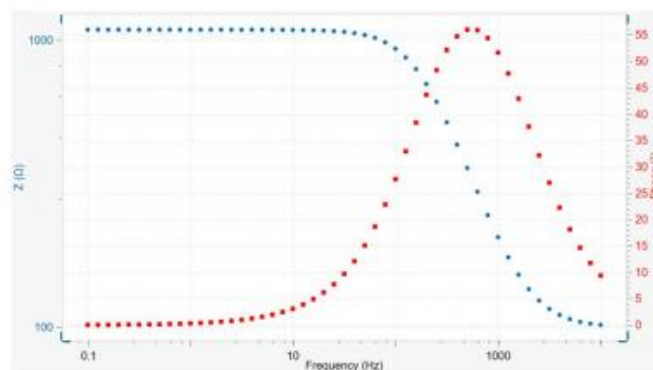
This electrode is connected through cell cables to one channel of a Multi Autolab M101 potentiostat/galvanostat, purchased from Metrohm Autolab B.V., Netherlands. This potentiostat is connected via an USB interface to the computer, where data analysis and elaboration can be performed with NOVA 2.1 software by Metrohm.

- Calibration was carried out using Electrochemical Impedance Spectroscopy (EIS) and consisted of measuring the impedance of the solutions over a wide frequency range. The starting point of all impedance methods is to apply a small amplitude sinusoidal excitation signal to the system investigated and measure the response. In this case the applied signal is a sinusoidal tension and the measured response is a current. The impedance  $Z$  [ $\Omega$ ] is the tendency of a system to oppose the passage of an alternating current (AC).  $Z$  is a complex quantity with a magnitude and a phase shift which depends on the frequency of the signal. Therefore, by varying the frequency of the applied signal, the impedance of the system as a function of frequency can be obtained. In this case a frequency range of 100 kHz – 10 Hz was used. The plot of the real part of impedance against the imaginary part gives the so-called Nyquist Plot, shown in Figure 3.15.



**Figure 3.15:** Nyquist plot

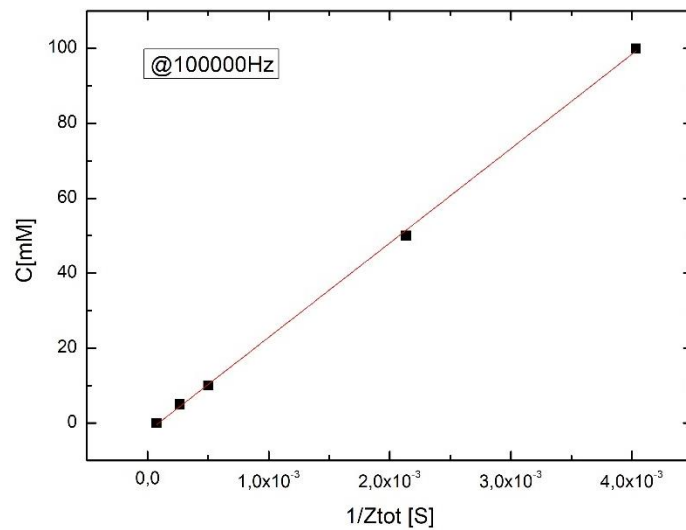
Instead the impedance modulus and the phase shift are plotted as a function of frequency in the so-called Bode plot, shown in Figure 3.16.



**Figure 3.16:** Bode plot. In blue the  $Z$  modulus vs. frequency. In red the phase vs. frequency.

Both these spectra of impedance are obtained using abovementioned NOVA software;

- In the case of NaCl, the six solutions prepared for serial dilutions were: 500mM, 100mM, 50mM, 10mM, 5mM, and 0mM (de-ionized water). In the case of Diclofenac, solutions prepared were instead 10 mM, 5 mM, 2,5 mM, 1 mM, 0,1 mM, 0 mM. For each solution the impedance was measured. Five impedance measurements were performed, in order to take into account any possible variation of experimental conditions. From each measurement the impedance was obtained in output, as a function of the varying frequency, as shown in Fig. 3.16;
- For each of the frequencies (41 frequencies from 100 kHz to 10 Hz) it was performed a linear fit between the impedances and the concentrations of the six solutions: concentration was plotted as a function of the reciprocal of impedance  $Z$ , as shown for example in Fig. 3.17 and 3.18. OriginPro software was used in order to perform this linear fit;
- Once obtained these linear fits, the squared deviation coefficient  $R^2$  was calculated for each line. The line with a coefficient  $R^2$  as close as possible to 1 was identified. The selected calibration line corresponds to a certain frequency, which has finally been set in the Autolab software as the working frequency. This frequency will be the one at which measurements will be carried out in diffusion transport study;
- In the case of probe calibration with NaCl solutions, the selected calibration line with  $R^2$  nearest to 1 is the  $C$  vs  $1/Z_{tot}$  line corresponding to 100.000 Hz, shown in figure 3.17.



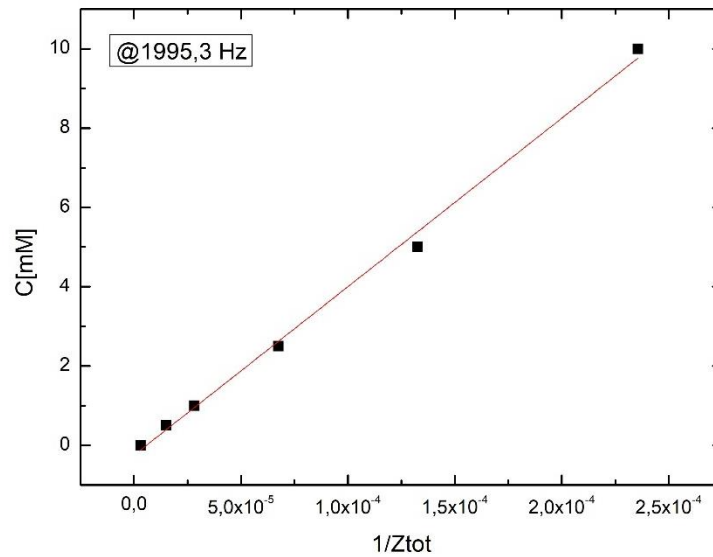
**Figure 3.17:** Calibration curve for NaCl solutions

Table 3.6 shows the values of  $R^2$ , slope and intercept of the calibration curve with relative errors, provided by the linear fit performed with Origin;

**Table 3.6:** Linear fitting data for NaCl solution

	Value	Standard error
Intercept	-2,31526	0,6561
Slope	25191,3175	319,12115
Average square deviation coefficient $R^2$	0,99936	---

- In the case of probe calibration with Diclofenac solutions the calibration line with  $R^2$  closest to 1 is the  $C$  vs  $1/Z_{tot}$  line corresponding to 1995,3 Hz, shown in Fig 3.28.



**Figure 3.18:** Calibration curve for Diclofenac solutions

Table 3.7 shows the values of  $R^2$ , slope and intercept of the selected calibration line with relative errors.

**Table 3.7:** Linear fitting data for diclofenac solutions

	Value	Standard error
Intercept	-0,24623	0,14166
Slope	42486,98527	1237,28974
Average deviation square coefficient $R^2$	0,99577	---

### 3.4.3 Transport study experimental procedure

Once completed the calibration procedure, the diffusion transport study was carried out following this experimental procedure:

- Both cell chambers are cleaned and air-dried every time before beginning the measurements, as well as each part of the Side-By-Side cell;
- Magnetic stir bars are put into both cell chambers;
- The membrane is put between the two cell chambers, with the graphene side facing the left chamber;
- The chambers of the cell are at this point clamped together using the cell clamp and regulating the tension knob, after positioning an o-ring between the chambers, next to the sample;
- In the left chamber are introduced 5 ml of 500mM NaCl solution or 5 ml of 10 mM Diclofenac solution, while in the right chamber are introduced 5 ml of de-ionized water in both cases;

- The stirrer is switched on before data acquisition, in order to magnetically stir both solutions during diffusion study, so to avoid effects of concentration polarization on the membrane surface;
- The platinum conductivity electrode is put into the right sampling port, dipping it in de-ionized water, as in Fig. 3.19. The ions diffuse through graphene membrane toward the de-ionized water side of the cell. In the right chamber the change in concentration  $[mol/l]$  with time  $[s]$  is monitored, by using the previously found linear correspondence between the conductivity measured by the probe with this in-line analysis and the concentration. This last is recorded every 20 seconds for one hour for each tested sample, with the software NOVA Autolab. The measurements are made at the frequency previously selected for calibration;
- After one hour the test is stopped, the stirrer switched off and the membrane removed, in order to wash every part of the system and re-start another test with another sample.

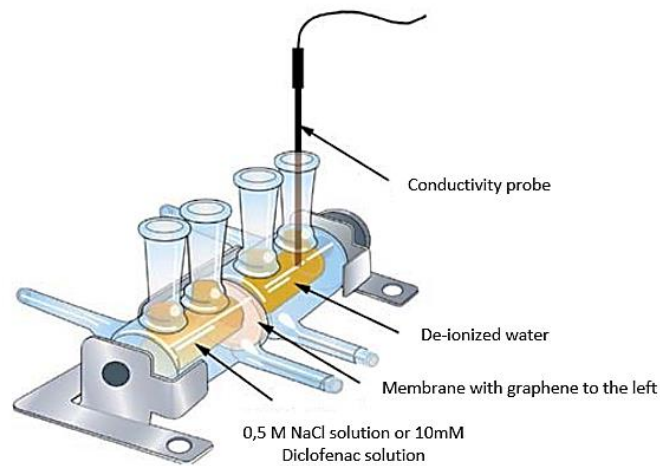


**Figure 3.19:** Diffusion transport study assembly. (In Side-bi-Side cell here used the sampling ports are one per chamber and not two). [22]

## 4. RESULTS AND DISCUSSION

### 4.1 Transfer process

The presence of a single layer or of multiple layers of graphene on PCTE is easily distinguishable after the transfer process by the naked eye. Actually, the colour of the starting PCTE membrane, which is white, changes to grey and becomes darker as the number of graphene layers is increased. This difference can be appreciated in Fig. 4.1. It is worth noting that the sample shown in Fig. 4.1 has been intentionally fabricated by using a graphene sample with an area lower than the size of the PCTE support. This was done to appreciate the effective presence of graphene after the transfer process, by optical contrast. All the membranes tested for filtration have been prepared with all the PCTE area covered with graphene, i.e. the active area of graphene sample coincides with the entire area of the PCTE membrane (PCTE membrane diameter is  $\approx 25$  mm).

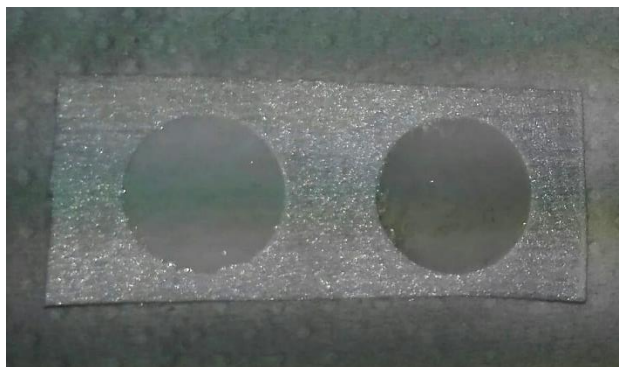


**Figure 4.1:** Colour difference between covered and uncovered areas of monolayer graphene/PCTE membrane

The quality of transferred graphene is generally affected by some features of the substrate support. The first one is the surface roughness of the substrate; the surface should be as smooth as possible, in order to provide a good contact with the graphene layer and avoid the formation of cracks. Secondly, if the pore size would be the smallest possible, a good suspension of the graphene film over the pores would be ensured, limiting the collapse of suspended graphene as much as possible. The last parameter is the substrate wettability, studied with contact angle tests, as follows. A hydrophobic surface is mandatory to exploit Van der Waals force electrostatic interactions and to favour the adhesion of graphene to the PCTE support.

### 4.2 Characterization of membranes

For comparative purposes, the characterization results of graphene/PCTE membranes will be compared with the ones of the supporting PCTE membranes, which is used as a reference material in this work.

### 4.2.1 Contact angle measurements on PCTE

The surface hydrophobicity of the substrate is necessary to promote an intimate contact between the graphene sample and the PCTE membrane. This also prevents the infiltration of the etching solution at the interface between graphene and the PCTE substrate during the transfer process, avoiding delamination. Contact angle measurements were carried out in order to determine the surface wettability of the substrate material. The average water contact angle for bare PCTE membranes has been estimated in triplicate as described in Materials and Methods section, and the results are shown in Table 4.1.

**Table 4.1:** Contact angle measurements for PCTE substrate

	Trial 1	Trial 2	Trial 3	Average
Contact angle [°]	78	83	84	81,7 ± 3

The measured contact angle approaches 90° and therefore it is representative of a hydrophobic behaviour.

In Fig. 4.2 there is an example of image obtained from water contact angle measurements by sessile drop method, on PCTE.



**Figure 4.2:** Water drop dispensed on PCTE and the corresponding contact angle value

### 4.2.2 Contact angle measurements on PCTE/graphene membranes

The contact angle values for PCTE/SLG membranes are reported in Table 4.2.

**Table 4.2:** Contact angle measurements for PCTE/SLG membranes

	Trial 1	Trial 2	Trial 3	Average
Contact angle [°]	84	89	89	87,3 ± 2,5

In Fig. 4.3 there is an example of image obtained from the contact angle measurements performed on PCTE/SLG.

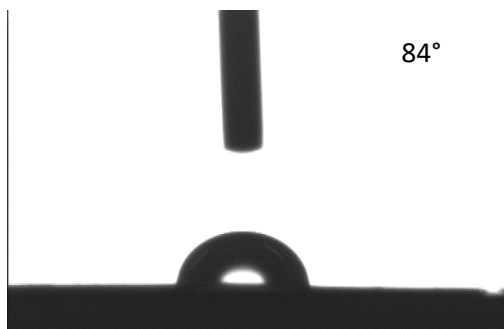


**Figure 4.3:** Water drop dispensed on PCTE/SLG and the corresponding contact angle value

The hydrophobicity of graphene is still a debated topic: the intrinsic hydrophobicity of graphene is in fact mainly supported by theoretical studies [15]. It is in fact practically impossible to measure the contact angle on an atomic thickness layer; being the graphene always supported on a substrate material, the interaction with the latter will always influence the final value of graphene contact angle. Many groups talk about the wetting transparency of single layer graphene [30,31], i.e. a notable dependence of graphene contact angle on the nature of substrate. In other terms, graphene coating does not induce a consistent variation in the wettability of the substrate. It has been demonstrated that substrate can considerably affect the wettability of graphene, but the inherent mechanism remains elusive. Here it is experimentally shown that between PCTE and PCTE/SLG membranes there is almost no difference in the contact angle value, a difference that instead is accentuated as the number of layers increases.

The contact angle values for PCTE/DLG membranes are reported in Table 4.3.

**Table 4.3:** Contact angle measurements on PCTE/DLG

	Trial 1	Trial 2	Trial 3	Average
Contact angle [°]	74	75	76	75 ± 1

In Fig. 4.4 there is an example of image obtained from the contact angle test on PCTE/DLG.

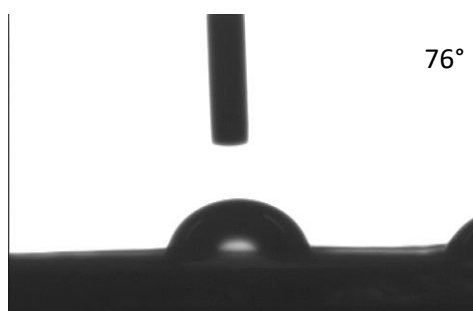


**Figure 4.4:** Water drop dispensed on PCTE/DLG

Finally, the contact angle values for PCTE/TLG membranes are reported in Table 4.4.

**Table 4.4:** Contact angle measurements on PCTE/TLG membranes

	Trial 1	Trial 2	Trial 3	Average
Contact angle [°]	64	65	71	66,7 ± 3,5

In Fig. 4.5 there is an example of image obtained from the contact angle test on PCTE/TLG.

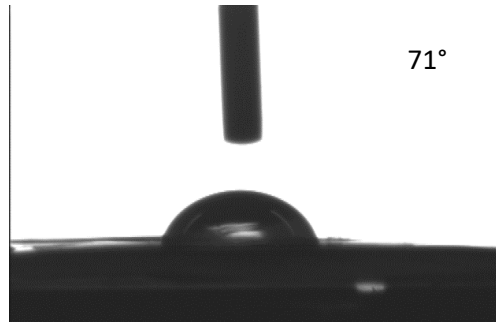


**Figure 4.5:** Water drop dispensed on PCTE/TLG

It can be stated from these data that the general trend is a decrease of the contact angle value as the number of graphene layers increases. It could be hypothesized that the effect of the defective graphene becomes predominant with respect to that of underlying PCTE. In fact, even if graphene should theoretically be hydrophobic, few defects are sufficient to make it less hydrophobic. Moreover, the contact angle technique is mainly sensitive to surface features not comparable with local defects or pores, as it is evaluated by the deposition of a macroscopic drop (average volume 1,5  $\mu\text{L}$ ). On the other hand, from a microscopic point of view some pores and defects in the graphene membranes could be locally hydrophilic, as the unstable dangling bonds at the edge of pores could be saturated with functional groups that give them a polar nature (such as -OH). This can lower the degree of hydrophobicity of this system. This effect of pore chemistry on membrane performance was studied by Tanugi and Grossman [13], which stated that water permeability for nanoporous graphene with hydroxylated pores (hydrophilic) was significantly enhanced compared to that of hydrogenated ones (hydrophobic), thanks to a remarkable hydrophilicity provided by hydroxylated pores. These could be some of the reasons why graphene does not show the lotus leaf effect that would be expected.

### 4.2.3 FE-SEM images of PCTE membranes

FE-SEM images in Fig. 4.6 show the typical surface morphology of 0,1  $\mu\text{m}$  PCTE substrate.

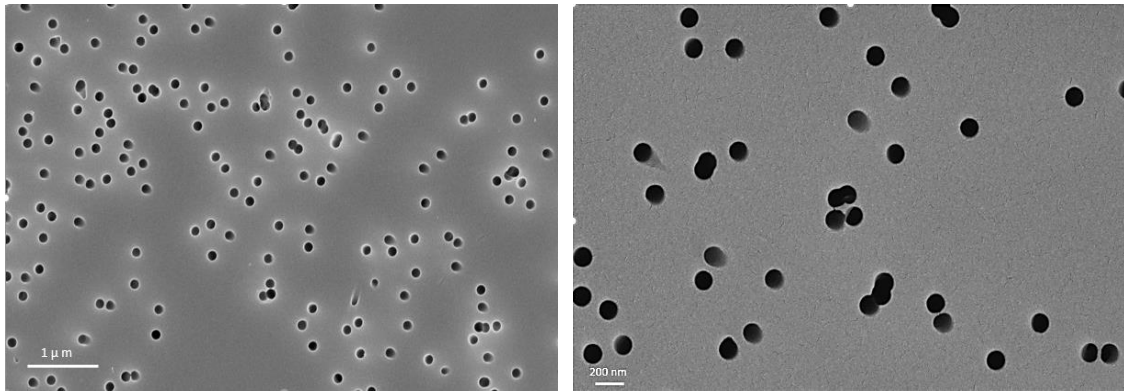


**Figure 4.6:** FE-SEM images of PCTE acquired at different magnifications. Left panel: 50kX. Right panel: 100kX

In the left panel some zones characterized by a greater pore density than others are distinguishable. Moreover, most membranes actually contain a distribution of pore sizes. The nominal pore size assessment typically refers to the predominant pore size (0,1 μm) but larger and smaller pores may be present too, as confirmed by Sterlitech company itself. In the right panel it is evident the coalescence of some pores, which joining together lead to a larger pore. Larger holes can lead to local rupture of graphene film and to its collapse into the pores. Both these phenomena can influence the homogeneity of the suspended graphene, as well as the presence of cracks and wrinkles.

#### 4.2.4 FE-SEM images of PCTE/graphene membranes

FE-SEM images in Fig. 4.7 show transferred SLG on PCTE substrate.

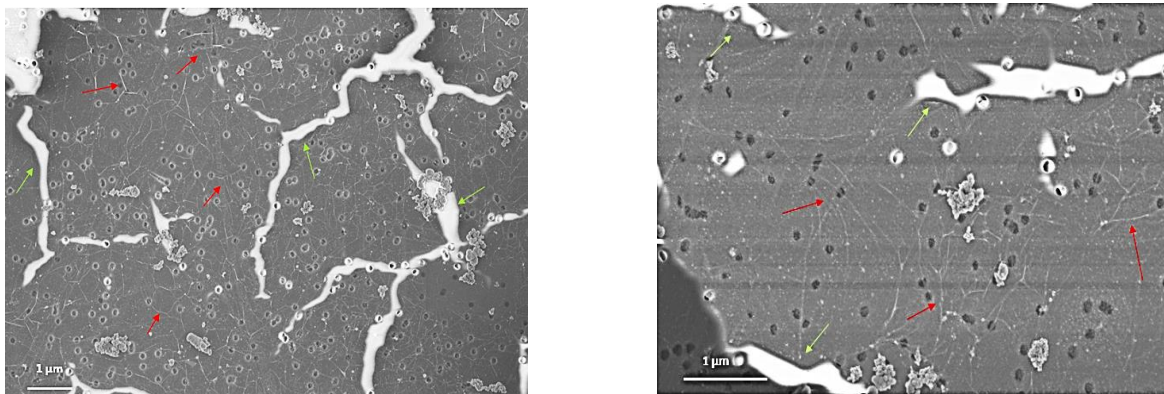


**Figure 4.7:** FE-SEM images of PCTE/SLG acquired at different magnifications. Left panel: 25kX. Right panel: 50kX

The areas characterized by the presence of graphene are clearly distinguishable thanks to the presence of wrinkles (some of them are indicated by red arrows), which are typical of graphene transferred on any substrate. The brighter areas are instead those where the PCTE is un-covered (indicated by green arrows). It can be also observed that most of the pores are covered with single layer graphene.

These FE-SEM images confirm a good coverage degree and a satisfactory quality of graphene film, but nanometer-scale intrinsic defects and micrometer-scale tears as well as

uncovered PCTE regions are still present, especially in proximity of the regions suspended over the substrate pores, as shown in Fig.4.8.

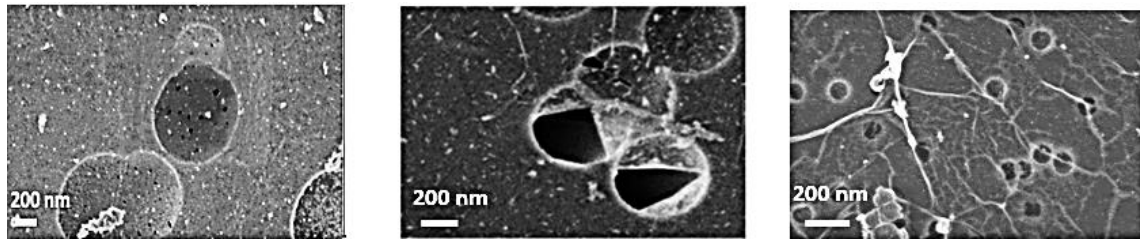


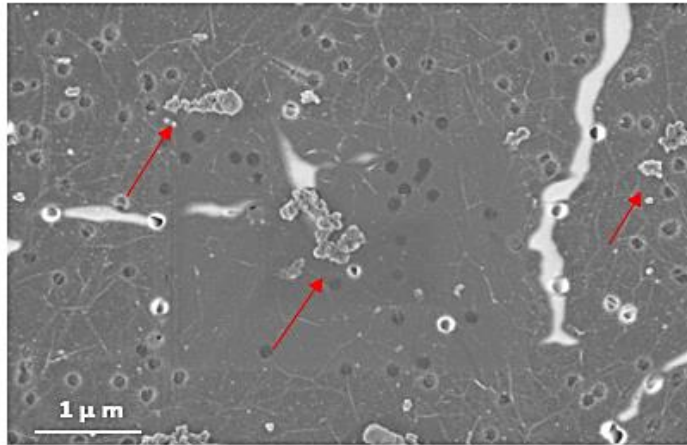
**Figure 4.8:** Left panel: nano-meter scale intrinsic defects. Central panel: partial coverage of pores. Right panel: rupture of graphene suspended over the pores

Depending on the origin and average dimension, defects within graphene can be grouped into intrinsic and extrinsic ones.

Intrinsic defects are nanometer-sized pores ( $< 20$  nm in size). It could be assumed that these defects are generated during the CVD graphene growth on Cu. It is known that Cu easily tends to return to its oxidized state CuO, that is the thermodynamically stable state. For this reason, H<sub>2</sub> reducing agent is injected into the reagents chamber during CVD process. However, if the reduction is not uniform over the entire Cu surface, some islands of CuO will remain, locally inhibiting the graphene growth, thus inducing pores of nanometric size. O'Hern et al. [19] confirmed that defects formed during the growth of graphene on Cu were responsible for these nanometer-scale pores. Analysing the graphene lattice structure via aberration-corrected scanning transmission electron microscopy (STEM), they observed that CVD grown graphene contained pores in the size range of 1-15 nm, which is comparable with pores observed for the PCTE/SLG membranes developed in this work.

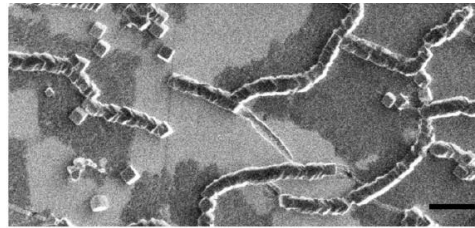
Extrinsic defects as cracks and tears that could derive from the transfer process and handling of the membranes. Defects induced by the transfer procedure could be related to the substrate features such as its roughness and wettability. Another important factor is the etching process, as the etchant could attack graphene domains, leading to a structural weakness of the graphene structure and its delamination from the polymeric support [22]. The partial coverage of the pores of the substrate and the rupture of graphene suspended over them are problems that can be minimized by choosing substrates with pores as smaller as possible. In this work, 0,1  $\mu\text{m}$  pore substrates were found to well prevent tearing of unsupported graphene domains, as shown by FE-SEM analyses.

The agglomerates indicated by arrows in Fig. 4.9 are extraneous to the rest of graphene film and are supposed to be contaminating residues of FeCl<sub>3</sub> etchant, which is very difficult to remove during the washing process of the membranes.



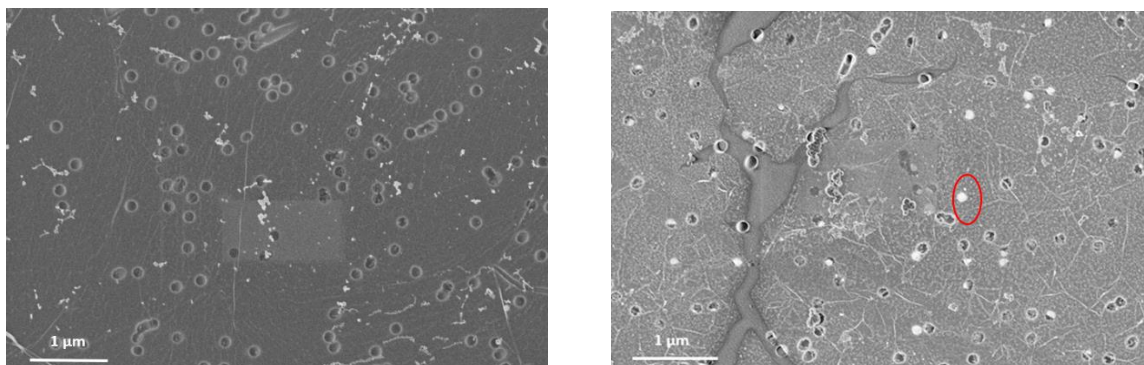
**Figure 4.9:** Contaminating residues of  $\text{FeCl}_3$

Fig. 4.10 from [19] shows a SEM image of graphene on Cu after exposure to  $\text{FeCl}_3$  etchant. It has been observed that crystalline reaction products tend to remain on the graphene surface and tear the graphene.



**Figure 4.10:** SEM image of graphene on copper after exposure to  $\text{FeCl}_3$  [19]. Scale bar  $1\mu\text{m}$

FE-SEM analysis on PCTE/SLG membranes was repeated after the NaCl filtration tests, in order to verify if the samples had been damaged during the test in Side-bi-Side cell or by simply handling the membranes during the various steps. The images would seem to confirm that the membrane was not damaged at all, in fact the appearance of the graphene film, the degree of coverage and the appearance of the pores seem to be very similar as before the ion transport measurements, as shown in Fig. 4.11.



**Figure 4.11:** FE-SEM images of PCTE/SLG. Left panel: image acquired before filtration test. 50kX. Right panel: image acquired after filtration test. 50kX

The only remarkable difference is the presence of white spots that are attributed to the adhesion of some salt crystals on the membrane surface during mass transport experiments. One of them is indicated by a circle.

FE-SEM images in Fig. 4.12 are referred to PCTE/DLG membranes and to PCTE/TLG membranes. The deposition of a greater number of layers can be deduced from the presence of wrinkles much more numerous and from a smaller number of uncovered areas.

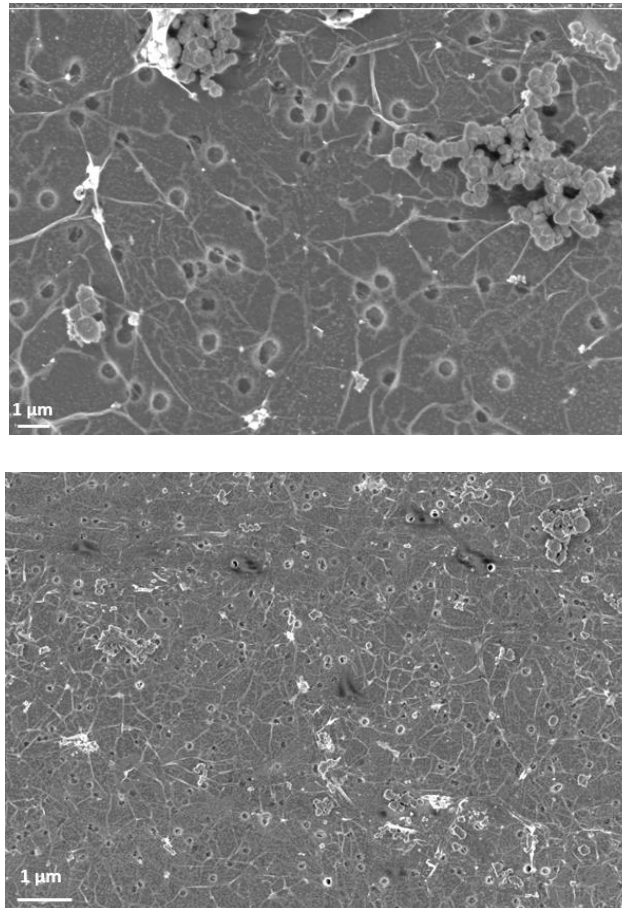


**Figure 4.12:** Top panel: DLG/PCTE. 25kX. Bottom panel: TLG/PCTE. 25kX.

#### 4.2.5 Raman spectroscopy

Raman characterization was performed on PCTE microporous support and on three graphene membranes (SLG, DLG, TLG membranes) in order to evaluate the quality of the graphene suspended over the PCTE support. Raman normalized spectra are reported in Fig. 4.13. Since they have been normalized with respect to the highest peak height, there intensity in the y-axis is reported in arbitrary units. Three vertical straight lines were drawn at the characteristic wavelengths of the D, G and 2D peaks.

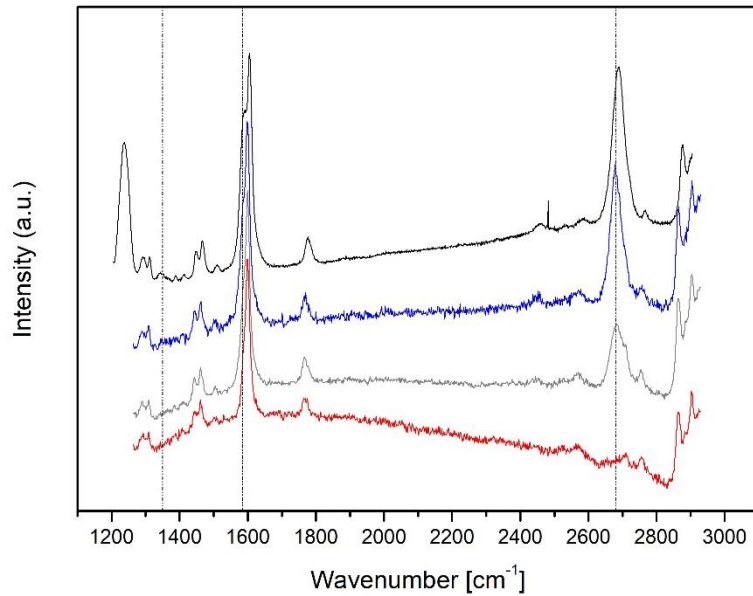


**Figure 4.13:** Red: PCTE Raman spectrum. Grey: PCTE/SLG Raman spectrum. Blue: PCTE/DLG Raman spectrum. Black: PCTE/TLG Raman spectrum. Each spectrum has been obtained with a laser wavelength of 532 nm, a beam power of 1% and a magnification of 50X.

As it emerges from Fig. 4.13 and from the zoom reported in Fig. 4.14, PCTE membrane has a main peak at the wavelength of  $1604\text{ cm}^{-1}$ , which corresponds to the phenyl ring vibration mode of polycarbonate [32]. Such resonance peak is close to the G peak of graphene noticed at  $1580\text{ cm}^{-1}$ . Due to this overlap, considerations on Raman spectra of graphene-based membranes will be made only with respect to 2D peak. This is also the reason why only 2D peak has been selected and mapped in intensity, as shown later. Actually, as indicated in spectra magnification in Fig. 4.15, this PCTE peak is shifted at a wavelength greater than that typical of G peak, whose presence is confirmed by a shoulder peak at  $1580\text{ cm}^{-1}$ . It derives from the reticular vibrations of the C-C bond in  $\text{sp}^2$  hybridization.

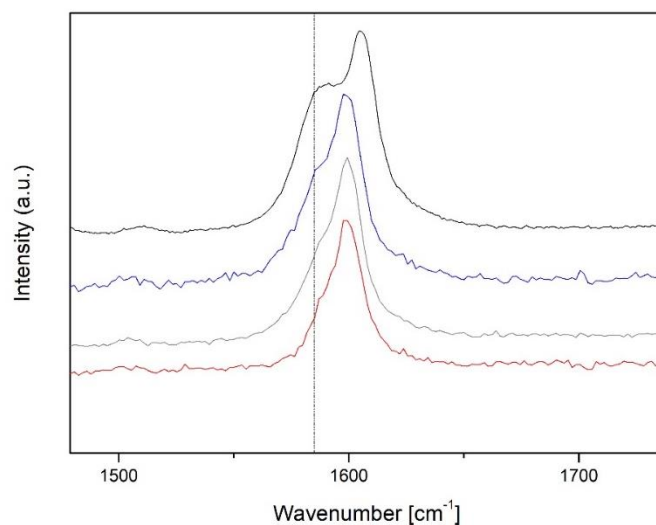


**Figure 4.14:** Raman spectra magnification of G peak. Red: PCTE Raman spectrum. Grey: PCTE/SLG Raman spectrum. Blue: PCTE/DLG Raman spectrum. Black: PCTE/TLG Raman spectrum.

- Therefore, it can be concluded that the Raman spectra collected from SLG, DLG, TLG membranes confirm the presence of graphene, whose fundamental peaks are G and 2D. In addition to these two peaks, there is also the D band, which is practically absent. It is in general positioned in the wavelength range from 1250 to 1400  $\text{cm}^{-1}$  and it is due to the “breathing modes” of carbon atoms of hexagonal rings [33]. Graphene D peak gives information on defects or disorder degree in graphene structure so it is a qualitative indication of crystalline quality of as-grown and transferred graphene. A magnification on the wavelengths corresponding to D band is shown in Fig. 4.15. Its absence indicates that the induction of defectiveness is really limited. Unexpectedly, by increasing the number of layers, the D peak is still absent, although an increase could have been expected due to the increased number of transfer processes.

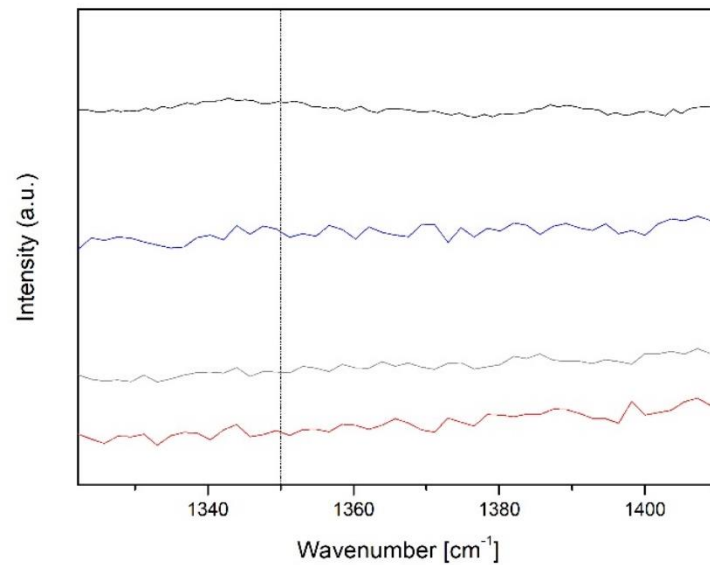


**Figure 4.15:** Raman spectra magnification of D peak. Red: PCTE Raman spectrum. Grey: PCTE/SLG Raman spectrum. Blue: PCTE/DLG Raman spectrum. Black: PCTE/TLG Raman spectrum.

Finally, in Fig. 4.16 a magnification on 2D peaks is reported. The position and the structure of 2D peak depend on the analysed carbon structure and on the number of its layers. In literature [34] it is possible to find that 2D peak is used for the recognition of graphene monolayer or the determination of the number of layers. In order to determine this last, the ratio  $\frac{I_{2D}}{I_G}$  is usually used. Ferrari et al. [34] stated that for a single layer, the intensity of the 2D peak is about four times greater than that of the G peak ( $\frac{I_{2D}}{I_G} \approx 4$ ) [34], and it decreases as the number of layer increases. In the same work they highlighted that as the number of layers increase, also the shape and position of the 2D peak change: for double layer graphene it moves to the right, becomes wider and not symmetrical, as shown in Fig 4.16 b. It is to be specified that these statements on the  $\frac{I_{2D}}{I_G}$  ratio and on the evolution of the 2D peak with the increasing number of layers are valid if a pristine isolated graphene is analysed, or at most for graphene placed on a substrate with which it has no interactions, such as silicon oxide. Therefore, in this case some deviations from these well known considerations are justified by the fact that the graphene is analysed at Raman on the support

of PCTE. In Fig. 4.16 there is a comparison between the trend of the ideal pristine graphene and the graphene on PCTE.

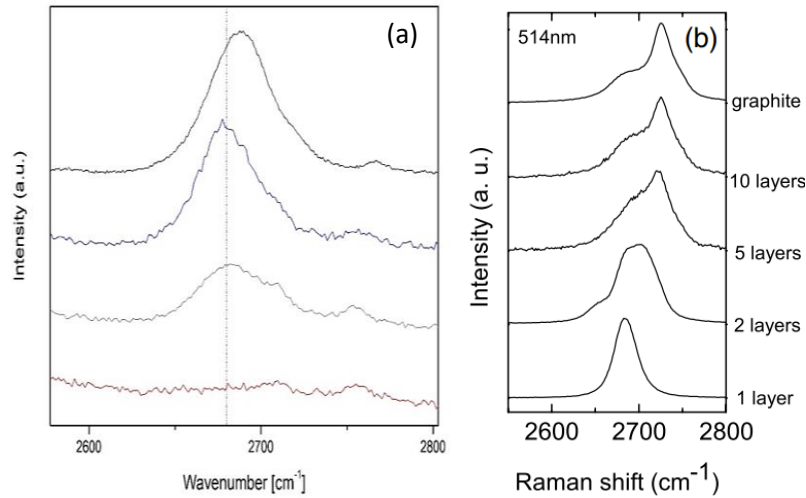


**Figure 4.16:** a) Raman spectra magnification of 2D peak here obtained. Red: PCTE Raman spectrum. Grey: PCTE/SLG Raman spectrum. Blue: PCTE/DLG Raman spectrum. Black: PCTE/TLG Raman spectrum. b) Evolution of the 2D peak with increasing number of layers in a pristine ideal graphene film [34]

In Fig. 4.16a it is possible to notice a more accentuated 2D peak as the number of layers increases and a shift to the right of the 2D peak in the case of the sample with a triple layer of graphene. Although the considerations regarding the shift of the 2D peak to the right as the number of layers increases are strictly valid only for pristine isolated graphene or for graphene on substrates with which it has not interactions, even in this case a similar trend can be observed.

The most important thing is that spectra of the membranes with different number of layers are very similar and consistent with each other, confirming that the stacking of several single layers on top of each other has been successful and the goal of minimizing defects and uncovered areas was achieved.

To have a more direct information about the graphene quality and coverage of PCTE, even after Diclofenac filtration test, a wide portion of TLG/PCTE, i.e. the membrane showing the best blockage of drug, was selected and Raman mapping has been carried out. The generation of images was obtained either horizontally following the surface topography or from vertical slices. The corresponding Raman map is represented in Fig. 4.17.

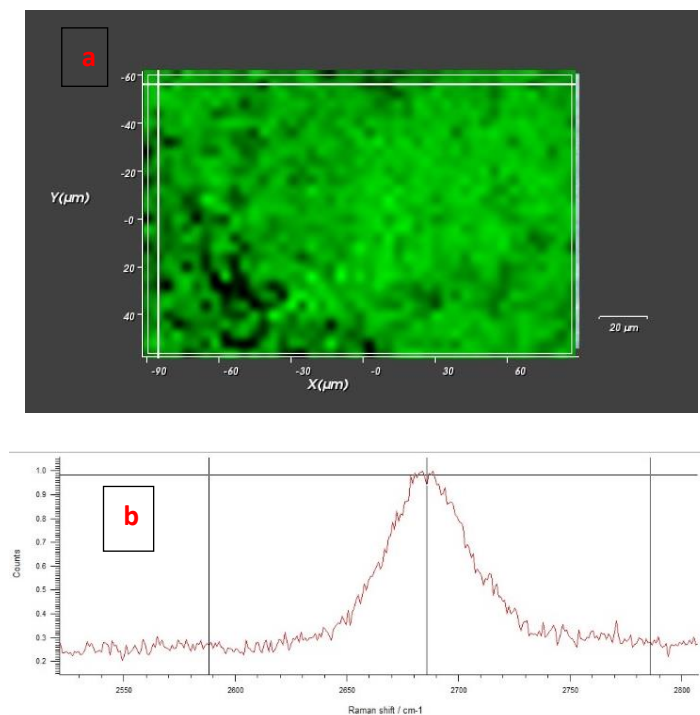


**Figure 4.17:** a) signal-to-baseline spatial Raman map of 2D band. b) Raman signal corresponding to green areas

The explored region is approximately 120 μm x 180 μm and was divided in ~2400 cells. For every cell a single Raman spectrum was acquired. Subsequently, the spatial Raman map was obtained by plotting the signal-to-baseline modality at 2680 cm<sup>-1</sup> (e.g. at the 2D peak), i.e. normalizing the maximum height peak with respect to the spectrum baseline created by the software. The signal-to-baseline value is associated with a colour map, where light green is the maximum and black is the minimum. Thus, it is possible to state that the green zones are those covered with graphene while the black ones are the uncovered ones. Actually, by pointing at the dark zones, in the underlying spectrum only noise is visible without the presence of the 2D peak, while by pointing at the green zones the spectrum returns a well delineated 2D peak, as shown in Fig 4.17 b. This mapping confirms once again an optimal coverage of the tri-layer graphene sample, indicating that the approach based on the use of multilayer graphene for sealing defects could be a good alternative to manufacture graphene/polymeric membranes with minimized leakage pathways.

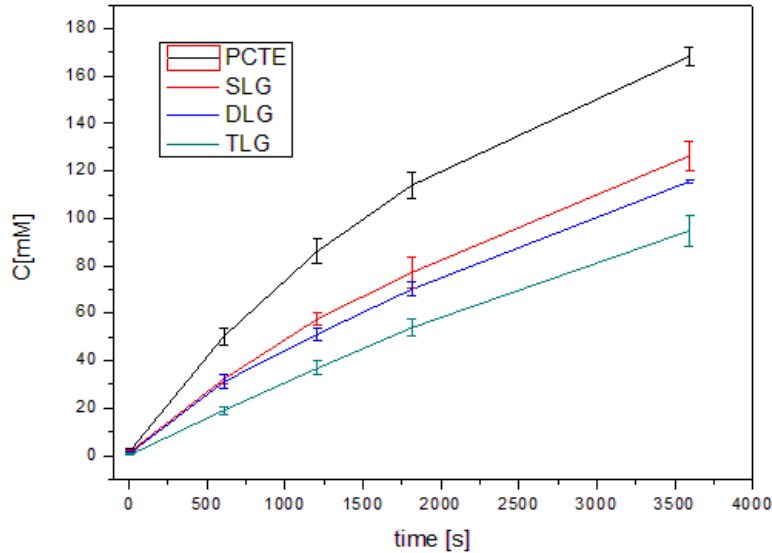
### 4.3 Transport measurements

As pointed out earlier, the quality of the transferred single layer or few layers graphene can be examined by using the ionic transport measurements through the membranes as a functional characterization. In this work, the quality of the transferred graphene is evaluated by monitoring the transport of 500 mM NaCl and 10 mM Diclofenac solutions through the graphene membranes. To ensure statistical relevance of the results, each experiment has been performed in triplicate, so the mass transport was always evaluated on 3 samples per type: 3xPCTE, 3xSLG, 3xDLG, and 3xTLG. In the graphs the curves are shown with the relative error bars. As can be deduced from the narrow error bars, the repeatability has been successfully confirmed.

### 4.3.1 NaCl transport measurements

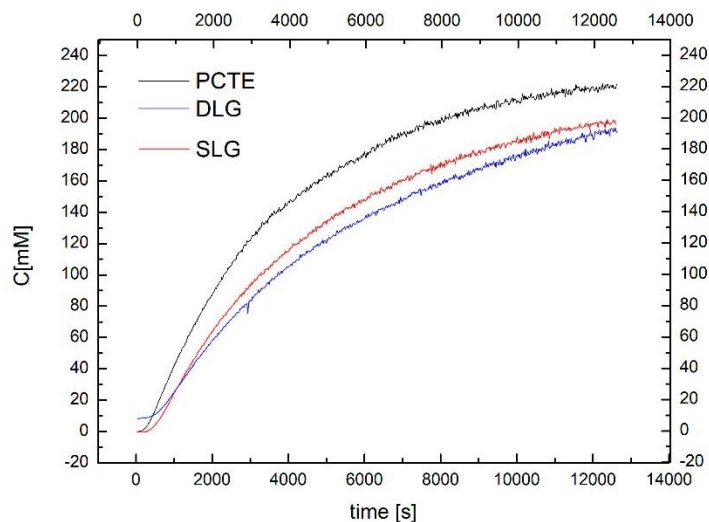
Fig. 4.18 and 4.19 show the results obtained from the NaCl ionic transport.

Fig 4.18 shows the NaCl concentration obtained in the permeate solution for up to 1h. It emerges that NaCl concentration increases with time, indicating the NaCl passage through the graphene/PCTE sample. Concentration versus time plot for the bare PCTE was taken as the reference curve for evaluating the effective ion blockage (% salt rejection).



**Figure 4.18:** NaCl concentration vs time

It is evident the increasing trend of molar concentration in the water side of the cell, but it can be demonstrated that it approaches saturation after a short time, as reported as an example in Figure 4.19. In the image it can be observed that after 3h and 30 minutes the concentration approaches to be constant and is more than halved compared to the initial one.



**Figure 4.19:** An example of NaCl concentration trend in the right side of diffusion cell up to 3,3h

Fig. 4.20 shows the salt rejection trend, defined as in the equation (1.2) of the 1<sup>th</sup> chapter, where  $C_f$  and  $C_p$  are respectively the concentration of the feed (that is constant, 500 mM) and the concentration of the permeate at a specific time. The rejection is calculated for 4 different times: 10 min, 20 min, 30 min, 1 h.

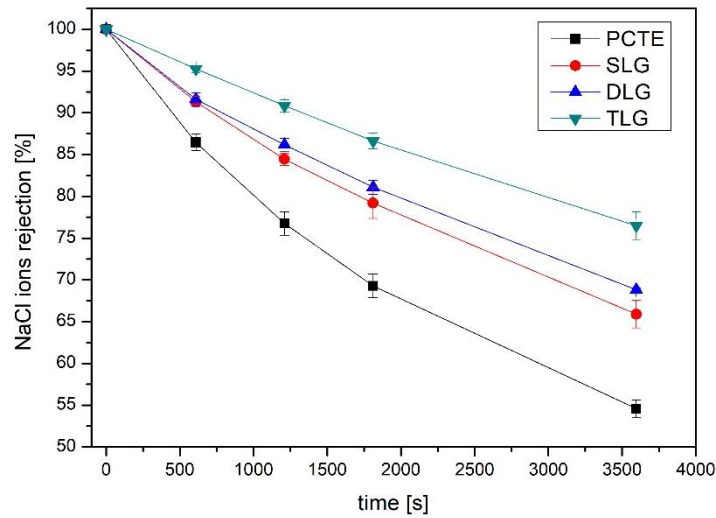


**Figure 4.20:** NaCl salt rejection [%]

The results indicate that the bare PCTE blocked 54,5% of the ion transport after 1h. Graphene single layer transferred on PCTE blocked 65,9% of the ion transport after 1h, while the double layer and triple layer graphene membranes blocked 68,8% and 76,5% of the NaCl transport, respectively. Although it has not reached a complete solute rejection as it would be expected from an ideal graphene film, these results are extremely promising considering that NaCl is one of the most difficult solutes to block because of its reduced size (0.716 nm), and that processes used for desalination purposes usually need costs and pressures far greater than those here used. However, these percentage-numbers are consistent with the FE-SEM characterization results, which has shown the presence of some defects and tears in the transferred graphene layers.

The ion transport flux for both graphene membranes and bare membranes is shown in Fig. 4.21. In order to obtain this column plot the concentration-time curves were linearly fitted and the ion diffusion fluxes were calculated through the slope of the plots. Being the molar concentration measured in mol/L and the time in seconds, the slop will be mol/L\*s, giving directly the ion flux.

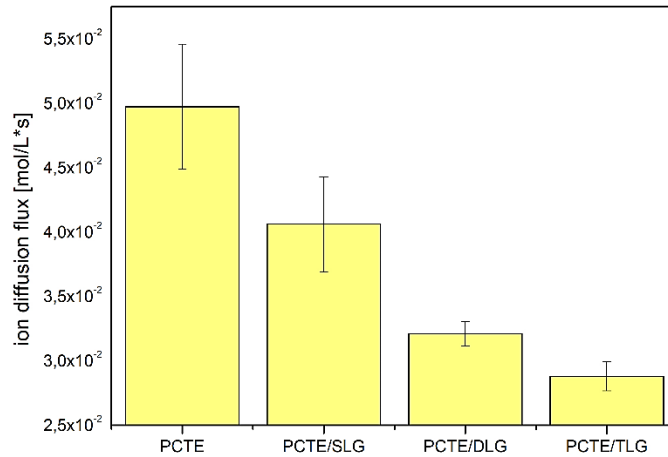


**Figure 4.21:** NaCl ion diffusion flux in all samples analysed

Graphene/PCTE membranes showed lower flux compared to bare PCTE membrane. A progressive lower flux as the number of layers increases indicates a lower leakage and therefore a higher blockage of ions through the graphene-based membranes.

### 4.3.2 Diclofenac transport measurements

Diclofenac is a drug with a brute formula  $C_{14}H_{11}Cl_2NO_2$ . Chemically, it is an acid whose molecule is significantly larger than that of NaCl. For this reason, a more efficient size-exclusion mechanism was expected by the membranes, and so a greater capacity of rejection. Fig. 4.22 shows the Diclofenac concentration trend obtained from monitoring the conductivity in the permeate (right side of diffusion cell) for 1 h.

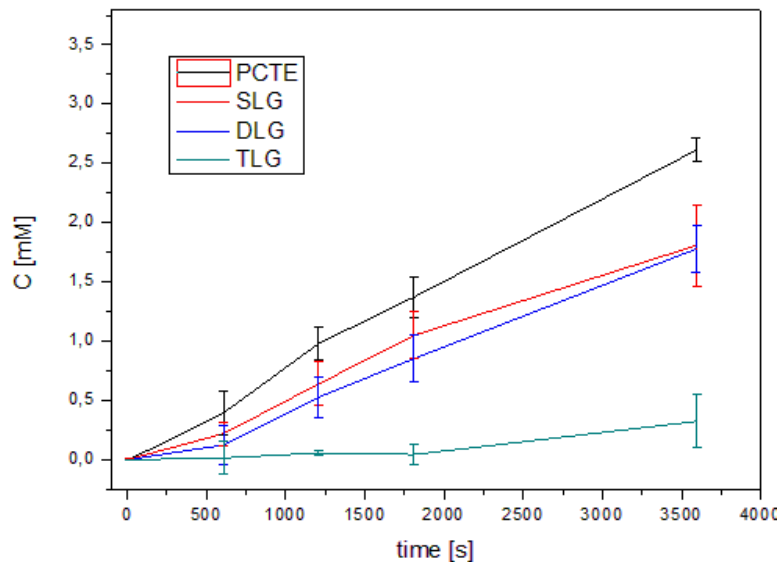


**Figure 4.22:** Diclofenac concentration versus time

Also in this case the concentration of solute increases over time, indicating that it diffuses through the graphene/PCTE sample but it remains after 1 h well below the initial

concentration of the feed (10mM). Concentration versus time plot for the bare PCTE was taken as the reference curve for evaluating the effective blockage (% rejection).

Fig. 4.23 shows the rejection R estimated at 4 different times: 10 min, 20 min, 30 min, 1 h.

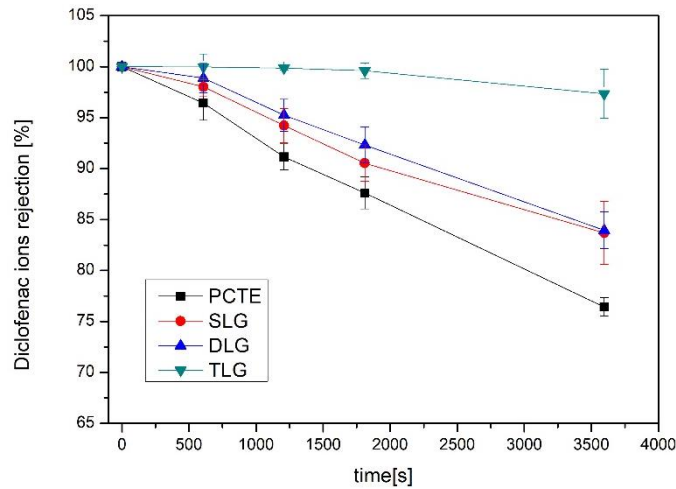


**Figure 4.23:** Diclofenac rejection [%]

Graphene single layer transferred on PCTE blocked 83,7 % of the ion transport after 1 h, while the double layer and triple layer graphene membranes blocked 84% and 97,3% of the Diclofenac transport, respectively.

The ion transport flux for both graphene membranes and bare PCTE membranes is shown in Fig. 4.24. The plot of the solute diffusion flux is obtained in the same way as explained for NaCl, with the same progressive decrease for Diclofenac flux.

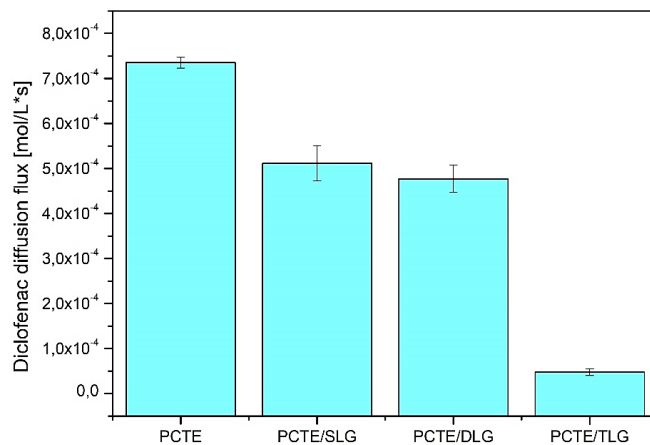


**Figure 4.24:** Diclofenac diffusion flux in all samples analysed

These results highlight that optimization of defect sealing by increasing the number of graphene layers can significantly improve the rejection ability of the membranes. This demonstrates that it is possible to achieve selective molecular transport through single layer or few layers graphene on PCTE.

## 5. CONCLUSIONS

In this work, we manufactured graphene membranes supported on a porous polymeric (PCTE) support and we analysed them with surface/morphological characterizations (contact angle and FE-SEM analysis), structural one (Raman spectroscopy), and functional one (mass transport measurements).

The first objective of developing a direct and simple transfer process has been fully achieved. The samples produced by our transfer process are quite homogeneous thanks to the minimum possible handling operations. Above all, they enjoy excellent repeatability, since all samples of the same type provided consistent results, both in morphological/structural and functional characterization.

With respect to wettability measurements, moderately high hydrophobicity of the substrate succeeded in promoting a conformal transfer of graphene to the substrate. Single layer transferred graphene was found not to change significantly the substrate wettability, while few-layers transferred graphene showed a decreasing wettability. We can only speculate that this occurs due to residual defects or to hydrophilic functional groups present at the graphene surface that may form during the membrane preparation processes.

Morphological and structural characterization confirm a good coverage degree of the support membranes with graphene, highlighting the presence of some intrinsic or transfer-induced defects.

While growth process of graphene on Cu is well known [10], the formation mechanism of pore defects occurring during this process is yet unexplored. Some research works [19] highlighted that they are probably due to defects in copper foil or to the presence of particulates on copper surface. This means that improvements in the quality of CVD graphene could further reduce the occurrence of defects. A great hurdle is to create a completely uniform layer of graphene on Cu substrate. It is quite difficult to obtain this homogeneity because the reactant gas concentrations punctually change within the space of a reaction chamber and in addition there might be a depletion of reactants by the time gas reaches the end of the substrate, leading to a local growth suppression. In order to overcome these technical issues, alternative techniques and guidelines to follow in order to create the highest possible quality of graphene are needed.

The filtration properties have been measured in a side-by-side apparatus in diffusion driven mode, by using a reliable in-line method. The results demonstrate that it is possible to achieve selective molecular transport through intrinsic defects of ultrathin graphene sheets with macroscopic areas.

The transport of molecules through intrinsic defects as well as larger defects forming during the membrane fabrication procedure has been successfully controlled via defect “sealing”. The latter has been achieved by stacking two or three layers of single layer CVD graphene: consequently, a reduction of leaks through areas not covered by graphene is observed. This implies an enhanced rejection ability and an optimization of size-exclusion mechanism. Mass transport study through graphene-based membranes was carried out by using 0,5 M NaCl solution and 10 mM Diclofenac solution, providing an indirect characterization of the defects induced by the transfer process. The single layer/PCTE graphene membranes blocked 65,9% of NaCl ions (i.e. 34,1 % leakage occurred through the defects) and the 83,7% of Diclofenac molecules (i.e. 16,3% leakage occurred through the defects). The sealing of the defects obtained by stacking two and three layers increased the blockage to a maximum of 76,5% for NaCl and 97,3% for Diclofenac. Thanks to the use of these two probe molecules it was therefore possible to better understand the dimensional exclusion properties of these membranes, demonstrating the greater feasibility of their application in the removal of polluting molecules from water (such as drug molecules). At this stage,

therefore, these membranes are not yet ready to be used effectively for reverse osmosis desalination applications. In fact, even if they have shown also excellent NaCl rejection ability compared to other sealing-defects techniques [22,23] with the further advantage of using a much less expensive technique, advanced graphene membranes for reverse osmosis desalination will require an additional effort in creating a controlled generation of sub-nanometric pores with defined size, to facilitate the passage of water while rejecting that of the ions. However, these membranes may be suitable for nanofiltration applications, as demonstrated by the ability to retain the diclofenac molecule which has an estimated size of 1,5 nm.

The ability here achieved to create graphene/polymeric membranes with low leakage and minimization of defects is an important step toward a scalable membrane manufacturing process and toward the realization of nano-porous molecular sieve membranes with a priori defined mechanism of dimensional exclusion.

## 6. BIBLIOGRAPHY

- [1] Judd S., Jefferson B., 2003, *Membrane for industrial Wastewater Recovery and Re-use* (1st ed.), Elsevier Advanced Technology, Oxford, UK
- [2] Wang L.K., Chen J.P., Hung Y.T., 2008, *Handbook of environmental engineering: Membrane and desalination technologies*, Humana Press, Totowa, USA
- [3] Bird R.B., Stewart W.E., Lightfoot E.N., 2006, *Transport Phenomena*, Revised 2<sup>nd</sup> edition, John Wiley & Sons, Hoboken, USA
- [4] "The Nobel Prize in Physics 2010". The Nobel Foundation. Retrieved 3 December 2013
- [5] Bunch J., Verbridge S., Alden J., Van der zande A., Parpia J., Craighead H., McEuen P., 2008, Impermeable atomic membranes from Graphene sheets, *Nano Lett.* **8**, 2548-2462
- [6] Wolf E., 2014, *Applications of Graphene: an overview*, Springer, Berlin, Germany
- [7] Nair R.R. et al, 2008, Fine Structure Constant Defines Visual Transparency of Graphene, *Science* **320**, 1308
- [8] Denis P., Iribarne F., 2013, Comparative study of defect reactivity in graphene, *J. Phys. Chem.* **117**, 19048-19055
- [9] Diankov G., Neumann M., Goldhaber-Gordon D., 2013, Extreme Monolayer-Selectivity of Hydrogen-Plasma Reactions with Graphene, *American Chemical Society* **7**, 1324-1332
- [10] Zhang Y., Zhang L., Zhou C., 2013, Review of Chemical Vapor Deposition of Graphene and Related Applications, *Accounts of chemical research* **46**, 2329-2339
- [11] Song N., Gao X., Mac Z., Wang X., Weia Y., Gao C., 2018, A review of graphene-based separation membrane: Materials, characteristics, preparation and applications, *Desalination* **437**, 59-72
- [12] Wang L., Williams C., Boutilier M., Kidambi P., Karnik R., 2017, Single-Layer Graphene Membranes withstand ultrahigh applied pressure, *Nano Lett.* **17**, 3081-3088
- [13] Tanugi D.C., Grossman J.C., 2012, Water desalination across nanoporous graphene, *Nano Lett.* **12**, 3602-3608
- [14] Suk M., Aluru N., 2010, Water transport through ultrathin graphene, *J. Phys. Chem. Lett.* **1**, 1590-1594
- [15] Leenaerts O., Partoens B., Peeters F.M., 2009, Water on graphene: hydrophobicity and dipole moment using density functional theory, *Phys. Rev. B* **79**, 235440.
- [16] Tanugi D.C., Grossman J.C., 2014, Mechanical strength of nanoporous graphene as a desalination membrane, *NanoLett.* **14**, 6171-6178
- [17] Drndić M., Fischbein M.D., 2008, Electron beam nanosculpting of suspended graphene sheets, *Appl.Phys.Lett.* **93**, 113107

- [18] Celebi K., Buccheim J., Wyss R.M., Droudian A., Gasser P., Shorubalko I., Kye J., Lee C., Park H.G., 2014, Ultimate Permeation Across Atomically Thin Porous Graphene, *Science* **334**, 289-292
- [19] O'Hern S.C., Stewart C.A., Boutilier M.S.H., Idrobo J.C., Bhaviripudi S., Das S.K., Kong J., Laoui T., Atieh M., Karnik R., 2012, Selective Molecular Transport through Intrinsic Defects in a Single Layer of CVD Graphene, *ACS Nano* **6**, 10130-10138
- [20] O'Hern S.C., Boutilier M.S.H., Idrobo J.C., Song Y., Kong J., Laoui T., Atieh M., Karnik R., 2014, Selective Ionic Transport through Tunable Subnanometer Pores in Single-Layer Graphene Membranes, *Nano Lett.* **14**, 1234-1241
- [21] Agrawal K.W. et al, 2017, Fabrication, Pressure testing, and Nanopore Formation of Single-Layer Graphene Membranes, *J.Phys.Chem.* **121**, 14312-14321
- [22] Kafiah F.M., Khan Z., Ibrahim A., Karnik R., Atieh M., Laoui T., Monolayer graphene transfer onto polypropylene and polyvinylidenedifluoride microfiltration membranes for water desalination, *Desalination* **388**, 29-37
- [23] O'Hern S.C., Jang.D., Bose S., Idrobo J.C., Song Y., Laoui T., Kong J., Karnik R., 2015, Nanofiltration across Defect-Sealed Nanoporous Monolayer Graphene, *Nano Lett.* **15**, 3254-3260
- [24] Surwade S.P., Smirnov S.N., Vlasiouk I.V., Unocic R.R., Veith G.M., Dai S., Mahurin S.M., 2015, *Nat. Nanotech.* **10**, 459-464
- [25] Kazemi A.S., Hosseini S.M., Abdi Y., 2019, Large total area membrane of suspended single layer graphene for water desalination, *Desalination* **451**, 160-171
- [26] Kazemi A.S., Abdi Y., Eslami J., Das R., 2019, Support based novel single layer nanoporous graphene membrane for efficacious water desalination, *Desalination* **451**, 148-159
- [27] Qin Y., Hu Y., Koehler S., Cai L., Wen J., Tan X., Xu W., Shen Q., Hou X., Xue J., Yu M., Weitz D., 2017, Ultrafast Nanofiltration through Large-Area Single-Layered Graphene Membranes, *ACS Appl. Mater. Interfaces* **9**, 9239-9244
- [28] Ferrari A.C., Meyer J.C., Scardaci V., Casiraghi C., Lazzeri M., Mauri F., Piscanec S., Jiang D., Novoselov K.S., Roth S., Geim K.A. C. Ferrari, 2006, Raman spectrum of graphene and graphene layers, *Phys. Rev. Lett.* **97**, 187401
- [29] Ferrari A.C., 2007, Raman spectroscopy of graphene and graphite: Disorder, electron-phonon coupling, doping and nonadiabatic effects, *Solid State Communications* **143**, 47-57.
- [30] Du F., Huang J., Duan H., Xiong C., Wang J., 2018, Wetting transparency of supported graphene is regulated by polarities of liquids and substrates, *Applied Surface Science* **454**, 249-255
- [31] Driskill J., Vanzo D., Bratko D., Luzar A., 2014, Wetting transparency of graphene in water, *The Journal of chemical physics* **141**, 18C517
- [32] Zheng N., Min H., Jiang Y., Cheng X., 2018, Polycarbonate as a negative-tone resist for electron-beam lithography, *Journal of Vacuum Science & Technology B, Nanotechnology and Microelectronics: Materials, Processing, Measurement, and Phenomena* **36**, 021603

- [33] Balan A., Kumar R., Boukhicha M., Beyssac O., Bouillard J., Taverna D., Sacks W., Marangolo M., Lacaze E., Gohler R., Escoffier W., Poumirol J.M., Shukla A., 2010, Anodic bonded graphene, *Journal Of Physics D: Applied Physics* **43**, 374013.
- [34] Ferrari A.C., Meyer J.C., Scardaci V., Casiraghi C., Lazzeri M., Mauri F., Piscanec S., Jiang D., Novoselov K.S., Roth S., Geim K.A. C. Ferrari, 2006, Raman spectrum of graphene and graphene layers, *Phys. Rev. Lett.* **97**, 187401

## 7. ACKNOWLEDGEMENTS

Il mio primo grazie va ai miei nonni, che oggi avrebbero vissuto questo momento con una gioia immensa. I vostri occhi sorridenti e l'entusiasmo che mostravate quando vi raccontavo di qualche mio piccolo successo sono stati molte volte il mio sprone nei momenti più duri di questo percorso universitario. È a voi che dedico col pensiero questo mio traguardo.

Ai miei genitori, che mi hanno sempre fatto sentire il loro supporto incondizionato anche a mille chilometri di distanza. Spesso e volentieri non riesco a trasmettere tutto l'affetto e l'ammirazione che provo per voi. Colgo quest'occasione per dirvi che siete due genitori meravigliosi. Grazie per avermi iniziato alla curiosità nei confronti di ciò che ci circonda, per avermi fatto capire l'importanza dello studio senza mai alcuna imposizione, e per avermi insegnato fin da bambina, con le parole ma soprattutto con l'esempio, l'importanza dell'umiltà.

Ai miei fratellini, Giulia e Armando, le persone più belle che possano esserci al mondo. Siete il mio porto sicuro, il mio primo punto di riferimento. Grazie per essere sempre stati i miei migliori amici oltre che i miei fratelli. La cosa di cui ho più certezza nella vita è la forza del nostro rapporto. Vi guarderò sempre con gli occhi della meraviglia e vi accoglierò sempre con lo stesso amore e la stessa gioia esplosiva con cui vi accoglieva quella bambina riccioluta di tanti anni fa quando tornavate da scuola.

Ad Antonio, il tuo sguardo genuino sul mondo e il tuo respirare la vita a pieni polmoni sono per me continua fonte di ispirazione. Grazie per essermi stato accanto in tutti questi anni e per averlo fatto ancora di più durante questo percorso di tesi. Grazie alla calma che sai infondermi nei momenti più burrascosi, ho affrontato le difficoltà con una visione nuova. Grazie per non stancarti mai di trasmettermi la tua positività e di ripetermi che ad ogni problema possiamo trovare una soluzione, insieme.

Ad Elisabetta, siamo il gatto e la volpe, si sa, ma non potremmo mai vivere l'una senza l'altra. Grazie per dimostrarmi quanto credi in me, quando io non riesco a farlo. Senza il tuo sprone di tutti questi anni probabilmente non sarei qui a scrivere.

A Claudia, per avermi ascoltata sempre con un'attenzione minuziosa e amorevole. I nostri discorsi interminabili mi hanno fatto crescere più di mille esperienze diverse.

A tutti i miei amici "di giù", e in particolare grazie a Elisabetta, Claudia G., Claudia M., Eleonora, Francesca, Stefania, Fabio, Marco, Davide. Siete la mia infanzia, la mia adolescenza, la mia giovinezza. Grazie per avermi dato la possibilità di capire il valore dell'amicizia. Siete la mia seconda famiglia, qualcuno su cui so di poter contare accada quel che accada. Se a volte ci sembrerà che gli anni e i chilometri ci stiano allontanando, ricordate quanto è raro crescere insieme, tappa dopo tappa. Per quanto le nostre personalità possano essere diverse, in ognuno di noi c'è un pezzo prezioso di tutti gli altri che abbiamo fatto nostro crescendo insieme, e che ci porteremo sempre appresso. Di questo sono estremamente fiera e felice.

A Gabriele, l'amico migliore che l'università potesse regalarmi. Assocerò per sempre gli anni universitari alle nostre tragicomiche, alle nostre risate, ai nostri pianti. Il tuo sapermi leggere dentro è stato la mia salvezza in molti casi. Grazie anche per aver reso le mille mila

ore passate sui libri meno faticose, per aver fatto diventare un'avventura divertente anche gli esami più ostici.

A Brunella, per avermi dato sempre il consiglio giusto al momento giusto, e per avermi fatto capire che non esiste il non riesco, in nessuna circostanza. La tua saggezza d'altri tempi mi ha aiutato a risolvere molti dei miei arcani.

Alla mia piccola grande Benni, la tua presenza mi ricorda sempre che il mondo ha anche tanto di buono da offrire. Grazie per avermi insegnato a vivere tutto con più leggerezza e spensieratezza. Il tuo spirito da eterna sognatrice continua ad essere per me un modello da seguire.

Ad Arianna, per avermi accolta fin da subito come una sorella e per avermi ascoltata ogni volta in cui ne avevo bisogno.

Ad entrambe un grazie enorme per avermi fatto vivere il periodo in assoluto più bello e più pieno di risate di questi anni torinesi: un pezzo grande del mio cuore rimarrà sempre in Corso Rosselli.

Infine, vorrei ringraziare i miei relatori Giancarlo Cicero e Marco Laurenti, e i professori Stefano Bianco ed Elena Tresso, per la grande disponibilità che mi hanno sempre mostrato e per aver arricchito il mio ultimo periodo universitario con tanti nuovi insegnamenti ed esperienze.

